THE HONG KONG
POLYTECHNIC UNIVERSITY
香港理工大學
Pao Yue-kong Library
包玉剛圖書館

Copyright Undertaking

This thesis is protected by copyright, with all rights reserved.

By reading and using the thesis, the reader understands and agrees to the following terms:

1. The reader will abide by the rules and legal ordinances governing copyright regarding the use of the thesis.

2. The reader will use the thesis for the purpose of research or private study only and not for distribution or further reproduction or any other purpose.

3. The reader agrees to indemnify and hold the University harmless from and against any loss, damage, cost, liability or expenses arising from copyright infringement or unauthorized usage.

Pao Yue-kong Library, The Hong Kong Polytechnic University, Hung Hom, Kowloon, Hong Kong

http://www.lib.polyu.edu.hk

The Thermal and Electrical Properties of Carbon Black/Liquid Crystalline Polymer Composites

by

Lo Kwan Leong

for the Degree of

Master of Philosophy in Physics

The Hong Kong Polytechnic University

February, 2000

Abstract

Carbon black/liquid crystalline polymer (CB/LCP) composites were mixed by blending the carbon black powder with Vectra A950 by extrusion. Film samples of 1 % to 7 % and 10 % CB were obtained from hot pressing the mixture in a mould with thin gaps.

Wide-Angle X-ray diffraction was employed to determine the molecular orientation of the LCP matrix. The results reveal that at lower CB volume fraction, the LCP in the composite has a higher orientation whereas the LCP become randomly aligned at high CB volume fraction composite. The surface morphology of the film samples were studied by optical microscope and scanning electron microscope. From the optical photomicrographs, an increase in the CB volume fraction would increase the probability of forming large clusters. There is an obvious change from 3 % to 4 % CB of which the clusters grow and make contact. The CB aggregates are discernible from SEM of which the average size is about a few microns.

The J-E characteristics of the CB samples reveal a linear relationship between the current and the applied voltage. It may be a result of highly conductive of the composites. Resistivities of the samples were also measured in the flow, transverse and thickness directions. The percolation threshold is found at between 3 % and 4 %. It is also found that the volume fraction dependence of resistivity satisfies the scaling law. The resistivity as a function of temperature was measured in the range from room temperature to 200 °C. The resistivities of samples below percolation threshold exhibit negative temperature coefficient and the drop in resistivity is about three orders of

magnitude. The resistivities against temperature of samples above the percolation threshold exhibit a negative slope at low temperature range. They reach a minimum at around 150 °C then change to a positive slope up to 200 °C.

Thermal conductivity and thermal expansivity of the composites were determined by the laser flash radiometry method and the thermal mechanical analyzer respectively. The results can be correlated to the molecular orientation of the LCP matrix. Low CB volume fraction composites correspond to high molecular order, thus heat diffuse more easy relative to the high CB volume fraction composites which have lower molecular order. The results of sheet moduli of the composites determined by the laser induced ultrasonic method revealed the elasticity of the composites is also dominated by the molecular orientation of the LCP matrix.

Acknowledgements

I'm especially grateful to my chief supervisor, Dr. Y. W. Wong, for his close supervision, precious advice and invaluable direction throughout the course of this research. He also deserves thanks for his suggestion regarding content and organisation of this thesis. I would also like to thank my co-supervisor, Prof. F. G. Shin for his enlightening suggestion and discussion. Apart from these, I owe debt of appreciation to many people: to the technical staff of our department and Mr. Yeung of MRC for technical support, to my companions Jimmy, Aaron, Alex, Mendel, Shiang, Fred, Crystal and Manliza for their support in this research period. Finally, I express my appreciation to my brothers and sisters in my church and my family for their spiritual encouragement and support.

Abbreviations

AsF$_5$ - Arsenic Fluoride

CB - Carbon Black

CF - Carbon Fiber

DSC - Differential Scanning Calorimeter

DSO Digitizing Storage Oscilloscope

EMT - Effective Medium Theory

FEF - Fast Extrusion Furnace

GEM - General Effective Media

HBA - p-Hydroxy Benzoic Acid

HDPE - High Density Polyethylene

HgCdTe - Mercury Cadmium Tellurium

HNA - 6-p-Hydroxy-2-Naphthoic Acid

KD*P - Potassium DiDeuterium Phosphate

LCP - Liquid Crystalline Polymer

LDPE - Low Density Polyethylene

LVDT - Linear Variable Differential Transformer

NTC - Negative Temperature Coefficient

OM - Optical Microscope

PE - Polyethylene

PS - Polystyrene

PTC - Positive Temperature Coefficient

PVC - Poly(Vinyl Chloride)

SBR - Styrene-Butadiene Rubber

SEM - Scanning Electron Microscope

SRF - Semi-Reinforcing Furnace

TEC - Thermal Expansion Coefficient

TMA - Thermal Mechanical Analyzer

Table of Contents

List of Figures

1 Introduction

1.1 Background

Electrically conducting polymers have attracted a great deal of scientific and commercial interest during the last few decades. Conducting polymers can be obtained in two ways: by producing a polymer that is intrinsically conducting, or by loading an electrically insulating matrix with conductive fillers. The former is basically the conjugated polymer doped with oxidative materials such as iodine or arsenic fluoride (AsF_5). For example, the polyacetylene doped with iodine, the polyphenylene doped with AsF_5 or even the undoped polypyrrole, all exhibit metallic conductivity.

The latter class of conducting polymers is the polymer loading with conducting particles for which the polymer matrix is an insulator, the resistivity is usually in the range of 10^{13} to 10^{16} Ω-cm, while the conductive phase of low resistivity include metallic powders [Mallaris et al., 1971, Kwan et al., 1980 and Coppard et al., 1990], carbon fibers [Lu et al., 1996], carbon black [Voet, 1981, Medalia, 1986 and Aminabhavi et al., 1990], or even with the intrinsically conductive polymeric powders, e.g. polypyrrole [Chen et al., 1995 and Ouyang et al., 1996]. Among the conductive additives, carbon black (CB) is the most common filler used for the extrinsic conducting polymers. The polymer matrix used for the conducting composites are the amorphous polymer e.g. styrene-butadiene rubber (SBR) and the semi-crystalline polymer e.g. polyethylene (PE).

It can be seen that both of these polymers have a relatively low working temperature e.g. the upper working temperature of synthetic rubber is about 100 °C. In addition, these polymers have a relatively poor mechanical strength, thus it will limit the applications of these composites in industry. In view of these shortcomings, a more demanding polymer matrix is required. A class of polymer so called liquid crystalline polymer (LCP) has been developed for two decades. It has a relatively high melting point, e.g. the Vectra A950 melts at nearly 300 °C. It has been found that the properties of ordinary engineering polymers can be greatly improved by blending them with liquid crystalline polymer. These composite materials may be processed by injection moulding, extrusion, thermoforming, or blow moulding, etc. Therefore, the work following is to investigate a new kind of polymer matrix which is Vectra A950 liquid crystalline polymer loading with a commercial carbon black. Other than the electrical properties, the thermal properties of the carbon black/liquid crystalline polymer (CB/LCP) composites are interested while the orientation and the surface morphology of the composites will also be studied in detail.

The behavior of conducting polymer composites is quite interesting. Firstly, a polymer composite could change from an insulator to a (semi) conductor over a very narrow range of filler concentration. At low filler concentrations, the composite remains an effective insulator. At a "critical volume concentration", the resistivity of the composite decreases sharply to a level at which the composite can be termed conductor of which the resistivity is of the order of 10^{-1} Ω-cm. An additional increase in filler concentration does not increase the conductivity further since it is very close to that of conducting filler.

1.2   Reviews on Carbon Black/Polymer Composites

1.2.1 Conduction Mechanism

The ability of polymers to act as electrical insulators is the basis for their manifold application in the electrical and electronics areas. But they can be modified by compounding with electrical conductive fillers to become relatively good electrical conductors. Many articles [Janzen, 1975, Michels *et al.*, 1989, Lee, 1992 Karasek *et al.*, 1996 and Nakamura *et al.*, 1997] have been published to describe the steep drop in electrical resistivity (increase in electrical conductivity) which occurs upon incorporation of increasing concentrations of a conductive particulate filler into an insulation matrix. The mechanism of conduction includes tunneling, ionic transport, electron hopping, dielectric breakdown, field emission, and simple interaggregate conduction. It is generally acknowledged that incipient formation of infinite contiguous particle chains is responsible for the sudden onset of conduction at a characteristic critical filler volume fraction [Janzen, 1975].

The electrical conduction process in carbon black/polymer composites is complicated and depends on a large number of parameters: particle size, surface area, surface condition, the volume fraction, filler matrix interactions, structure and dispersion of conducting particles and processing techniques are all the key factors in determining the electrical properties. In addition, the thermal expansion of polymers also plays an important role in the conduction process of these composites.

A simple theory of conductive paths, which is used to explain the conduction mechanism of carbon fibers (CF) or conductor-filled polymer composites [Lu *et al.*, 1996]. Lu *et al.* suggested that the existence of conductive paths (fibers or particles contacts) that results in the conductivity of the composites. With increase of the content of the fibers or the particles, conductive connection among the fibers or the particles increase, and the average distance between the fibers or the particles becomes smaller; thus, the resistivity of the composites decreases.

Sherman *et al.* [Sherman *et al.*, 1983], introduced three vital processes controlling conduction (percolation, tunneling and thermal expansion) which were required to explain electron transport in conductor-filled polymer composites. Percolation theory predicts a filler loading threshold where the composite system makes a transition between tunneling and conductor-filler ohmic conduction. The electrical resistivity changes from 'opaque' to 'transparent' on adding conducting-fillers. Below the percolation threshold, tunneling dominant and the conductor-fillers carry the current while beyond the threshold. Tunneling occurs when the conductor-fillers whose separation is small so that electrons may tunnel quantum mechanically between conductive elements, leading to a lower resistance than would be expected from the insulator alone. They also demonstrated the thermal expansion changes the physical dimensions of the entire electrical network and leaded to the changes in the relative magnitudes of the various processes. Since the thermal expansion coefficients are generally greater in polymers relative to the metallic-like materials used as fillers. As a consequence, the volume fraction of fillers and the distance between adjacent individual filler elements can be expected to vary easily with respect to temperature.

For the quantum mechanical tunneling, Sheng *et al.* [Sheng *et al.*, 1978], suggested a tunneling conduction mechanism for disordered materials in which the modulation of tunneling barriers by thermal fluctuation plays an important role in determining the dependence of the conductivity on temperature and electric field. In addition, they have supplemented this type of treatment with a novel mechanism and claimed its application on carbon black/poly(vinyl chloride) (CB/PVC) composites at cryogenic temperature. They found that at low temperature, the transport properties of CB/PVC composites are governed by tunneling of carriers across a barrier that is modulated by temperature-activated fluctuations.

Lundberg *et al.* [Lundberg *et al.*, 1986], described the conducting mechanism for carbon black-filled conducting polymer (ET-Semicon®) must be based on at least two effects: percolation and quantum mechanical tunneling between the conducting particles. When the filler volume fraction is comparable to or smaller than the critical volume fraction, tunneling has important consequences. The extra current provided by this mechanism decreases the resistivity relative to the case of pure percolation, but the exact amount is very sensitive to temperature, volume fraction, and a number of geometrical factors pertaining to the junction.

Kozlowski [Kozlowski, 1995], studied the carbon black-filled polystyrene, polyethylene and their blends. He reported the classical conducting mechanism of the quantum mechanical tunneling between the conducting particles and the interfacial phenomena at the carbon black/polymer matrix surface, which are prevailing at the critical volume

fraction. Below the percolation threshold, the hopping charge carrier transport has the highest contribution to the conductivity mechanism.

The current-voltage characteristics of samples of butyl rubber loaded with two different types of carbon black have been studied at different temperature by Abo-Hashem [Abo-Hashem, 1992]. He described the conduction mechanism for the fast extrusion furnace (FEF) composite is a conventional band model as the temperature increase from room temperature up to 333 K. He also concluded that the conduction mechanism above the transition temperature is the hopping mechanism with activation energy ($E=0.8$ eV). The reason for this is as the temperature increase, the bandwidth and mobility decrease, and the transition from the band conduction model to the hopping model at a certain temperature.

In Lux recent extended review [Lux, 1993], he depicted a number of models that were proposed to explain the conductivity of mixtures on the basis of different factors such as volume fraction of the conductive phase, the specific conductivity of the fillers, the probability of the development of at least a one-dimensional conductive network and the interfacial interactions at the boundary between the individual filler and the polymeric matrix. Lux concluded that currently no existing model is able to explain all of the different results of experimental studies. Furthermore, no model is able to account for the extensive influence of different processing methods on the percolation process.

Since the percolation theory is limited in which the percolation equation is valid near the percolation threshold only when the ratio of the resistivities of the two components

is infinite. This can be a problem when dealing with a real system where all components have finite resistivities which corresponding to the composites above the percolation threshold [Blaszkiewicz *et al.*, 1992]. Percolation theory is not valid in these cases with the use of scaling factors. Thus a quantitative general effective media (GEM) [Deprez *et al.*, 1988 and Blaszkiewicz *et al.*, 1992] equation is used to describe a broad range of experiment resistivity-volume fraction results for graphite/polymer and carbon black/polymer composites.

For detailed GEM, which combines most aspects of both Bruggeman's effective media and percolation theories into a single GEM equation [Mclachlan *et al.*, 1990]. They showed that the GEM equation quantitatively fits electrical resistivity as function of the volume fraction data for binary composites. The GEM equation can gives a quantitative method of analyzing the actual experimental composite media of electrical resistivity results.

1.2.2 Carbon Black Filled Polymer Composites

The interest in composites made with carbon black is due to the fact that carbon black of high degree of permanent particle structure generally give low value of resistivity and its low cost. So that carbon black becomes the additive most widely used to make conducting polymer composites nowadays [Voet, 1981, Yacubowicz *et al.*, 1986, 1990, Ghofraniha *et al.*, 1988, Jia *et al.*, 1994 and Modine *et al.*, 1996]. Some popular researches in carbon black/polymer systems were reviewed as following.

Carbon Black/Poly(vinyl chloride)

Sheng *et al.* [Sheng *et al.*, 1978], have presented evidence that in carbon black/poly(vinyl chloride) (CB/PVC) composites, consisting of aggregates of carbon black dispersed in the insulating matrix, the electrical conductivity can be ascribed to a novel mechanism of tunneling with potential barrier modulation by thermal fluctuations. This evidence plays an important role in determining the dependence of the conductivity on temperature and electric field.

Electrical conductivity of CB/PVC composites results from percolation of electrons in the carbon black networks. When the carbon black concentration is low, conduction is dominated by electron tunneling across small barriers separating large conducting regions. As the carbon black concentration is high, the composite turns to the carbon black conductivity.

Carbon black impregnated polymer such as carbon black/poly(vinyl chloride) have also been studied by Sichel et al. [Sichel et al., 1978]. They found that the transport properties of CB/PVC composites are governed by tunneling of carriers across a barrier which is modulated by temperature activated fluctuations at low temperature. As the carbon black concentration increases, the CB/PVC composites become more conductive and the conductivity is less sensitive to temperature. In addition, the energy required for an electron to cross the PVC gap between carbon black aggregates also decreases.

In the investigation of the temperature dependence of resistivity of CB/PVC composites above 100 K, they introduced two competition effects. As temperature increase, the tunneling current increases because the thermal fluctuations decrease the potential barrier between carbon black aggregates. On the other hand, the PVC expands more rapidly than the carbon black that widening the gap between carbon grains, and increasing the resistivity as the temperature rises. At a certain temperature, there is a crossover occurs and the CB/PVC composites have resistivity minimum.

Carbon black/Polyethylene

The *I-V* characteristics of carbon black filled crystalline polyethylene (CB/PE) composite was investigated at room temperature and at few degrees above the melting temperature by Al-Allak et al. [Al-Allak et al., 1993]. The composite has a large carbon black content of 28 parts per hundred by weight and displayed a strong positive temperature coefficient of resistance (PTCR) effect with a sharp resistivity increase of four orders of magnitude. The resistivity above melting point did not show a steep reduction with temperature. Logarithmic current-voltage plots were found to be linear

slopes at temperature above and below melting temperature. They introduced a new model capable of explaining both the positive temperature coefficient resistance (PTCR) effect and the steep reduction in resistivity above melting point. This model invokes the co-operative effects of changes in crystallinity and volume expansion as the key factors responsible for this PTCR effect. A higher degree of crystallinity implies more interruptions in the conductive chains on approaching melting point resulting in an enhanced PTCR effect.

The conduction mechanism for a carbon black filled high-density polyethylene (CB/HDPE) composite was investigated by Tang *et al.* [Tang *et al.*, 1996]. Percolation and the quantum mechanical tunneling effect were the two models which were used to illustrate the electron transport process. The minimum electrical resistivity occurs near the glass transition temperature T_g of HDPE. It can be concluded that electron tunneling is an important mechanism and a dominant transport process in the CB/HDPE composite. For the temperature dependence of the resistivity investigation, this phenomenon competed with the expansion of the polymer matrix in the CB/HDPE composite, that a minimum resistivity can be occurred near the glass transition temperature of HDPE.

In the article of percolation threshold of carbon black/polyethylene (CB/PE) composites investigation by Nakamura [Nakamura, 1997], the percolation threshold based on the change in resistivity and relative permittivity for loading of carbon black, the electric field dependence of current and the critical exponent of conductivity. The change of insulating to non-insulating properties of the composites is called percolation threshold.

Three kinds of CB, Ketjenblack, #45 and Ashi-thermal were used in this study and their percolation threshold were 3.9, 14.0, 38.5 wt. % respectively. It is found that the tunneling gap exists even beyond this transition and interrupts to form infinite clusters of carbon black aggregates. It is further found that the critical exponent of conductivity estimated by the transition of resistivity from the tunneling to ohmic conduction mechanism is satisfied with the universal law of conductivity. The mechanism for changing between the carbon black aggregates into ohmic contacts has been considered the same as that of continuous conducting bonds above the percolation threshold in a random resistor network system. Therefore, it is concluded that the percolation threshold is defined at the volume fraction where the ohmic current behavior appears after the disappearance of the non-ohmic current behavior.

Carbon black/Rubber

In the study of butyl rubber mixed with SRF carbon black by Abo-Hashem *et al.* [Abo-Hashem *et al.*, 1994], the concept of percolation is able to explain the sharp increase in the electrical conductivity of composites above a certain concentration of carbon black, percolation threshold, which is about 21 % of CB. The variation of conductivity with temperature below the percolation threshold was characterized by thermally activated behavior above a certain temperature. The temperature dependence of conductivity above the percolation threshold was attributed to both breakdown and re-formation of carbon black clusters with temperature.

The percolation concept holds true for composites of crystalline chloroprene rubber mixed with fast extrusion furnace (FEF) carbon black and the percolation threshold is

found about 20 % phr of CB [Ali *et al.*, 1995]. It is found that the percolation threshold holds true for the composites where the conductivity shows a sharp increase when the mass fraction of FEF carbon black in the mixture exceeds 20 %. The temperature dependence of conductivity is thermally activated for the composites below and at the percolation threshold. As the temperature increase, two processes take place. One is the breakdown of the extended clusters while the other is the thermal expansion of rubber itself. Both processes increase the separation distance between the carbon black clusters. This leads to the decrease in conductivity with increasing temperature. But higher than the critical temperature of 60 °C, there is a change of conductivity from decrease to increase. This change is expected due to the fact that the increase in the separation distance with temperature reaches a critical value at which the size of carbon black clusters changes from infinite to finite and hence the temperature dependence of conductivity change.

1.3   Characteristics of Liquid Crystalline Polymer and Carbon Black

1.3.1 Liquid Crystalline Polymer (LCP)

The polymer matrix used in this project is the Hoechst-Celanese, Vectra A950 which is a copolyester of about 70 mol % p-hydroxybenzoic acid (HBA) and 30 mol % 6-p-hydroxy-2-naphthoic acid (HNA) [Choy et al., 1991]. The molecular structure of A950 is shown in Figure 1.1.
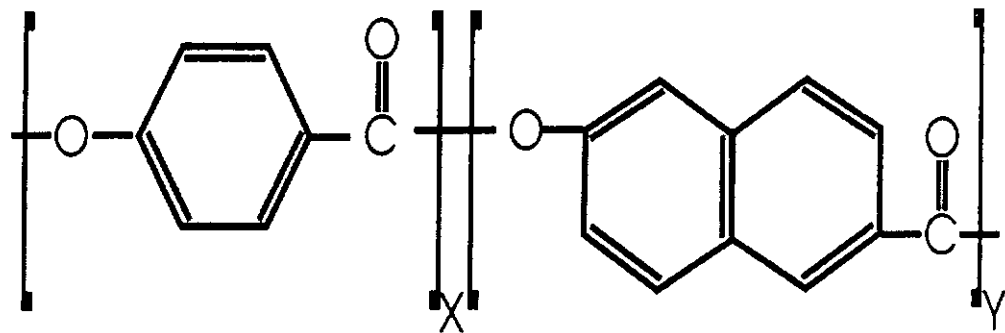
Figure 1.1   Molecular structure of Liquid Crystalline Polymer Vectra A950

The motivation for using LCP as polymer matrix to make the conducting polymer because it has a relatively high melting point (285 °C), highly anisotropic after processing because of its rod-like molecular structure (Figure 1.2) and it is also a good insulator.

In addition, the LCP blended with carbon fibers have higher stiffness and strength than that obtained with glass fibers. Carbon fiber modified composites are electrically

conductive and generally applied where the highest possible modulus is required. Carbon fiber reinforced Vectra (A230, B230) composites attain with 30% reinforcement in strength. However, conducting particles filled LCP is still a open topic. Therefore, it is interesting is to attempt this new polymer composite which is Vectra A950 liquid crystalline polymer loaded with carbon black powder.
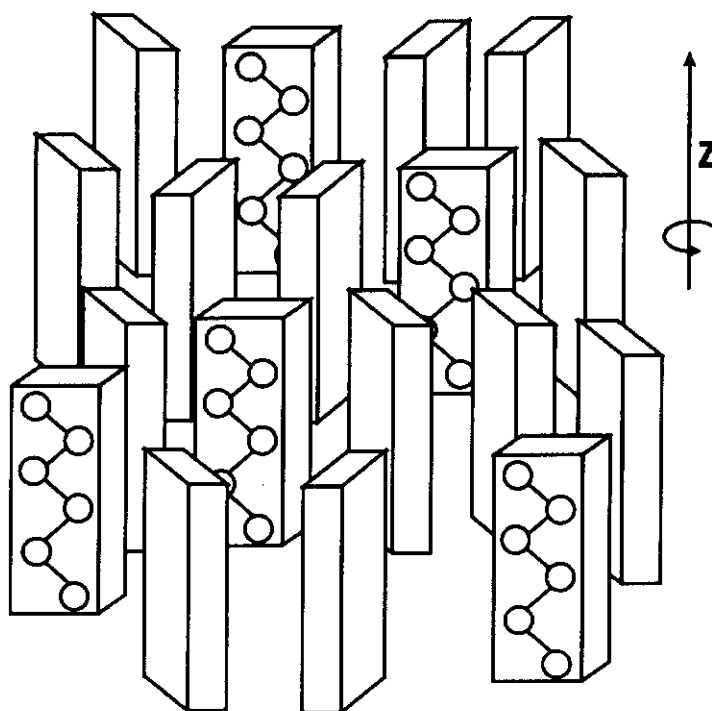
Figure 1.2   Rigid-rod like LCP

Research on LCP is diversified, covering topics in chemistry, physics and engineering. This section is not intended to be a comprehensive review of the state-of-the art for LCP. Instead, we seek to provide a brief review of the current trends in LCP research.

The first thermotropic LCP was reported in the mid-1970' by Rviello *et al.* and Jackson *et al.* [Rviello *et al.*, 1975 and Jackson *et al.*, 1976]. Since then, a large number of LCP

researches have been reported. In the 1980's, several thermotropic aromatic copolyester

LCPs were commercialized as shown in Table 1.1. Typical LCP structure is shown

schematically in Figure 1.3 [Ober *et al.*, 1990]. The major milestone in the development

of LCP was the synthesis of a family of thermotropic LCP based on hydroxybenzoic

acid (HBA) and hydroxy naphthoic acid (HNA) by Celanese Research Company. These

LCP was first commercialized in 1985 under a trade name Vectra [Isayev, 1996].

Trade Name	Company
Vectra	Hoechst-Celanese
PET-80PHB (XG-7)	Eastman Kodak
Xydar	Dartco
Granlar	Granmont
Hx-200	Dupont

Table 1.1   Representative commercial thermotropic LCPs
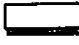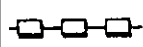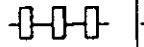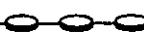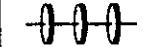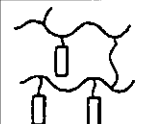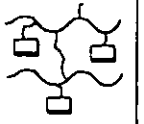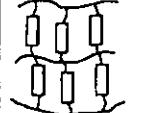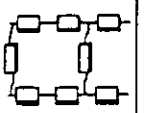
Figure 1.3   Examples of Liquid Crystalline Polymer architectures
[Ober *et al.*, 1990]

LCP has rigid-rod like (mainly due to the rigidity along the backbone) molecules and thus can be easily ordered (Figure 1.2), both in the melt state and solid state. Though highly ordered, the molecules flow readily in the melt state providing good moulding characteristics, which also can be compounded with reinforcements and fillers, forming unique compounds. The injection-moulded filled and reinforced Vectra A950 has high degree of anisotropy, physical properties in the flow direction differ from those in transverse to flow. In addition, a well-known skin-core effect is presented in these materials, where surface is a highly aligned monodomain material and the bulk is remaining of the polydomain structure. It thus has strong influence on the mechanical properties of components moulded from LCP.

Liquid crystalline polymer has very good thermal and mechanical properties as well as good chemical resistance, low flammability, very good dimensional stability. Besides, LCP also is an excellent electrical insulator even at elevated temperature, its resistivity at room temperature is of the order of 10^{16} Ω-cm. In addition to their good product properties, they show remarkable ease of processing due to their low melt viscosity and high melt strength. LCP generally has lower viscosity, longer melt relaxation time and higher melt strength than ordinary thermoplastics. The lower viscosity of LCP is explained by the rod alignment in the melt and the ease of rods sliding past each other, which is similar to shear thinning in flexible polymer systems in the non-Newtonian region as the molecules become elongated and somewhat oriented [Jackson *et al.*, 1991].

Unlike metals, LCP enable moulders to achieve very precise dimensions and tolerances without expensive machining. The alignment of rigid rod molecules results in a very low thermal expansion coefficient (TEC) minimizing shrinkage as parts cool from the melt. Low TEC also minimizes expansion when parts are sterilized or soldered. In most metal forming processes, tight tolerances on critical features require some machining. Even with computer controlled machining, the overall process remains operator intensive and therefore more expensive and less efficient than injection moulding.

LCP is a unique material for blending with other thermoplastics because of its outstanding mechanical properties and relative chemical inertness. The higher strength of the LCP results from the molecular orientation in the nematic phase during processing [Viswanathan, 1995]. Thus when the LCP is blended with a thermoplastic in an elongational and shear field, highly fibrillar structures of LCP domains in the thermoplastic matrix are obtained. This leads to *in situ* reinforcement of the thermoplastic.

A major expansion of research in blending of LCP with thermoplastics started after the publications by Isayev *et al.*, Blizard *et al.*, Kiss and Weiss *et al.* [Isayev *et al.*, 1987, Blizard *et al.*, 1987, Kiss, 1987 and Weiss *et al.*, 1987], indicating that one can obtain LCP/thermoplastic blends with good or synergistic mechanical properties even in the absence of the miscibility of components. This synergism is achieved due to a so-called self-reinforcing effect of LCP. In particular, during the process of mixing and shaping, LCP creates *in situ* high strength and modulus fibers within thermoplastic matrix. Thus, the concept of the self-reinforced or *in situ* composites has appeared. Evidently, in self-

reinforced composites, fibers can easily transfer mechanical load even in the absence of good adhesion at the interface between the LCP fibers and the matrix. It is also obvious that properties of these self-reinforced composites can be further enhanced by an improvement of the interfacial interaction.

Recent papers concerning blends of a LCP with flexible polymers include polycarbonate [Choy *et al.*, 1996, Mucha, 1989, and Magagnini *et al.*, 1992] and poly(ethylene terephthalate) [Li *et al.*, 1992], some attention was also paid to blending of two LCPs [Akhtar *et al.*, 1993]. The major objective of these studies was to obtain new LCP materials with improved mechanical properties. Number of investigations was carried out to look at the phase behavior, flow behavior (rheology), morphology and mechanical properties. Concerning rheology of LCP/LCP blends, as indicated earlier. LCP has the characteristic of extremely low viscosity compared with other engineering plastics. Akhtar *et al.* reported the viscosity of LCP could be modified by an addition of another LCP. They also reported the viscosity ratio of pure LCP melts exceed values of 10 over a wide range of shear rates, with the viscosity of the LCP/LCP blends lying between those of the pure components. Kiss [Kiss, 1987], concluded the low viscosity of LCP is that the viscosity of the blends with an isotropic polymer is usually lower than that of the isotropic polymer by itself. This reduction of viscosity is reflected in the processing parameters when working with such blends, such as the extruder torque, the extruder melt pressure, and the injection pressure.

The morphology of the blends is important as it directly affects the final properties of the resultant products. Morphological studies revealed, in many cases, the existence of

two phases of heterogeneous structure in blends [Isayev, 1991, Akhtar *et al.*, 1993 and Ding *et al.*, 1995]. Injection moulded samples in some cases indicated some unusual morphology with a highly oriented skin later encasing the core region [Akhtar *et al.*, 1993]. An enhancement of fibrillation and orientation of one LCP in the presence of other LCP are also postulated [Kenig *et al.*, 1991, Isayev, 1991, Akhtar *et al.*, 1993 and Ding *et al.*, 1995]. In these cases, a significant synergism of mechanical properties of mouldings was found. LCP/LCP blends were also spun into fibers. It was found that the major factor affecting fiber modulus and the order parameter was the draw ratio [Lee *et al.*, 1993]. Further studies on LCP/LCP blends will undoubtedly lead to creation of new materials with performance characteristics superior to those of high performance engineering thermoplastics.

It is well known that the mechanical properties of thermoplastic polymers can be greatly affected by the blends of other polymers. Akhtar *et al.* [Akhtar *et al.*, 1993], reported a substantial increase in the impact and tensile properties of the blends. The properties obtained are remarkably higher than those known for any high performance engineering thermoplastics. It is shown that such remarkable performance characteristics are due to the effect of self-reinforcement during the processing step when a LCP is presented in another matrix in the forms of *in situ* fibers.

Many potential applications of LCP can be envisioned, and they are expected that the level of both academic and industrial interest in these remarkable materials will continue to grow. The major areas of application of LCP (Hoechst/Celanese) have been reported by Jansson as shown in Table 1.2 [Jansson, 1992]. While LCP is appropriate,

or even essential, in many applications, their cost is very high relative to other polymers. The cost is likely to drop with expanding volume and increasing demand. One way of enjoying some of the attractive properties of LCP, while reducing the cost is to mix the LCP with less expensive polymers.

Electronics/electrical	Connectors, surface-mount components, relays bobbins, capacitor housings, potentiometers, switches.
Fibre-optics	Strength members, couplers, connectors.
Automotive	Fuel-system components, electrical systems.
Industrial	Motor components, lamp housings, conveyor belt components, and gears.
Chemical process	Tower packings, pump housings, pump shafts, valves.
Domestic equipment	Compact disc components, microwave equipment and turntables.
Others	Medical components, watch components, safety equipment, chemical analysis equipment, leisure goods.

Table 1.2   Applications of LCP (Hoechst/Celanese) [Jansson, 1992]

1.3.2 Carbon Black

Carbon black (CB) is one of the most versatile fillers used in compounding polymers. It provides varying levels of conductivity and at the same time serves as effective and moderately low-cost fillers. Carbon black is an electrical conductor and its resistivity is in the range of 10^{-2} to 10 Ω-cm depends on the size and the shape of particles. Carbon black is widely used because it is less expensive and lighter than metallic particles. Due to its dominant advantages, it can replace the metal as the conducting fillers. It imparts good conductivity to polymers and is consequently used at low concentrations in the manufacture of conducting compounds. In some cases, the addition of fillers may deteriorate the mechanical properties of polymer, using the lowest possible filler concentration offers advantage.

Carbon black is usually produced by incomplete combustion of hydrocarbon vapors. It has generally been preferred for the addition of particulate fillers in the conducting polymer composites because it is a compatible material, mixing in, and adhering to, the matrix rather well, it does not change the overall density very much. Traditional carbon black particle is a small spherically shaped and non-discrete component of an aggregate. The model we use is a highly graphitized carbon black particle in hollow polyhedron shape as shown in Figure 1.4. It is separable from the aggregate only by fracturing, but are generally fused into aggregates in an early stage of formation.

One of the useful and interesting property of the carbon black is that it exhibit a negative temperature coefficient (NTC). Thus, any discontinuities in resistivity with

temperature of carbon black filled polymers are mainly due to transitions in the polymer phase. For nonporous carbon black, the particle size is a major property affecting resistivity. However, there is a general trend toward higher resistivity with increasing particle size [Aminabhavi *et al.*, 1990]. Since there is a small difference in the thermal expansion coefficient (TEC) of carbon black and it does a very small contribution in the resistivity change upon temperature increase.
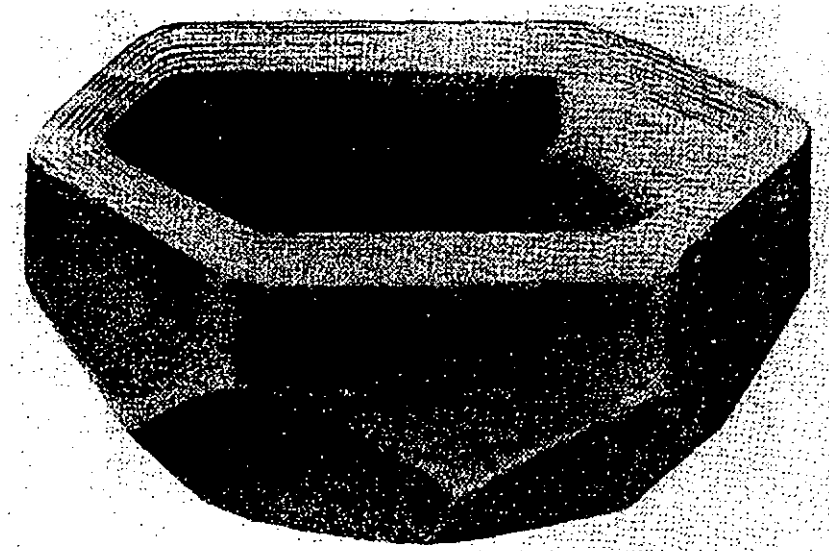
Figure 1.4   Model of highly graphitized carbon black particle
[William, 1993]

However, the use of a particular carbon black depends many factors [Probst, 1993]: (1) the ability of the polymer to accept a certain carbon black concentration, (2) the critical volume fraction at which the electrical percolation occurs, (3) processability of the final composite, (4) the overall mechanical property balance achieved at the desired conductivity level. We will consider in the electrical behavior and the thermal behavior of the carbon black filled LCP composites.

The carbon black used in this work is provided by 廣東開平市南方化工染料有限公司 with the trade name 華光導電炭黑. The resistivity of this kind of CB is 0.33 Ω-cm at room temperature and the particle size is approximately 33 nm which is correlated to the size of primary structure. The density is about 1.9 g/cm, while the surface area is 1080 m^2/g and the PH value is 6.5.

2 Theory Aspects

2.1 Electrical Conduction in Carbon Blacks Composites

With regard to the reviews on the conduction mechanism on carbon black/polymer composites in the section 1.2, various mechanisms have been proposed by various authors. Sherman *et al.* [Sherman *et al.*, 1983], proposed two important processes (tunneling and percolation) which were used to explain electron transport in conductor-filled polymers. Below the percolation threshold, tunneling is dominant, while percolation theory is suitable for near percolation threshold. There is a sudden drop in resistivity at this critical filler volume fraction. But percolation theory is limited when the filler concentration is far from the percolation threshold. Thus, an effective medium theory is employed to explain the conduction of high volume fraction of conducting fillers.

2.1.1 Tunneling Effect

Tunneling is a quantum mechanical process in which the wave function of the electron is not confined entirely within a potential box, but has a small tail extending beyond the potential barrier. Because of the tail, a very small fraction of the electrons will penetrate the barrier and reach the next aggregate.

As shown in Figure 2.1, a simple barrier having an energy V_o above the reference level

($E=0$) and a width w. If a stream of particles that obey classical mechanics approach the

barrier from the left, no particles will be observed to the right of the barrier unless they

have a kinetic energy E greater than V_o. On the other hand, if the particles are electrons,

a fraction of the current incident on the barrier will be observed on the right-hand side

even if E is less than V_o. This is a consequence of the wave nature of the electrons.
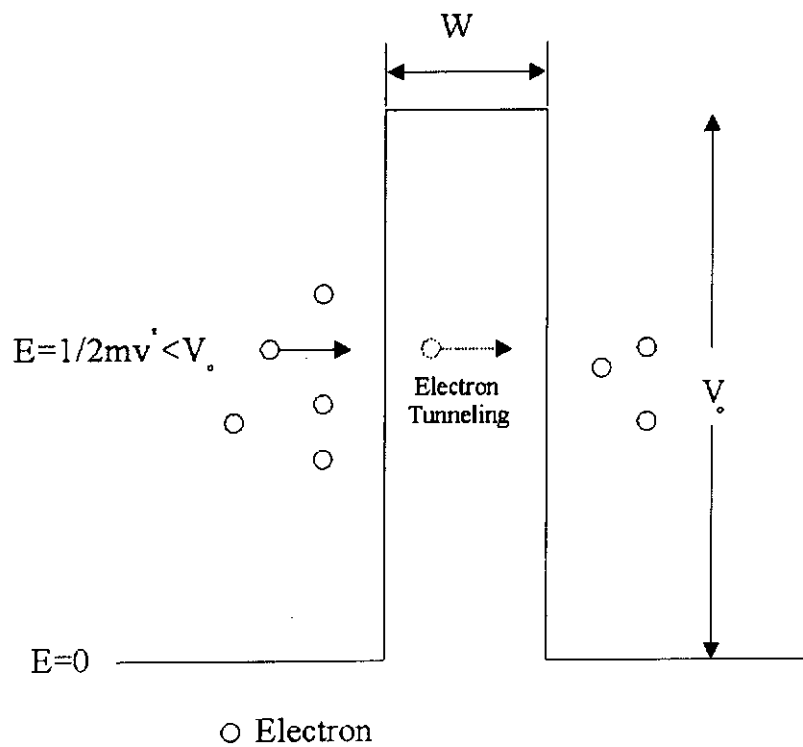
Figure 2.1   Diagram of electron tunneling: electrons with kinetic energy
             E less than potential energy barrier V_o can appear on the
             right-hand side by the process of tunneling across the width
             w between adjacent sites

There is no continuous conducting path between any pair of attached electrodes. Therefore, for the materials to exhibit finite dc conductivity, electrons hop from conductor to conductor by tunneling through the insulating barrier. Tunneling can be essentially regarded as between two bulk conductors. Consider one of the tunnel barriers in the form of a plane parallel junction of area A and separation w. The barrier potential will be taken to be symmetrical. When an electric field ε is applied to the junction, the potential barrier is both lowered and narrowed. It is shown that the tunneling current density j has the form

$$j(\varepsilon) = j_o \exp\left[-\frac{\pi\chi w}{2}\left(\frac{|\varepsilon|}{\varepsilon_o} - 1\right)^2\right], \quad |\varepsilon| < \varepsilon_o, \quad (2.1)$$

where we have neglected the small backflow current; w is the gap width, $\chi=(2mV_o/\hbar^2)^{1/2}$ is the tunneling constant, m is the electron mass, $\hbar$ is Planck's constant divided by 2π, and V_o is the potential barrier; $\varepsilon_o=4V_o/ew$ where e is the charge of an electron. j_o is the pre-exponential factor which contains all the weak (nonexponential) temperature and electric field variations of j [Sheng et al., 1978].

The tunneling current is an exponential function of the gap width; thus tunneling takes place almost exclusively between very closely neighboring carbon black aggregates, with virtually no conduction between aggregates which are separated by somewhat larger gaps (Figure 2.2).

Over a region of values of ε_o, the tunneling current is a quasi-exponential function of the electric field. Thermal fluctuations in the material give rise to voltage fluctuations

across the gap, of root mean square magnitude $(kT/C)^{1/2}$, where k is the Boltzmann

constant and C is the capacitance of the junction formed by the small regions of the

carbon black aggregates (of area A) on either side of the gap. In carbon black

composites, C is small, therefore the voltage fluctuations are of appreciable magnitude.

Now, because of the quasi-exponential dependence of j upon ε, the current is increase to

a great extent by fluctuations which increase ε by a given amount, then it is decreased

by fluctuations which decrease ε by the same amount. Thus, the net effect of the

thermally induced voltage fluctuations is to increase the conductivity.
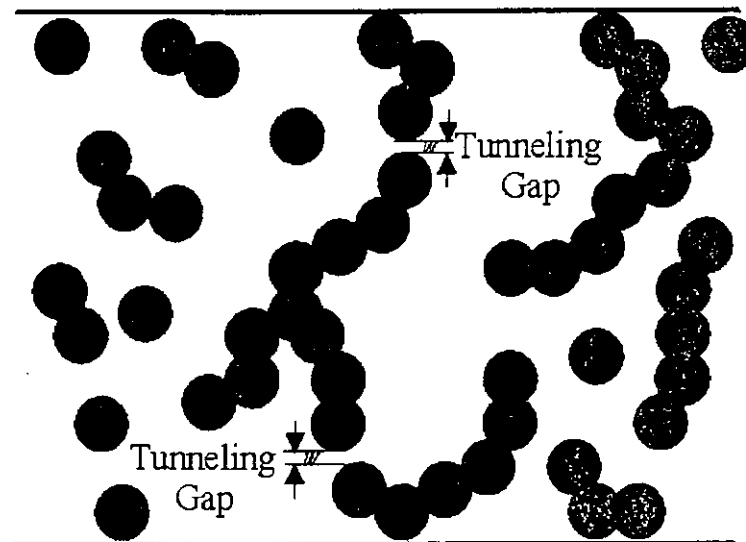
Figure 2.2   Diagram for electron tunneling between adjacent aggregates,
electron can tunnel across the gap width w

2.1.2 Percolation Theory

Percolation was first studied formally by Hammersley and Broadbent [Hammersley, 1957]. They originally dealt with the concept of the spread of hypothetical fluid particles through a random medium. The term as fluid and medium were viewed as totally general: a fluid can be liquid, vapor, heat flux, electric current, a solar system, and so on. In general, the spread of a fluid though a disordered medium involves some random elements. This model requires fluid to flow through the bonds which connect nearest neighbors in regular lattice of sites. Disorder may be introduced in a variety of ways. The most common statistical assumptions are known as the site percolation and bond percolation models. [Frisch *et al.*, 1963; Shante *et al.*, 1971].

Site and Bond Percolation

Imagine each site of the lattice to be occupied, and lines were drawn between neighboring lattice sites as shown in Figure 2.3a. Then each line can be an open bond with probability ϕ, or a closed bond with probability $(1-\phi)$. A cluster is then a group of sites connected by open bonds. When measuring the size of a cluster, one has to define whether one counts the site content or the bond content. To convey the concentration or density-dependence that is an important aspect of most phenomena, which can be modeled as site-percolation processes, connected and disconnected sites are usually referred to as filled and empty sites, respectively. The counter part of site percolation is called bond percolation as shown in Figure 2.3b [Stauffer, 1985]. For given a set of

sites, percolation theory attempts to determine the distribution of cluster sizes as a function of the bonding criterion.
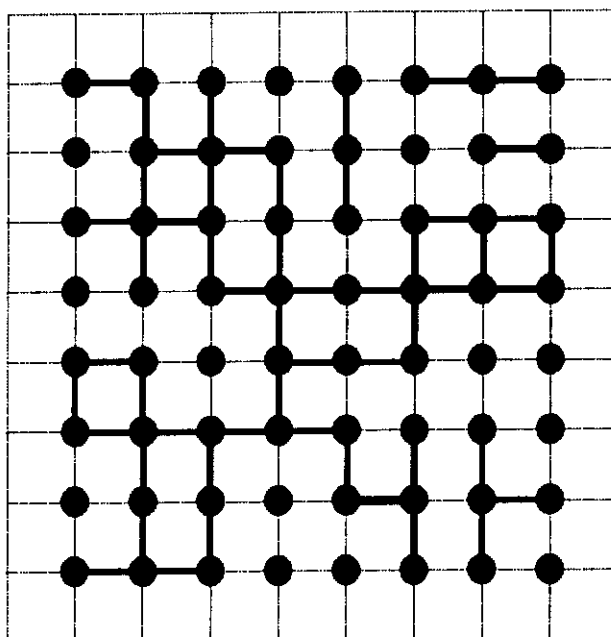
Figure 2.3a   Example of site percolation
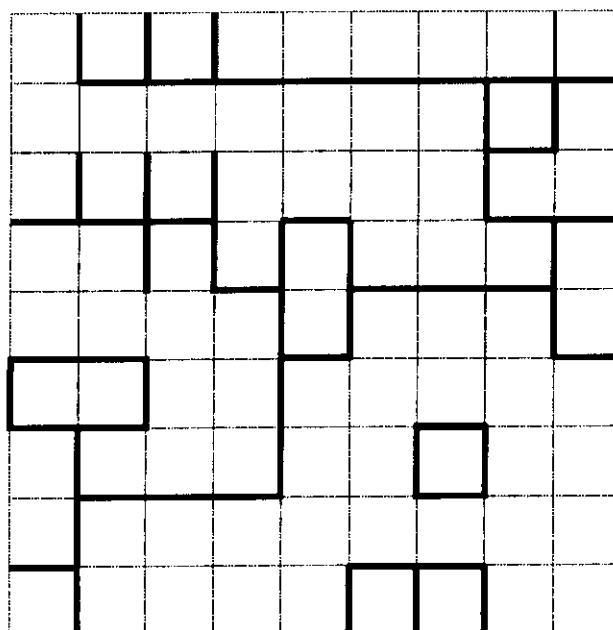
Figure 2.3b   Example of bond percolation

The percolation threshold ϕ_c is that the concentration ϕ at which an infinite network appears in an infinite lattice. For all $\phi > \phi_c$ one has a cluster extending from one side of the system to the other, whereas for all $\phi < \phi_c$ no such infinite cluster exists. Generally, above ϕ_c, the percolation path exists; below ϕ_c, it does not. From $\phi = \phi_c$ to $\phi = 1$, the percolation path fleshes out until it fills the entire lattice. Usually, the percolation threshold is defined at the probability, which is the volume fraction of conductive bonds in the random resistor network system, where an infinite cluster is formed for the first time.

Percolation Theory for the of Carbon Black/Polymers

The percolation phenomenon can be applied to the electrical conductivity of conducting polymer systems. The behavior of composites made with an insulator polymer and carbon black is quite interesting, especially the critical composition at which a dramatic resistivity change occurs, i.e., the insulative to conductive transition, is of special interest. The common explanation for such a drastic change in the resistivity with various CB concentration curves is related to the filler mode of dispersion.

As shown in Figure 2.4, for the low concentration region, the CB incorporated in the form of small particles (aggregates) of different shapes, is homogeneously distributed in the insulating matrix where adjacent CB particles are far apart, that the composite remains an effective insulator depicted as insulation region. With increasing CB concentration, larger aggregates of the CB particles are formed, in which particles are in contact. At a certain critical CB concentration, the aggregates grow to a size that makes

large scale contact possible, forming a compact nearly three-dimensional network of the

conducting phase within the polymer matrix. The first appearance of the network results

in a transition depicted by a drastic decrease in the resistivity of the mixture, which

called percolation threshold [Kirkpatrick, 1973] and the percolation region named. The

critical concentration for percolation is depended on the packing mode and conductivity

of CB. Following the initial formation of the conductive network and upon the sharp

transition completion, additional CB causes the resistivity of the mixture to gradually

further decrease because of a slight improvement of the conductive network quality. At

the end, the addition increase in CB concentration has a much small effect which

depicted as the conduction region. The resistivity then approaches monotonously the

resistivity of the conducting phase.
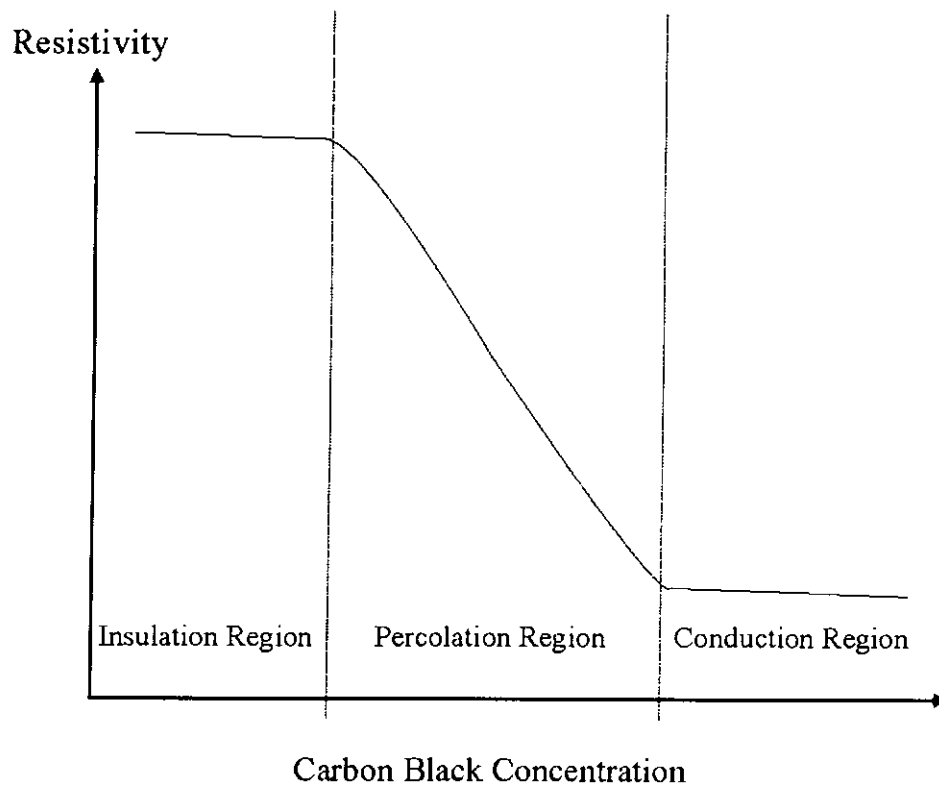
Figure 2.4   Schematic resistivity versus CB concentration
                curve for carbon black/polymer composite

In fact, in an insulating matrix containing randomly dispersed conductive particles, probability calculation predicts a sharp change in resistivity when the volume fraction of the conductive particles reaches the percolation threshold. One of the most convincing theoretical approaches to the calculation of resistivity is in terms of percolation theory. The theory of power of dependence predicts the correlation of the resistivity ρ of composites, with the volume fraction ϕ of the conductive filler [Kirkpatrick, 1973]

$$\rho = \rho_o(\phi - \phi_c)^{-\beta} \tag{2.2}$$

where ρ_o is a constant, ϕ is the volume fraction of the filler, ϕ_c is the volume fraction at percolation threshold, and β is a quantity determining the power (critical exponent) of the resistivity increase above ϕ_c.

2.2   Effective Medium Theory

Blaszkiewicz *et al.* [Blaszkiewicz *et al.*, 1992] has pointed out that the percolation equations are valid in the range near the percolation threshold with the condition that the ratio of the resistivities of the two components is infinite. This could be a problem when dealing with real systems where all components have finite resistivities. Therefore, a semi-phenomenological general effective media (GEM) [McLachlan *et al*, 1990] were proposed and applied to predict the effective or the large-volume average of electrical resistivity.

In the GEM theory, Mclachan has used two morphological parameters, the critical volume fraction and an exponent parameter in the model equation. Blaszkiewicz *et al.*, [Blaszkiewicz *et al.*, 1992], applied this model equation to a carbon black/epoxy and a graphite/epoxy composites systems. The former composite shows segregated filler distribution, the critical volume fraction is about 7 %. The latter composite has a higher critical volume and exhibit similar behaviour to a random distribution system.

The successful of the GEM theory on these two extreme composite systems encourages us on a trial model to reduce the number of free parameters in GEM to one, the critical volume fraction.

It is well-known that a Bruggeman symmetric system exhibits an evident transition behaviour. It can be verified by plotting the conductivity of the composite σ against the volume fraction ϕ according to the Bruggeman equation:

$$\phi \frac{\alpha - \sigma}{\alpha + 2\sigma} + (1 - \phi)\frac{x - \sigma}{x + 2\sigma} = 0 \qquad (2.3)$$

where α and x are the conductivities of filler and matrix respectively.

As shown in Figure 2.4, the transition occurs at a filler volume fraction of about 30 % and it can be shown that it is independent on α and x.
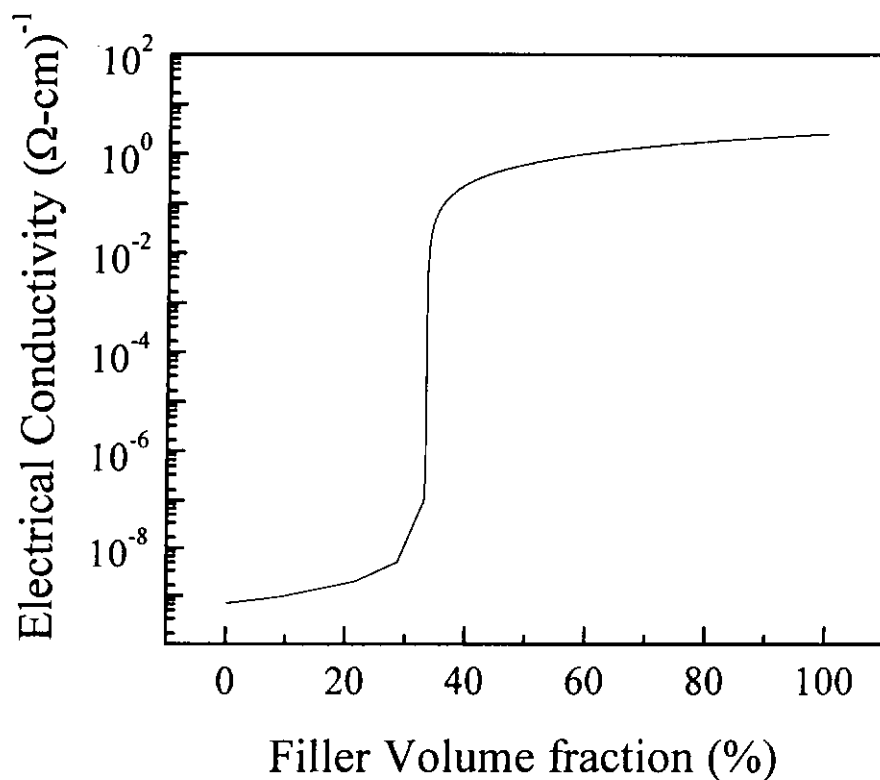
Figure 2.5   Electrical conductivity of the composite plotted against the filler volume fraction according to symmetrical Bruggeman equation 2.3

Shin *et al.* [Shin *et al.*, 1990], has proposed a scheme based on the effective medium theory (EMT) to derive a formulation for describing the dielectric property of a binary mixture, they claimed that this scheme can also be applied to the electrical conductivity of composites.

If the EMT concept is valid, equation 2.3 can be rewritten in a differential form as follow

$$[1 + (1 + k)\phi]\frac{\partial\sigma}{\partial\phi} = \frac{3x(\alpha - x)}{\alpha + 2x}\frac{\partial\sigma}{\partial x} - k\frac{3\alpha(\alpha - x)}{x + 2\alpha}\frac{\partial\sigma}{\partial\alpha} \qquad (2.4)$$

when $k = \dfrac{1}{\phi_c} - 1$ and ϕ_c is the critical volume fraction.

In a real system, it can be assumed that $\alpha \gg x$, equation 2.4 can be solved and resulted in two solutions

$$\sigma = x\left[1 - (1 + k)\phi\right]^{-\frac{3}{1+k}} \qquad (2.5)$$

$$\sigma = \alpha\left[\frac{(1 + k)\phi - 1}{k}\right]^{\frac{3k}{2(1+k)}} \qquad (2.6)$$

Equation 2.5 is valid for low volume fraction end while equation 2.6 is valid for the high volume fraction part. Both equations approach each other at $\phi = \phi_c$.

3 Sample Preparation and Characterizations

3.1 Sample Preparation

The CB/LCP sample preparation process is shown in Figure 3.1. First of all, the LCP pellets were milled into powders form in a cryogenic grinder at liquid nitrogen temperature. Before mixing with the milled LCP, carbon black powders were dried in oven at 100 °C for at least 2 hours, then they were premixed in a grinder. The mixture were blended in a ¼ inch single screw extruder (Rancastle RCP0250) with L/D=24/1 and equipped with a 1 mm conical die. The CB/LCP composites were extruded as thin rods and subsequently chopped by the pelletizer. The barrel temperature settings in zone 1, 2, 3, and 4 were 285, 285, 290 and 290 °C respectively. The screw speed is 10 to 15 rpm.

Mixing of CB & LCP	Cryogenic Grinder (with Liquid Nitrogen)
Milling of LCP	Cryogenic Grinder
Extrusion	Rancastle Single Screw Extruder
Peletization CB/LCP Composites	Pelletizer
Injection Moulding	Carver Hot Press with Stainless Steel Mould
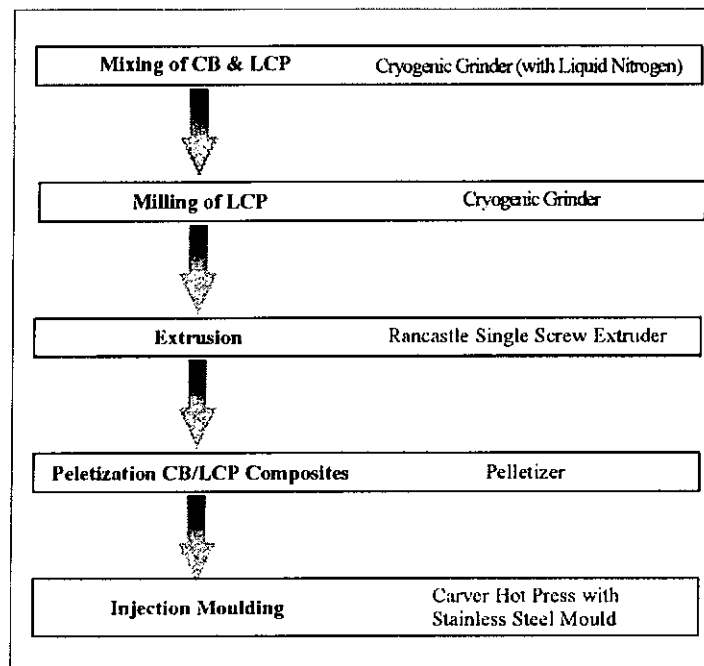
Figure 3.1   Sample preparation process

In order to prepare samples in thin film shape with specified flow of material, a special stainless steel injection tool was made. It consists of a piston and the mould with side gaps of 20 mm long and 0.2 mm thick. The pelletized CB/LCP composites were put into the mould. The mould and the composites were heated to 290 °C for 30 minutes at the hot press machine (Carver 2699) as shown in Figure 3.2. Thin film samples were obtained by pressing the molten composites rapidly into the gaps and then quenched in room temperature water.
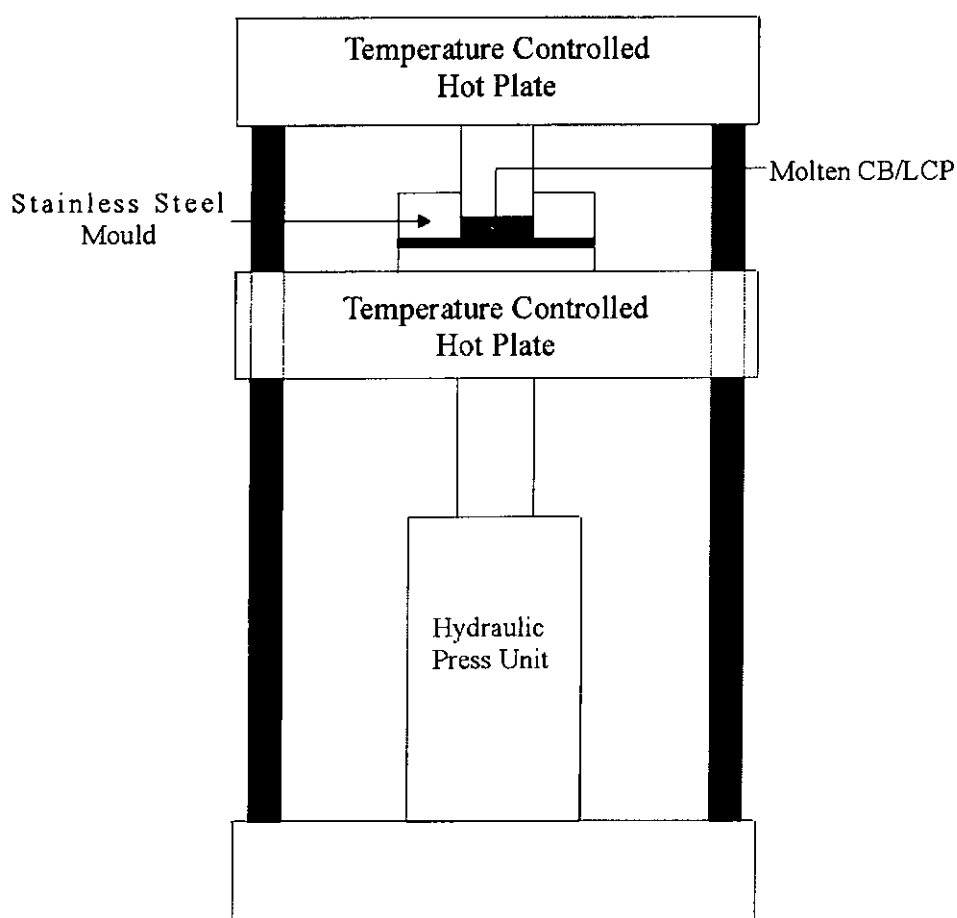
Figure 3.2   Schematic diagram of the hot press machine and stainless steel mould

The densities of pure LCP and CB were taken to be 1.4 and 1.9 g/cm^3 respectively, which were determined by the flotation method and density bottle method. The volume fraction of CB can be easily obtained from its weight fraction and the conversion are tabulated in Appendix A. The CB volume fraction of the composites varied from 1 % to 7 % in step of 1 % and 10 %.

3.2   Flotation Method

The densities (d) of the CB/LCP samples were determined by flotation method. It is a simple method to measure the density of solid. When the solid is immerged in a solution of identical density, it will neither sink or float but remain suspended.

In order to measure the density of CB/LCP samples by flotation, a solution with density equivalent to the sample was prepared. It was done by mixing two clear miscible liquids, they were dibromomethane and ethyl alcohol with densities of 2.4969 and 0.7893 g/cm^3 respectively. They were then mixed in various proportions such that the sample can suspend in the mixed solution. The density of the mixed solution were then determined by a 25 ml density bottle. The volume of the bottle was calibrated by pure water at the same temperature.

The results are tabulated in Appendix B, which are used for the determination of thermal conductivity and sheet modulus.

3.3   Specific Heat Measurement

The specific heat C_p of the samples were determined by the Differential Scanning Calorimeter (DSC) (Perkin-Elmer DSC-7). It is a power compensation type calorimeter which can be operated from -150 to 450 °C. More testing information was shown in Appendix C1.

To determine specific heat, a baseline was established by measuring the temperature difference of the two empty aluminum crucibles as the temperature is changed at a constant rate over the temperature range of interest. The scanning rate is 10 °C per minute in a nitrogen environment. Sample about 10 mg was used. Thermal response records were then acquired for a reference and a composite under identical conditions as the baseline. The specific heat, C_p, is calculated from the difference in heat flow, ΔQ, between the baseline and the sample needed to change the temperature by ΔT :

$$C_P = \frac{\Delta Q}{m\Delta T} \tag{3.1}$$

where m is the mass of the composite sample.

The results are tabulated in Appendix B, which are used for the determination of thermal conductivity.

3.4 Determination of Orientation Function by X-ray Diffraction Method

The orientation of the CB/LCP composites were determined by using X-ray diffraction method. Figure 3.3 shows the schematic diagram of Bragg's diffraction of a crystal. When X-rays irradiate on atoms in the crystal lattice, each atom scatters a small fraction of the incident beam. Thus, the reflected beams from all atoms in the crystal planes involved may interfere and the resultant reflected beam is only enhanced if the path difference from successive planes is a whole number of wavelength of the incident X-ray radiation. Thus, reinforcement only occurs for planes 1 and 2 when $BA'+CA'=n\lambda$, where n is an integer and λ is the wavelength of the X-ray. If a is the distance between plans of the atoms and θ is the angle between the X-rays beam and the crystal plane, then $BA'+CA'=2a\sin\theta$ and the reflect beam has maximum intensity when

$$2a\sin\theta = n\lambda \qquad (3.2)$$

For polymeric materials, it is generally agreed that the observed X-ray reflections arise as a result of the diffraction from the crystalline region as well as the amorphous region. Sharp and well defined diffraction peaks are attributed to the crystalline phase while the broad 'halo' is the contribution from the amorphous phase. Liquid crystalline polymer has rigid rod-like molecules, the aperiodic arrangement of the rigid-rods would result in crystal-like reflections. The half-width of these reflections gives an indication of the coherence length of the diffraction unit of about 10 monomers. The azimuthal intensity distribution of the strongest meridional reflection thus will provide information about

the orientation of the molecular chain of the polymer. If ψ is the azimnthal angle and I

is the peak intensity of the meridional reflection at the diffraction angle 2θ, then the

orientation function f can be expressed in term of the mean value of the $cos^2 \psi$ as shown

in the following equation:

$$f = \frac{1}{2}\left(3\langle\cos^2 \psi\rangle - 1\right)$$ (3.3)

and

$$\langle\cos^2 \psi\rangle = \frac{\int_0^{\pi/2} I(\psi)\cos^2 \psi \sin\psi d\psi}{\int_0^{\pi/2} I(\psi)\sin\psi d\psi}$$ (3.4)

As shown in Figure 3.4, the azimnthal angle is defined as the angle between the

direction of the liquid crystalline phase and the flow direction of the sample. For perfect

orientation in the fiber direction (perfect alignment), $f=1$, and complete random

orientation ($<cos^2 \psi>=1/3$) and hence $f=0$.

●   Lattice Point

Figure 3.3   Schematic diagram of X-ray diffraction of a crystal

In our experiment, we have used the Philips Xpert diffractometer equipped with

a pole figure attachment. The CuKα radiation of $\lambda=0.154$ nm was applied to record the

meridional scan profile of the sample. A meridional peak of the LCP at $2\theta=44.5^{\circ}$ was

used to monitor the intensity distribution at various azimuthal angle.
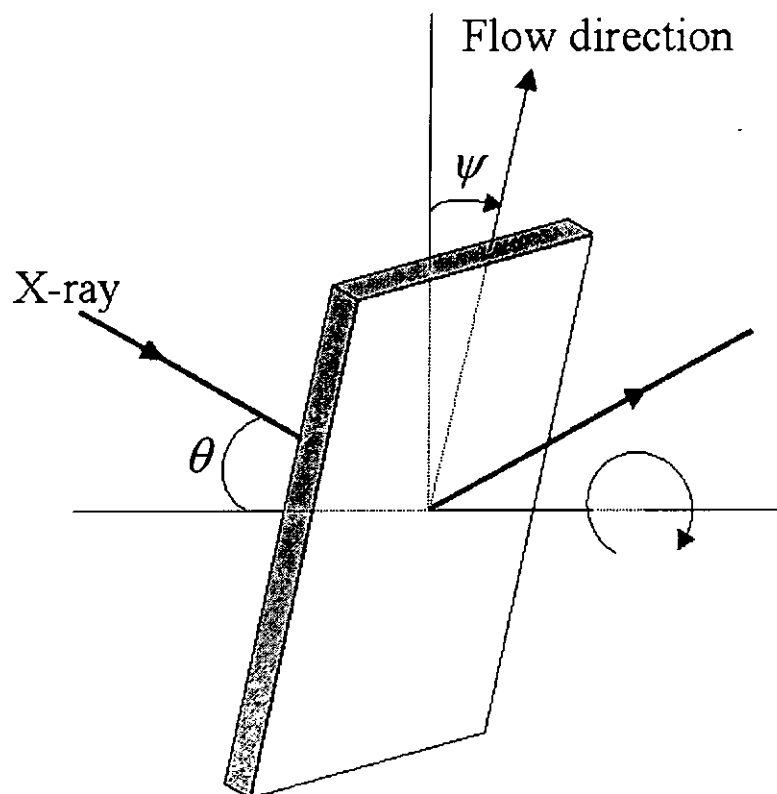
Figure 3.4   Schematic diagram for orientation determination

3.5   Surface Morphology

The surface morphology of CB/LCP composites was observed by the Nikon Microphot FXA optical microscope (OM). Film shape samples with 0.2 mm thickness from injection moulding were polished flatten prior to viewing through a pair of polarizers. They were rotated with respect to each other until the CB clusters in the surface can be seen under the magnification of 400.

Scanning electron microscope (SEM) (Cambridge Stereoscan 250 Mk 2) was also used for the observation of surface morphology. In order to have better image about the CB particles dispersed in the LCP, sample surfaces were polished with 6 microns and then 1 microns diamond plates. The samples were then gold coated so that the sample surfaces become more conductive to prevent any charge accumulation.

3.6   Thermal Expansivity

The volume expansivity α (or expansivity in short) is defined by the following equation [Choy, 1998]:

$$\alpha = V^{-1}\left(\frac{\partial V}{\partial T}\right)_P = \left(\frac{\partial \ln V}{\partial T}\right)_P \tag{3.5}$$

where V is volume, T is temperature and P is pressure. Similarly linear isobaric expansivity, can be defined by

$$\alpha_L = l^{-1}\left(\frac{\partial l}{\partial T}\right)_P \tag{3.6}$$

where l is the length of the sample. For cubic and isotropic solids to the first approximation, α and α_L are related by the following equation:

$$\alpha = 3\alpha_L \tag{3.7}$$

The expansivity of solids mainly depends on the strength of interaction between its constituent atoms or molecules. For polymers in which the molecular chains are held together by weak van der Waals forces, the thermal expansivity is larger compare with the covalently bonded solid like carbon.

The thermal expansivity was determined by measuring the extension of the thin film CB/LCP composites at various temperature using the Thermal Mechanical Analyzer (Perkin-Elmer TMA-7). The block diagram of TMA-7 is shown in Figure 3.5. It consisted of a highly sensitive linear variable differential transformer (LVDT) capable

of detecting displacements of the order of nanometers. Expansion of the samples in temperature controlled chamber was transmitted to the LVDT by a quartz probe, thus any minute expansion or contraction of the samples could be detected. In the TMA measurement, the probe in contact with the sample is under a predetermined constant load (100 mN). Any change in displacement of the probe is recorded as a function of temperature. A thermocouple which is used to monitor the sample temperature is placed in proximity of the sample. A computer was linked to the TMA for data acquisition and temperature controlling. The temperature of the chamber could be stabilized at ± 0.2 °C. Samples were measured in the flow and transverse directions at the temperature range of 20 to 200 °C with a heating rate 10 °C per minute. More testing information was shown in Appendix C2. Before the measurement, samples in the two directions were slightly polished to make the both surfaces flat and parallel to the quartz probe.
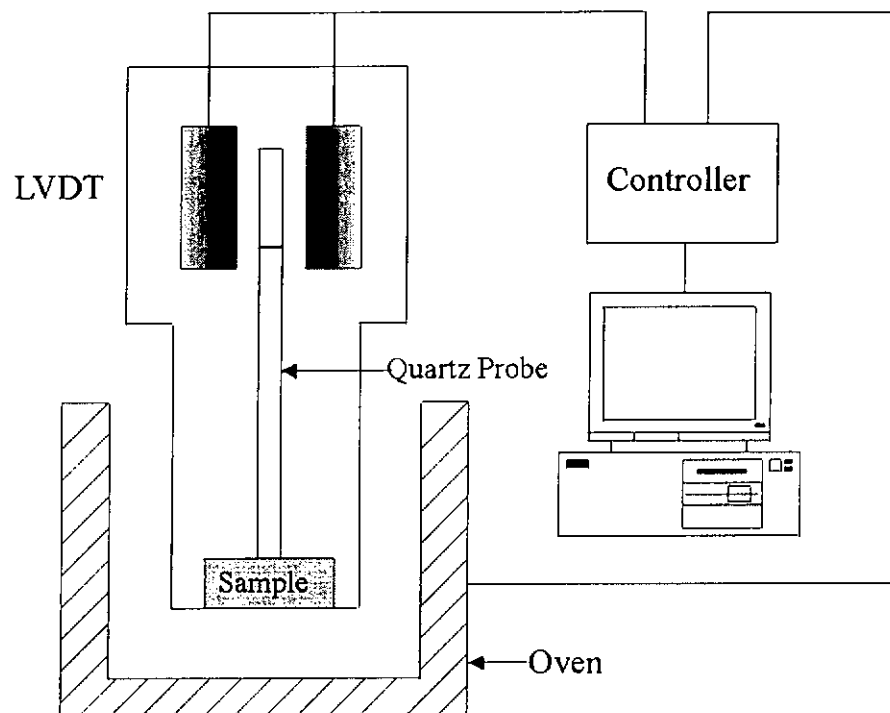
Figure 3.5   Schematic diagram of TMA for thermal expansivity measurement

3.7   Results and Discussion

Orientation of CB/LCP Composites

The orientation of the CB/LCP composites was investigated by Wide-Angle X-ray (WAX) diffraction. The peak intensity of the meridional diffraction $2\theta=44.5^\circ$ was used for the characterization of molecular ordering in terms of Hermans orientation function which may be interpreted as the spread on the mean molecular orientation averaged over the thickness of the samples. The X-ray diffraction pattern of pure LCP and 10 % CB/LCP composite are shown in Figure 3.6a and b respectively. ψ is the azimuthal angle of the sample measured with respect to the flow direction.

For the pure LCP, the X-ray peak intensities decrease as the ψ angle increase. On the contrary, the X-ray peak intensities of 10 % CB/LCP composite almost unchange in the whole range of ψ. These two graphs represent two extreme samples. It is evident that pure LCP has relative higher degree of molecular orientation while the high CB volume fraction sample has very low degree of molecular orientation. It seems that CB weakens the LCP molecular chain alignment and causes the disordering in the composites.
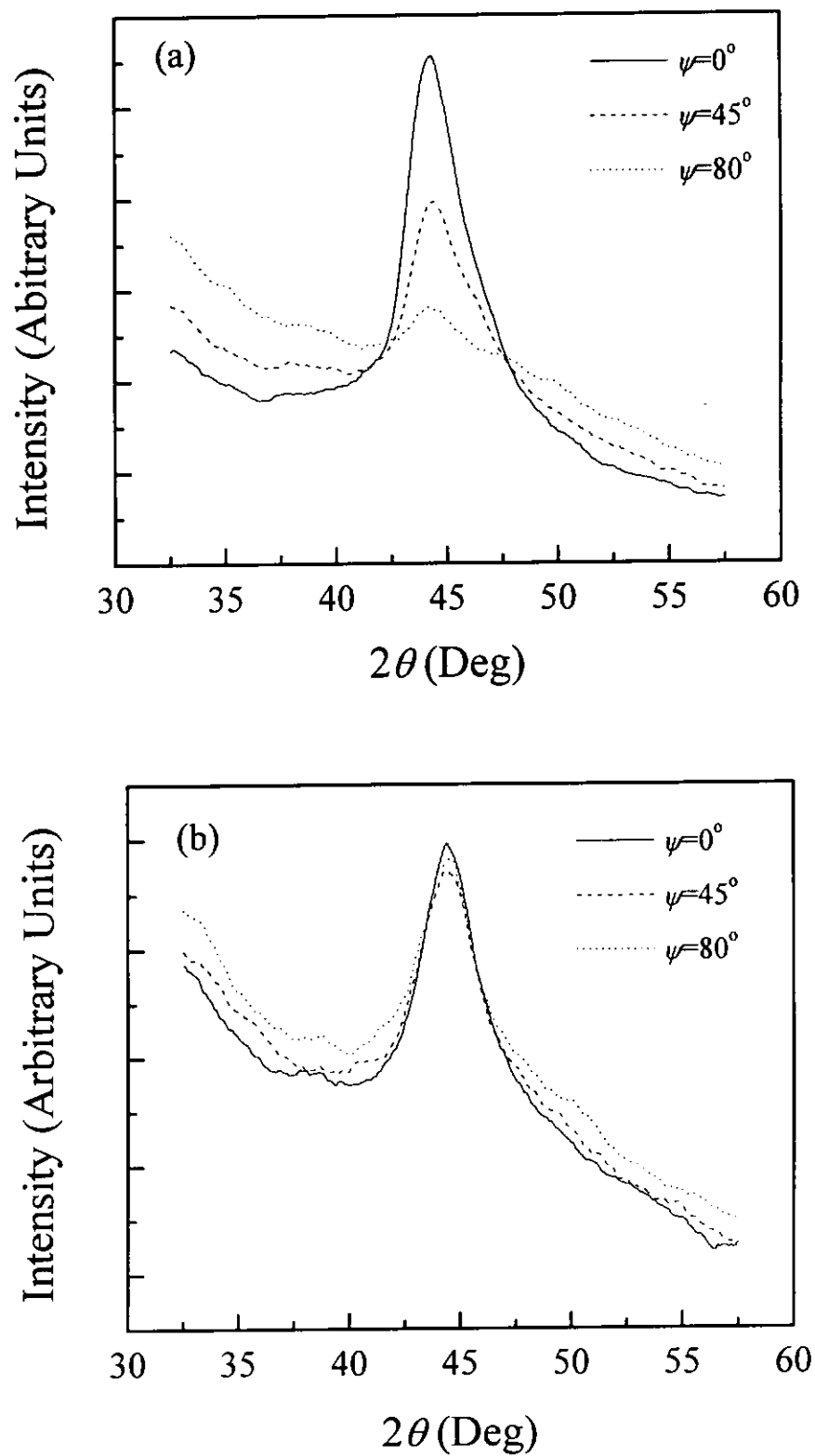
Figure 3.6   The θ-2θ scan diffraction profiles of (a) pure LCP and
(b) 10 % CB/LCP composite at various azimuthal angle

Figure 3.7 depicts the orientation function calculated from equation 3.3 for different CB

volume fraction (data were tabulated in Appendix D). The orientation function

decreases rapidly at 1 % CB/LCP sample and then decreases gradually at higher CB

volume fraction. It is quite obvious that the CB clusters is a hindrance to the LCP

molecular alignment, the more CB clusters, the poorer the alignment. The CB/LCP

sample losses its anisotropy completely at high CB volume fraction.
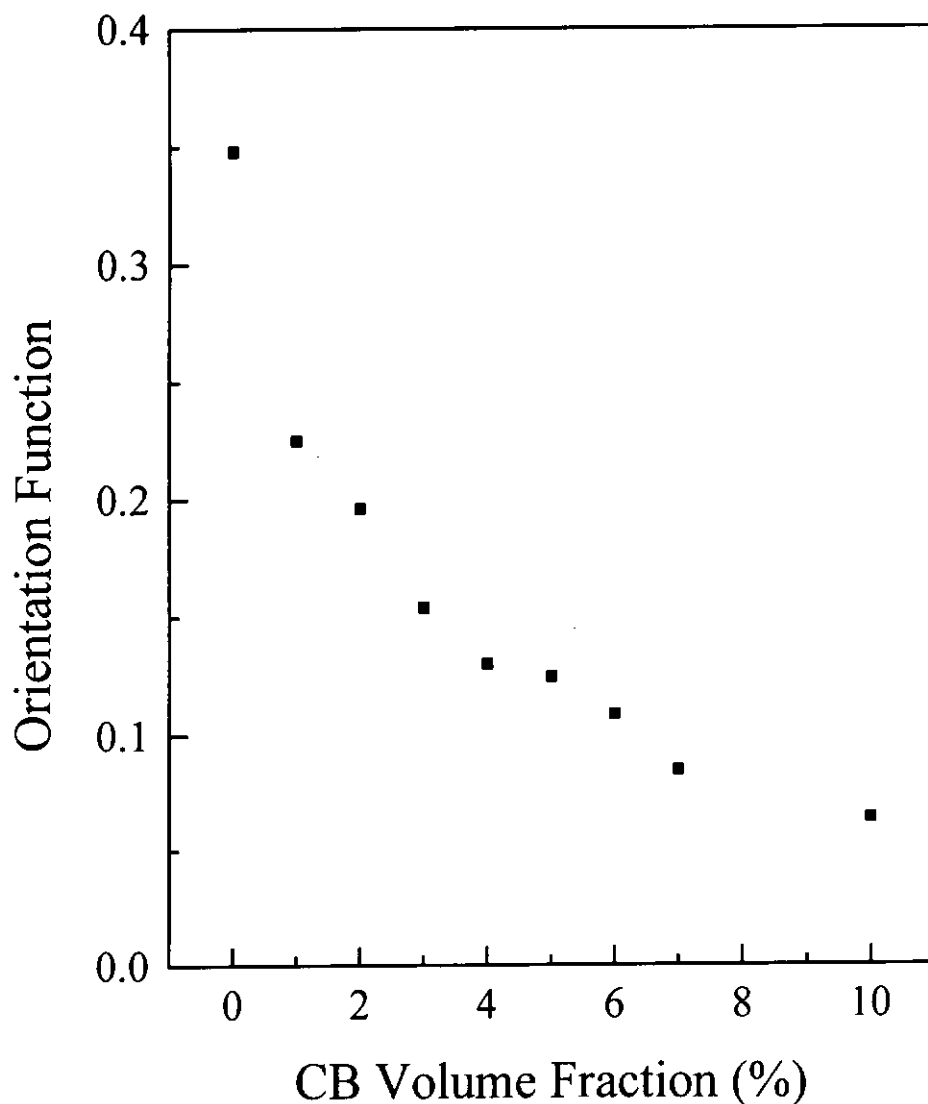
Figure 3.7   Orientation function versus volume fraction of CB

In the traditional injection of the flat plated mould process, pure LCP or LCP blends with thermoplastics are strongly aligned along the flow and highly depends on the flow rate. It also exhibits skin-core effect in the sample and has higher molecular ordering and the orientation function is close to unity [Xu et. al., 1996]. But the filling of CB in the LCP matrix may retard the formation LCP fibrils and making the LCP molecules aligned randomly.

Surface Morphology

The CB clusters distributed in the sample can be observed by a polarizing optical microscope. As shown from Figure 3.8a to Figure 3.8i, the photomicrographs of the series of composites clearly illustrate a continuous network of CB were formed at above 4 % of CB. Figure 3.8a for the pure LCP shows a homogeneous matrix. The discreted black spots shown in Figure 3.8b for 1 % CB/LCP sample indicates the random distribution of CB clusters in the sample. As the CB volume fraction increase, the clusters of CB form larger aggregates and distribute evenly in the samples. It is evidently shown in Figure 3.8c and Figure 3.8d for 2 % and 3 % CB respectively. A definite transition is occurred at about 4 % CB, as shown in Figure 3.8e, the CB phase almost form a continuous distribution in the sample. Further increase of CB volume fraction exhibit similar surface morphology, the continuous dark area appear in the sample surface as shown in Figure 3.8f to Figure 3.8i for the higher CB volume fraction composites illustrate the formation of continuous CB networks.

Scanning electron microscopy (SEM) was also used for the observation of surface morphology. The results of 2 %, 4 %, 6 %, and 10 % CB/LCP composites were shown in Figure 3.9a to Figure 3.9d For the lower CB volume fraction, e.g. 2 %, few CB particles and clusters can be observed (Figure 3.9a). The size of clusters also is in the range from 0.1 μm to 1 μm. The 4 % micrograph (Figure 3.9b) has greater in number of the CB particles and clusters. The 6 % (Figure 3.9c) and 10 % samples (Figure 3.9d) micrographs show particles of size greater than 1 μm or larger. It indicates the aggregation of CB particles at higher CB volume fraction.

The SEM micrographs and the photomicrographs both indicate the CB can easily form aggregation in the LCP matrix. As the CB volume fraction increase, more CB clusters distributed and connected in the polymer matrix. While increasing to about 4 %, the large dark area shows the formation of continuity of CB network and larger dark area and more darkness revealed the formation of larger agglomerates at the higher CB volume fraction.

20 µm

Figure 3.8a   Pure LCP photomicrograph at 400×

20 µm
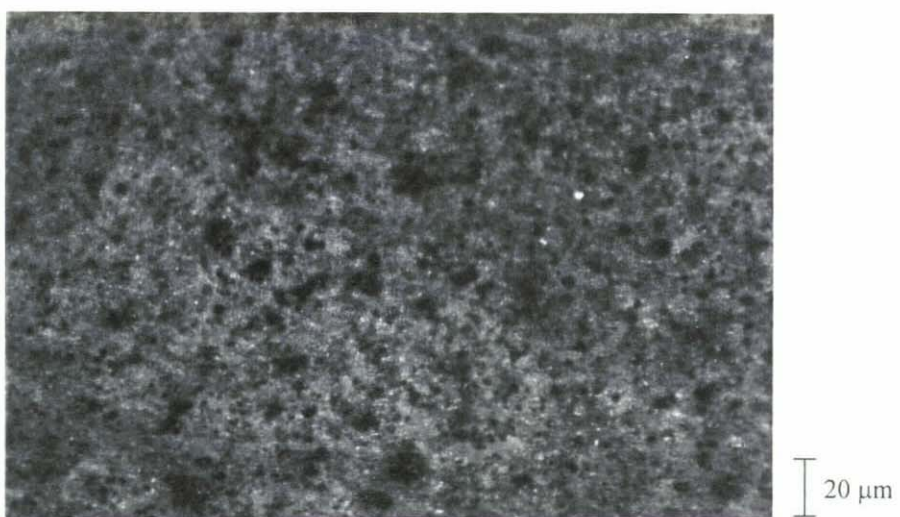
Figure 3.8b   1 % CB/LCP photomicrograph at 400×

20 µm
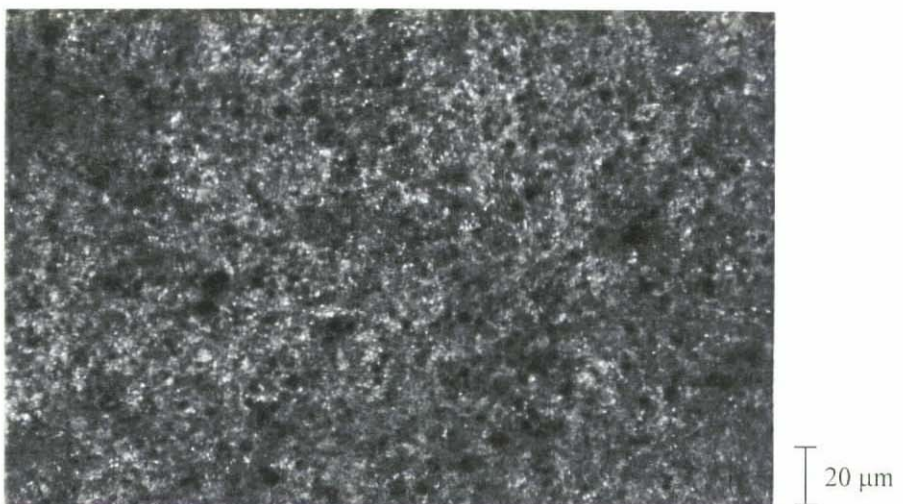
Figure 3.8c   2 % CB/LCP photomicrograph at 400×

20 μm
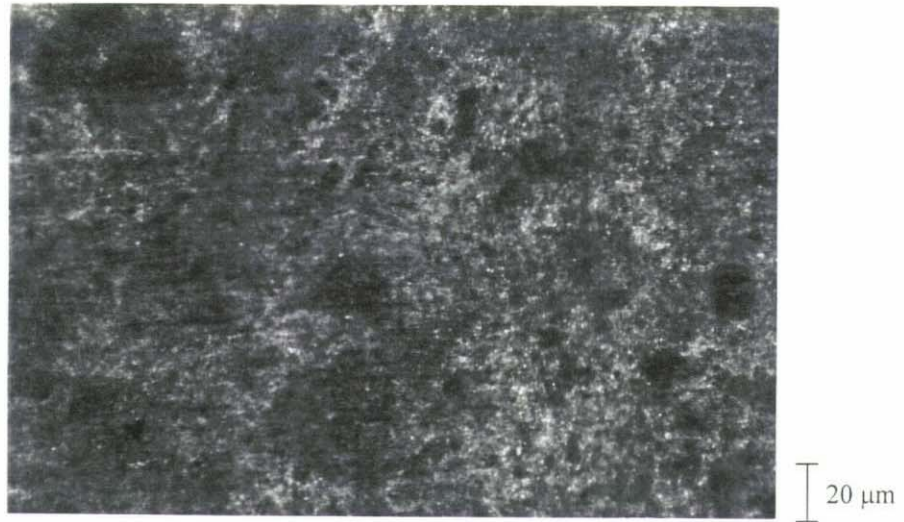
Figure 3.8d   3 % CB/LCP photomicrograph at 400×

20 μm
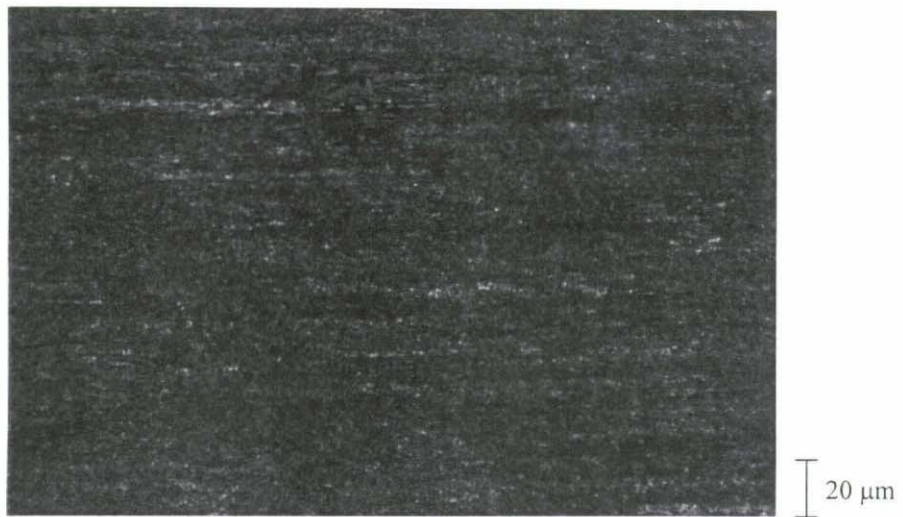
Figure 3.8e   4 % CB/LCP photomicrograph at 400×

20 μm

Figure 3.8f   5 % CB/LCP photomicrograph at 400×

20 μm

Figure 3.8g   6 % CB/LCP photomicrograph at 400×

20 μm
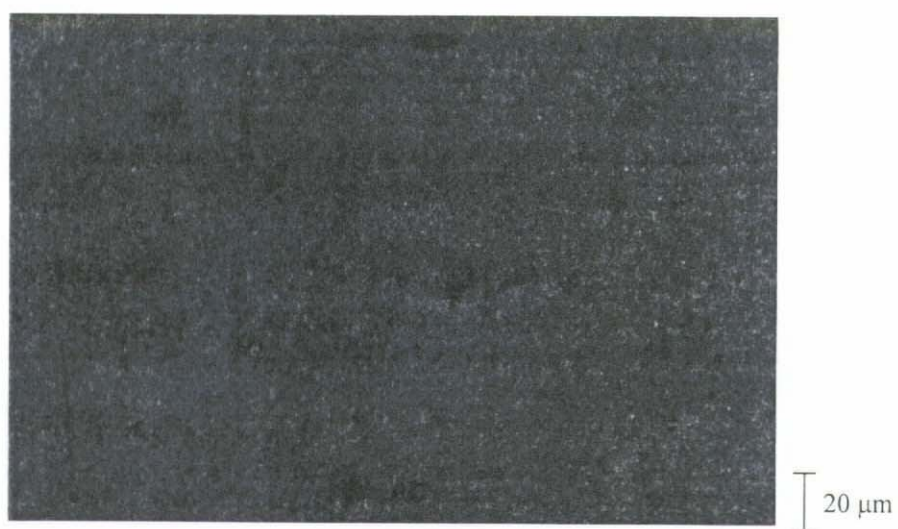
Figure 3.8h   7 % CB/LCP photomicrograph at 400×

20 μm
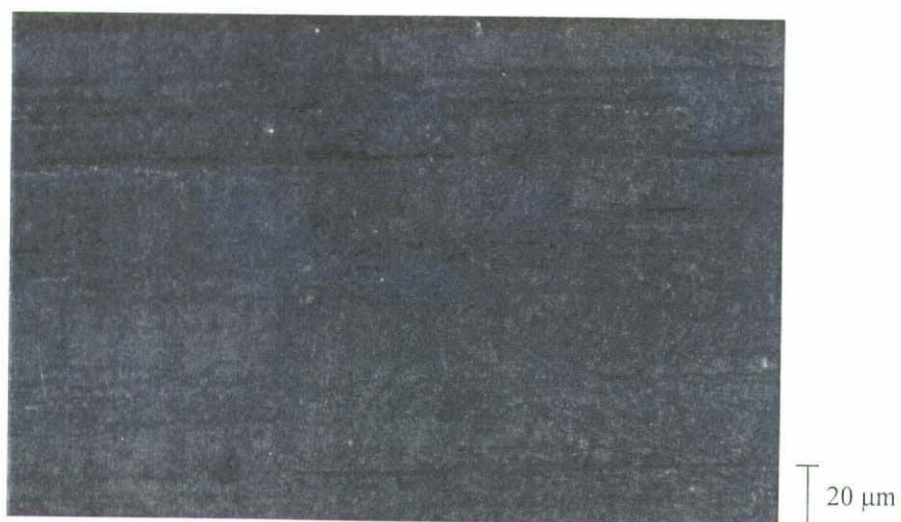
Figure 3.8i   10 % CB/LCP photomicrograph at 400×
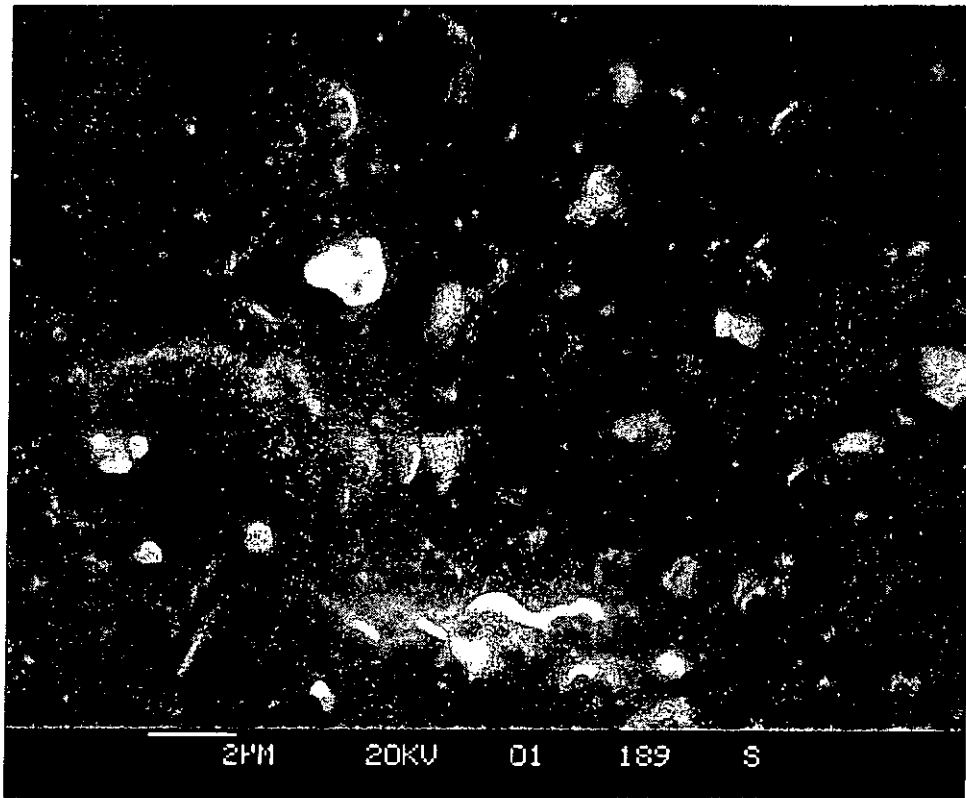
Figure 3.9a   Surface micrograph of 2 % CB/LCP composite
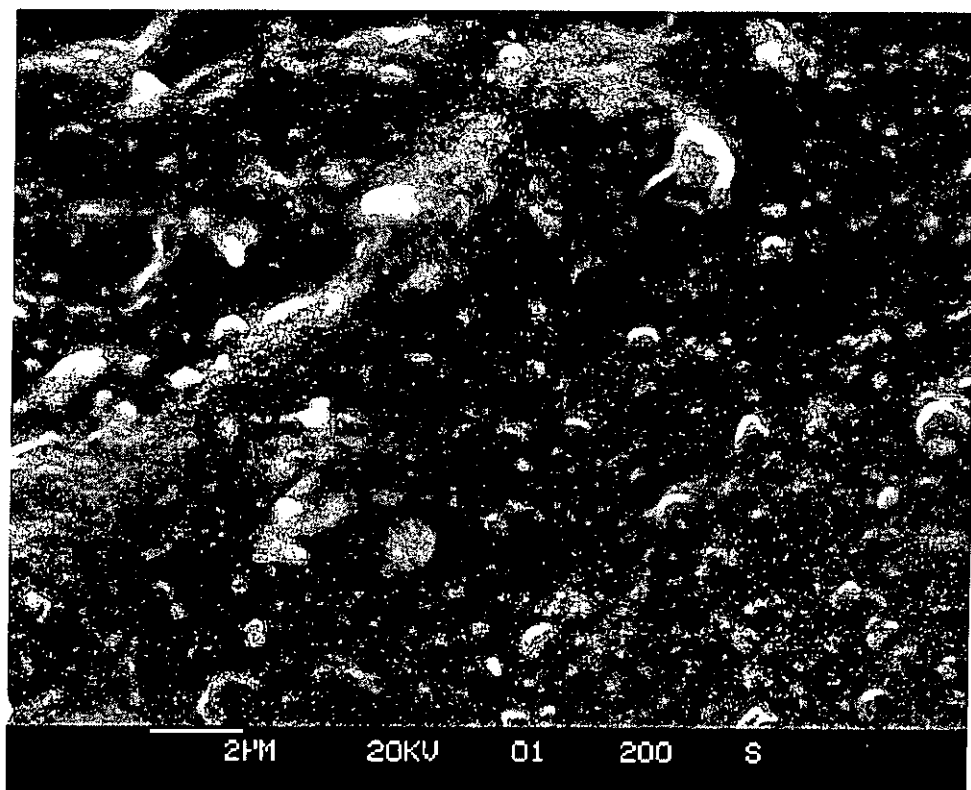
Figure 3.9b   Surface micrograph of 4 % CB/LCP composite
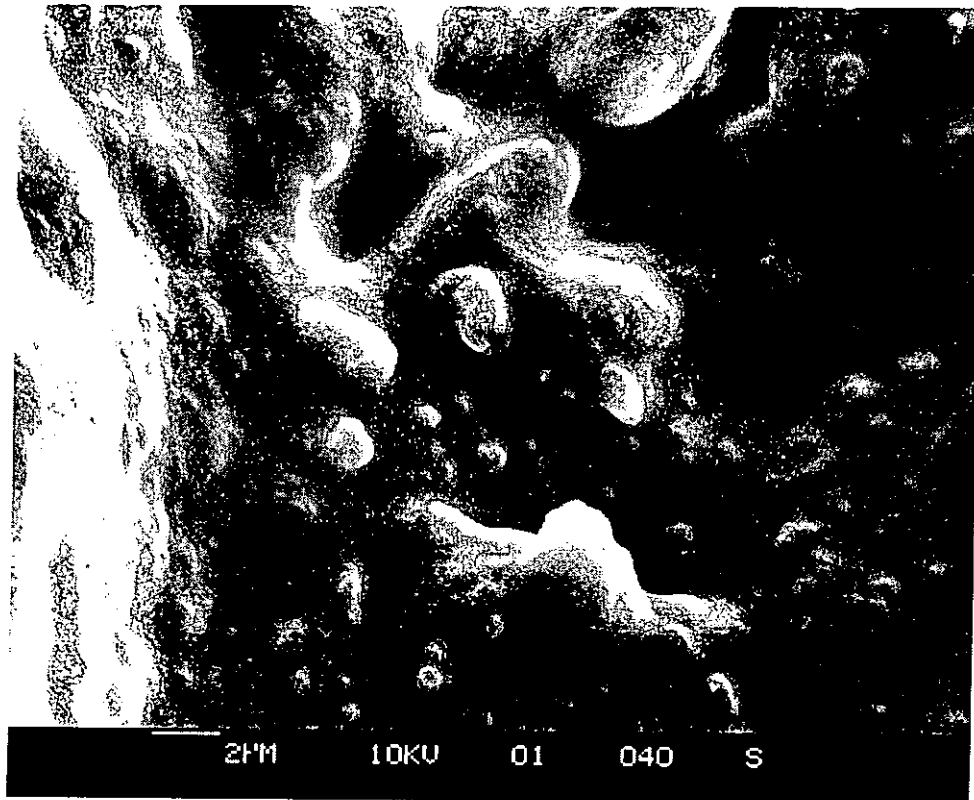
Figure 3.9c   Surface micrograph of 6 % CB/LCP composite
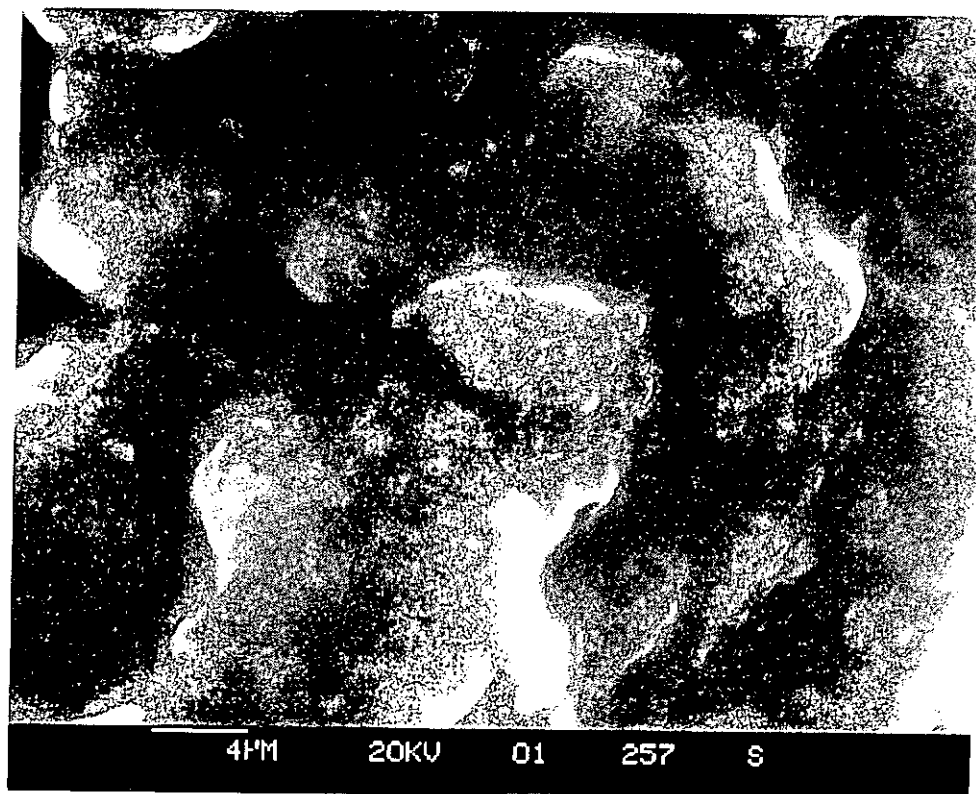
Figure 3.9d   Surface micrograph of 10 % CB/LCP composite

Thermal Expansivity

In chapter 2, we have described about the conduction mechanisms of the CB/polymer systems. In particular, the temperature dependence of the electrical resistivity would be affected significantly by the thermal expansion of the polymer matrix at elevated temperature. As the polymer matrix expands, the separation of the conducting particles will increase, on the contrary, if the matrix contract, it would squeeze the particles and push them close together. Therefore, we have measured the thermal expansion of the CB/LCP samples in both flow direction and transverse directions in order to correlate with the temperature dependence of electrical resistivity. As show in Figure 3.10a, all the samples exhibit expansion in temperature rise, but the pure LCP and low CB volume fraction samples have lower expansivity. It is more interesting to note that the pure LCP and 1 % sample exhibit slightly contraction at above 150 °C. A well aligned or highly oriented LCP contracts in the molecular chain direction [Choy, 1995]. Sine our pure LCP sample has an orientation function value of 0.35 which indicates the sample is not well aligned, thus it appears to expand. For those higher CB volume fraction samples, the orientation function even lower, therefore they expand as those linear thermoplastics.

Furthermore, the increasing slope of the thermal expansion curves as shown in Figure 3.10a reflects a certain degree of molecular chain alignment for lower CB fraction samples which do match the X-ray orientation measurement results.

The thermal expansion measurements of the composites in the transverse direction

behaviour similarly. All the samples expand as temperature rise. From the Figure 3.10b,

it can be clearly seen that the slope of the expansion curves for all volume fraction

samples are similar. It is expected that there are no preferred chain orientation in the

transverse direction.

Since all the samples have less than one millimeter (0.2 mm) in thickness, the thermal

expansion measurements in the thickness direction render no reliable results.
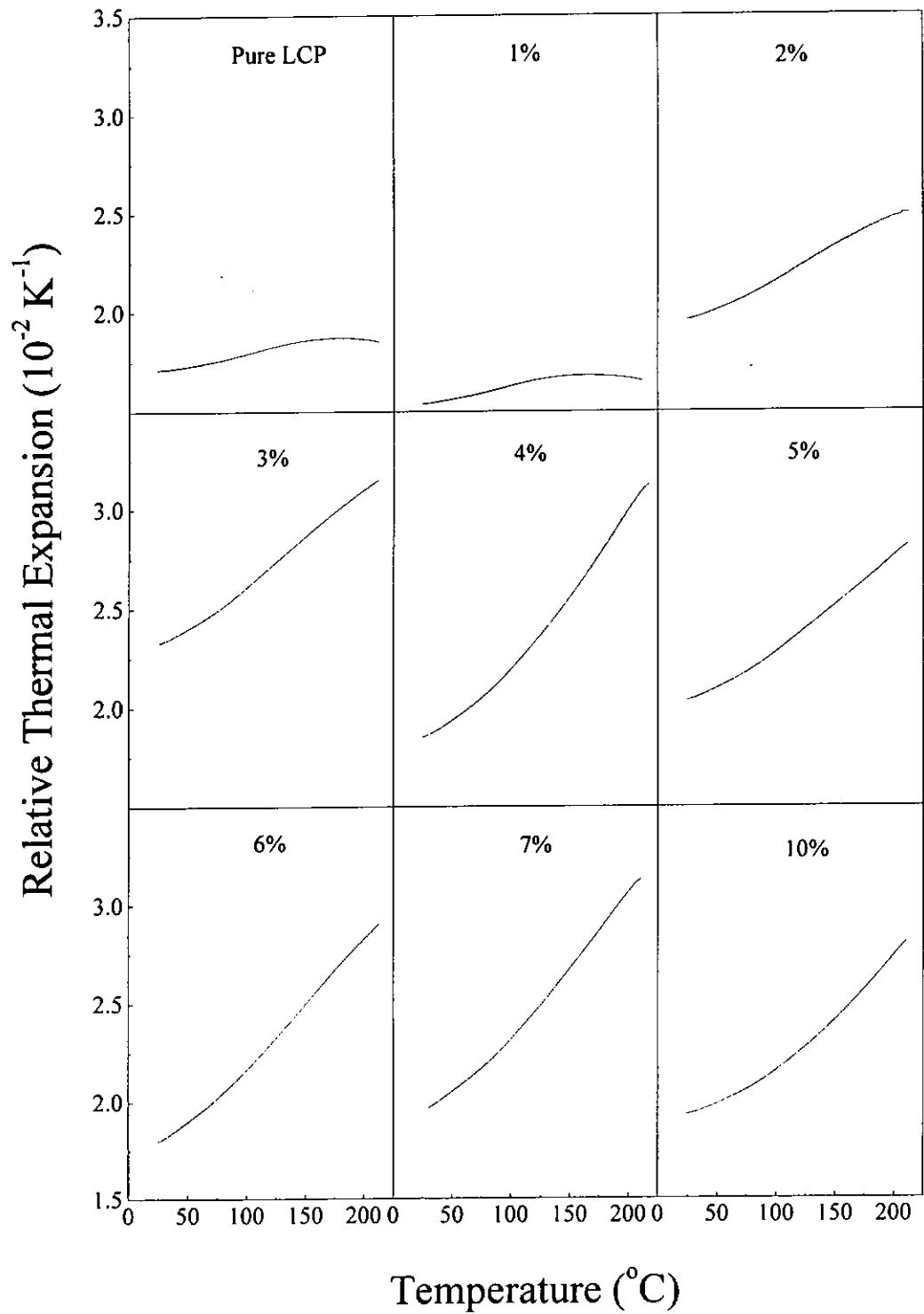
Figure 3.10a   Relative thermal expansion of CB/LCP
                      composites in the flow direction
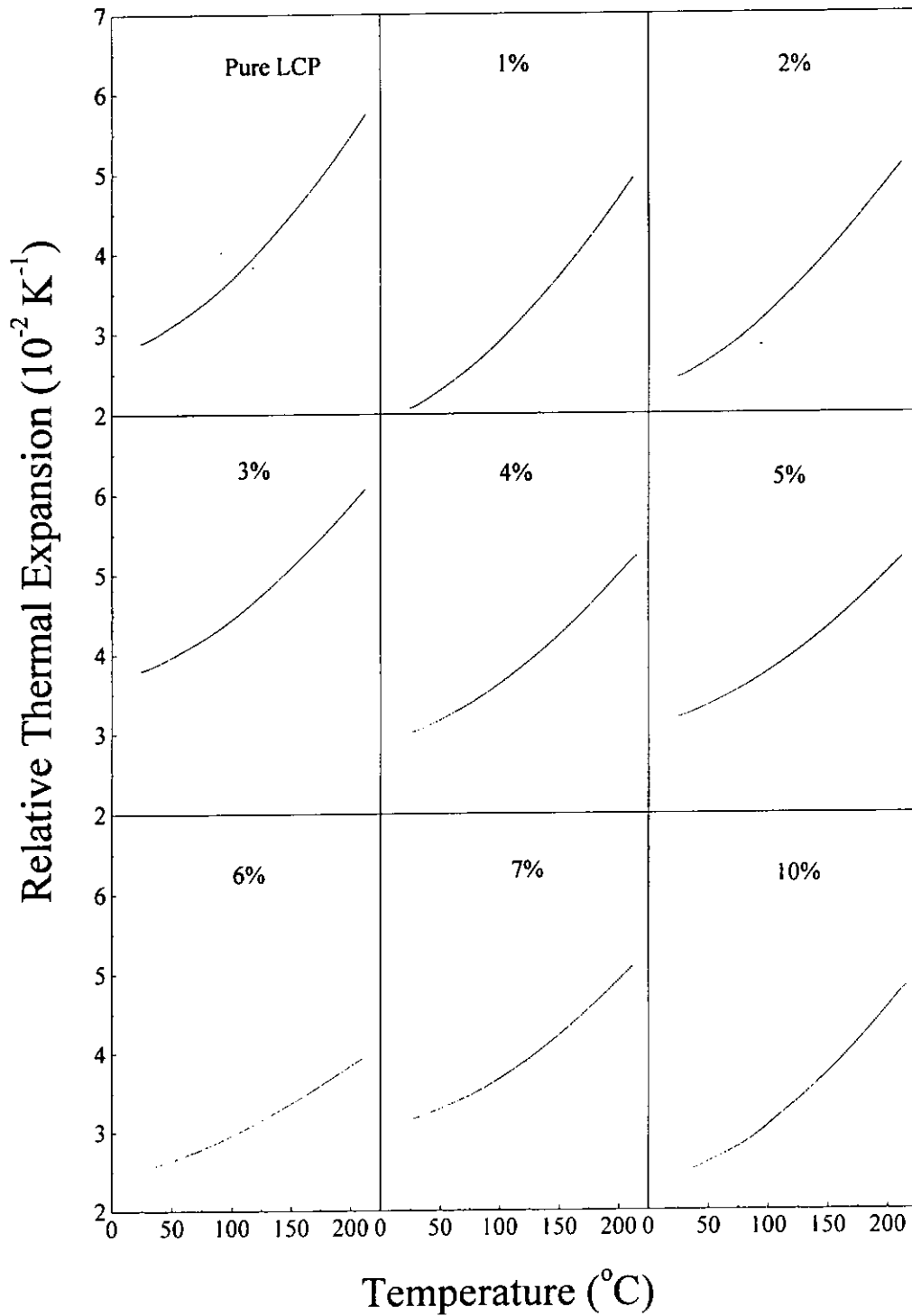
Figure 3.10b   Relative thermal expansion of CB/LCP
                      composites in the transverse direction

4 Electrical Properties

4.1 *J-E* characteristics

Current density-electric field (*J-E*) characteristics of CB/LCP composites were measured at room temperature. The simple circuit for this measurement was shown in Figure 4.1. In order to prevent self-heating effect, the voltage was applied momentarily about one second for each measurement. The voltage drop (V_R) across a standard resistor connected in series with the sample was recorded by a digital voltmeter (Keithley 197) so that the current through the sample can be obtained. Another multimeter is used to monitor the output voltage (V) of power supply and thus the voltage across the sample can be deduced. By normalizing the dimension of the sample, the characteristics of *J-E* can be obtained.
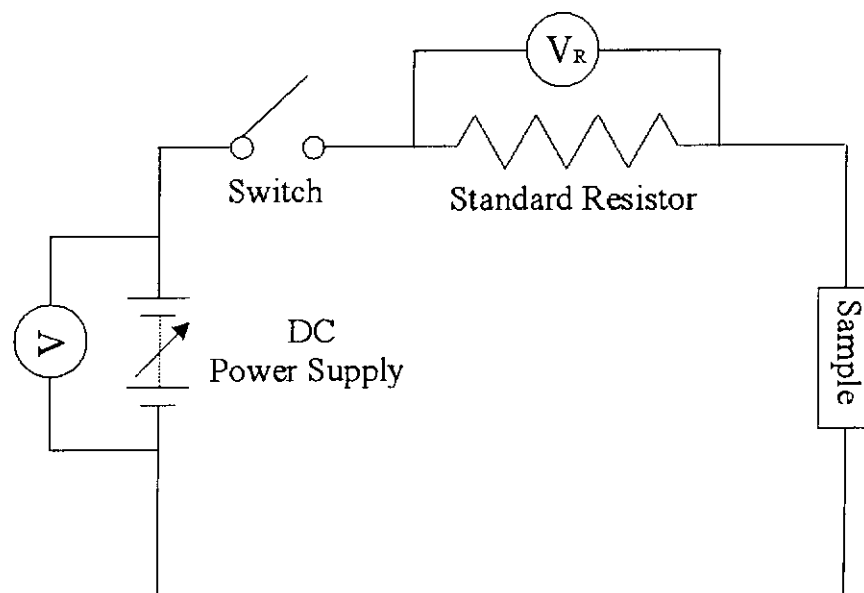
Figure 4.1   Circuit diagram for *J-E* characteristics measurement

4.2   Electrical Resistivity Measurement

We have used two different methods for the resistivity ρ measurement, i.e. the two-point and four-point method. Two-point method is particularly useful for measuring high resistivity materials. In other words, it is suitable for measuring samples of CB volume fraction below percolation threshold. Four-point method is more appropriate for measuring low resistivity samples where the electrode contact resistance may be eliminated. Therefore, it is suitable for measuring samples of CB volume fraction above percolation threshold.
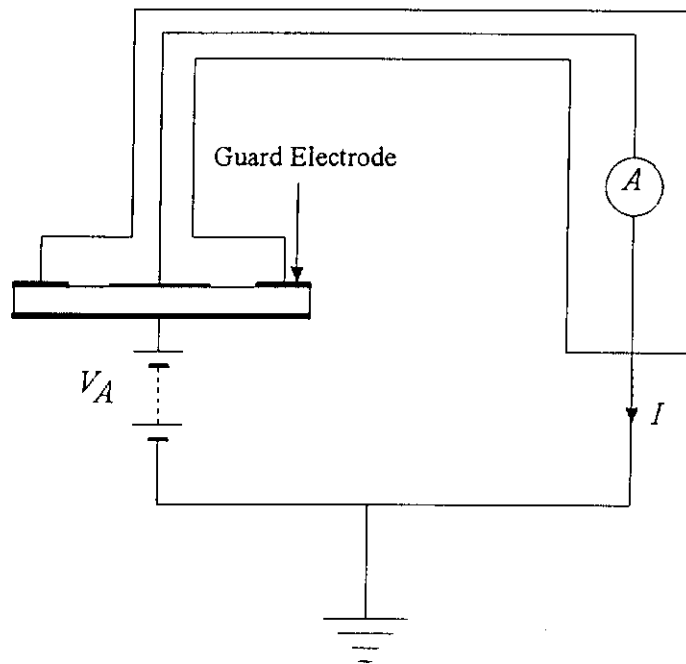
Figure 4.2   Two-point method with guarding

Two-Point Method

As shown in Figure 4.2, the electrodes were applied on the ends or two surfaces of the rectangular samples. The resistivity ρ of the sample can be calculated from the following equation [Blythe, 1979]:

$$\rho = \frac{RA}{l} \tag{4.1}$$

where R is the resistance, A and l are the cross-sectional area and the length of the sample between the electrodes respectively.
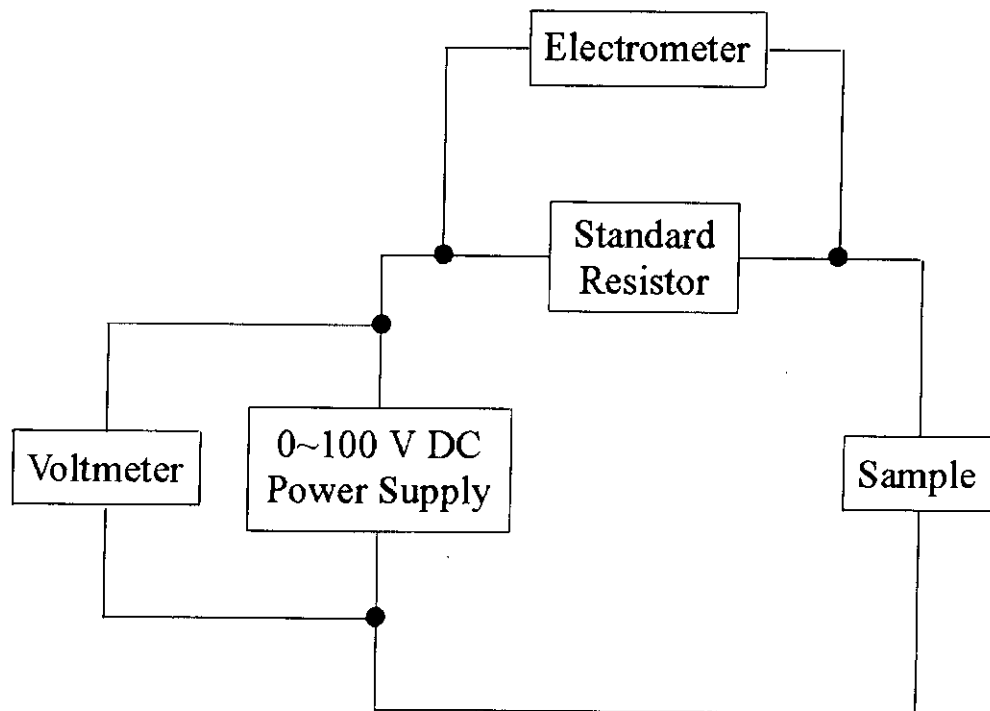
Figure 4.3   Block diagram of resistivity measurement

CB/LCP samples in the shape of sheets with dimensions 0.2 mm thick and 5 mm×5 mm were cut from the moulded piece for resistivity measurement. Silver paint was applied as electrodes. As shown in Figure 4.3, the current passing through the sample was determined from the potential difference of a standard resistor which was in series with the sample. A Keithley 197 digital multimeter was used to monitor the output voltage of a DC power supply and a Keithley 610C electrometer was used to measure the potential difference of the standard resistor. The resistance R of the sample is obtained from the equation:

$$R = \left(\frac{V}{V_S} - 1 \right) R_s \qquad (4.2)$$

where R_S is the resistance of standard resistor, V is the voltage of power supple and V_S is the potential difference across the standard resistor.

When making measurements of a high resistivity sample, the current leakage between the electrodes via routes other than the bulk volume of the sample becomes a major problem. Sample surface often provides a low resistance path through the accumulation of dirt and moisture on them. One can usually overcome the problem to a large extent by the use of an extra guarding electrode on the sample as shown in Figure 4.2. The guard is connected to earth and surrounds that electrode which is connected to the highly insulated side of the circuit. Any leakage currents over the surface of the sample are then collected by the guard electrode and are not contributed in the measured current.

Four-Point Method

Figure 4.4 shows the schematic diagram of the four-point method. A known current I is injected from electrode 1 and collected at electrode 4 through the sample, whilst the potential difference ΔV between electrodes 2 and 3 is measured. Resistivity ρ can then be obtained by the follow equation [Blythe, 1979]:

$$\rho = \frac{\Delta V \pi d}{I \ln 2} \qquad (4.3)$$

where d is the separation of electrodes.
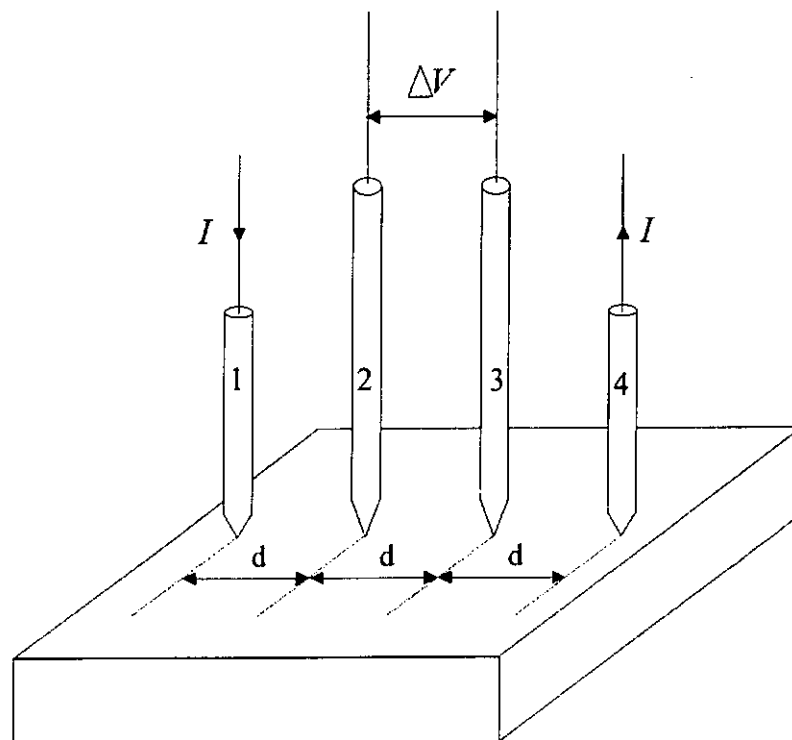
Figure 4.4   Diagram of resistivity measurement with four-point method

Four-point method measurements are very reliable and they have been used extensively for measurements on inorganic semiconductors. This technique has the advantage that the contact resistance between the electrode and the sample would not make contribution to the measurement since the voltage between probe 2 and 3 is determined by a high impedance voltmeter. The practical upper limit of resistivity that can be measured by the four-point method is about 10^6 Ω-cm.

4.3 Temperature Dependence of Resistivity Measurement

For the temperature dependence of resistivity measurement, the sample was placed in a vacuum chamber as shown in Figure 4.5. Inside the chamber, the sample is attached to a brass stage to which a heater is attached. A cover was used to maintain uniform ambient temperature around the sample. The temperature was controlled by a temperature controller (manufacturer, CAL 3200). The temperature was maintained for 5 minutes at a measuring temperature before each measurement was made to ensure that the sample was at thermal equilibrium.
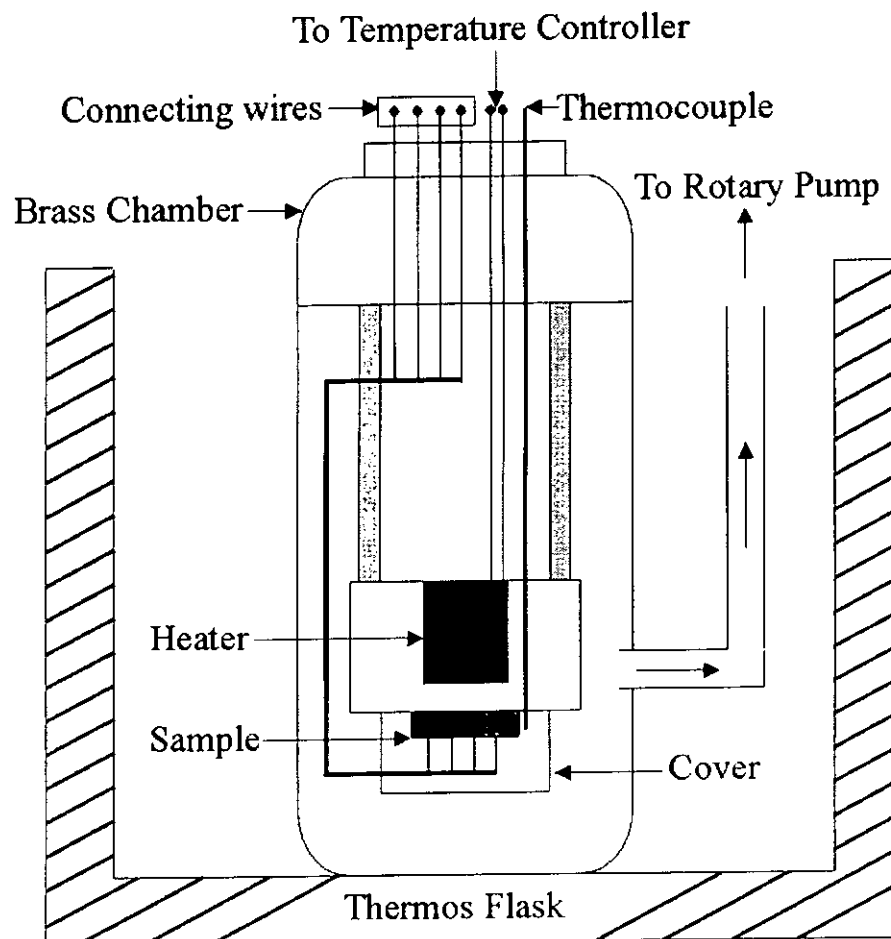
Figure 4.5   Diagram shown the arrangement of temperature dependence of resistivity measurement

A rotary pump was used to maintaine the chamber at 10^{-1} torr through out the whole experiment to prevent condensation of moisture at low temperature and reduce heat loss at high temperature.

Before the measurement, the sample was heated to 100 °C in the chamber and was kept for one hour in order to eliminate any moisture that was trapped inside the sample. The temperature was measured in 10 °C interval from room temperature to 200 °C. During the whole experiment, the sample was kept at constant voltage.

4.4   Results and Discussion

J-E Characteristics

For the current density-electric field (*J-E*) characteristics measurement, conductive silver paint was used as electrodes and adhered on both end of the sample with dimension of 5×5×0.2 mm. The results of CB/LCP samples in the flow, transverse and thickness directions were measured at room temperature and the results were shown in Figure 4.6a to Figure 4.6h. Figure 4.6a, Figure 4.6b and Figure 4.6c are the *J-E* curves for CB volume fraction of 1 %, 2 % and 3 % respectively. All of these samples in the three directions exhibit linear *J-E* relation. There are no particular trend for the three directions of the *J-E* curve intercepts in the log-log plot. In other words, there are no prefer charge transportation direction of the samples. Even though the applied electric field is high (1000 V/cm), the current densities are just few milli-ampere. It is the characteristic magnitude of an insulating polymer. It shows that the CB aggregates distributed separately in greater distance and randomly in the matrix. Mainly is the LCP matrix responsible for the electrical conduction.

In the case of 4 % CB as shown in Figure 4.6d, the current density increases several orders of magnitude at the same applied electric compared with those low CB fraction samples. It is quite obvious that the separations between the CB aggregates become close for electron tunneling across the small barrier. The tunneling effect may also be responsible for the slightly nonlinear behavior of the *J-E* characteristics.

For higher CB volume fraction samples, the 5 %, 6 %, 7 % and 10 % samples, their *J-E* curves are shown in Figure 4.6e to Figure 4.6h respectively. The current density that carried by the samples are increasing with respect to higher CB volume fraction. Due to the large current density magnitude, the CB aggregates are expected becoming large and are in contact with each other. Meanwhile, the tunneling gaps also change into ohmic contact and form the continuous conducting chains. The samples become highly conductive and current are passed directly through the carbon black aggregates that result in the linear Ohmic *J-E* behavior as depicted in the figures. Although the slopes of the *J-E* curves are different in three directions, there are no systematic variations been found between different CB volume fraction, it indicates only a sample fluctuation. Since the electrode distance is shorter in the sample thickness direction, for the same applied electric field, a shorter electrode distance produces at higher electric field.
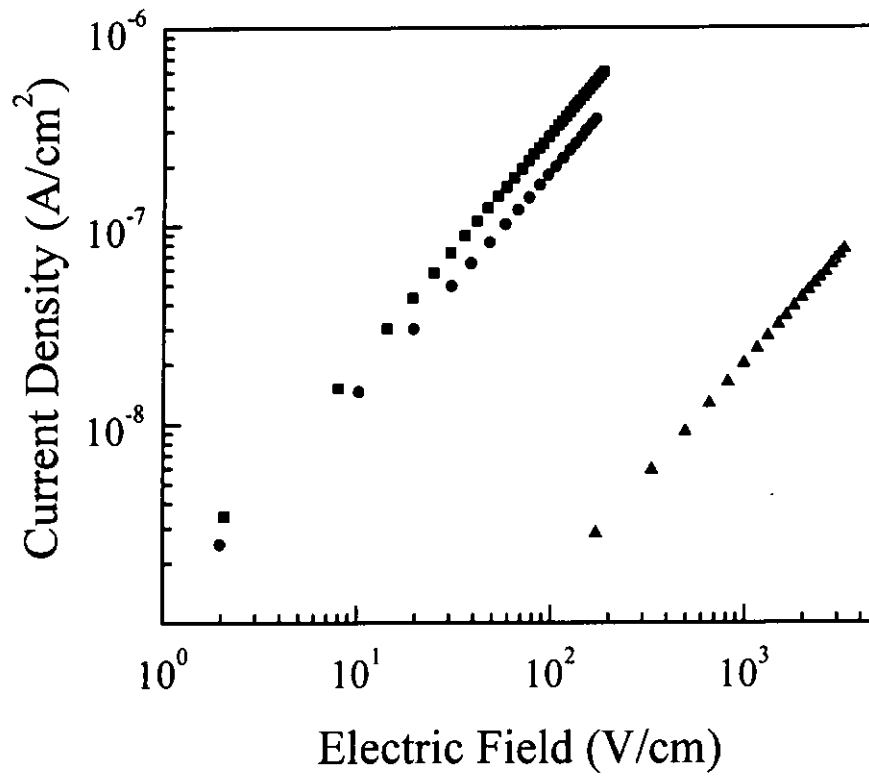
Figure 4.6a   *J-E* characteristic of 1 % CB/LCP composites in the
flow (■), transverse (●) and thickness (▲) directions
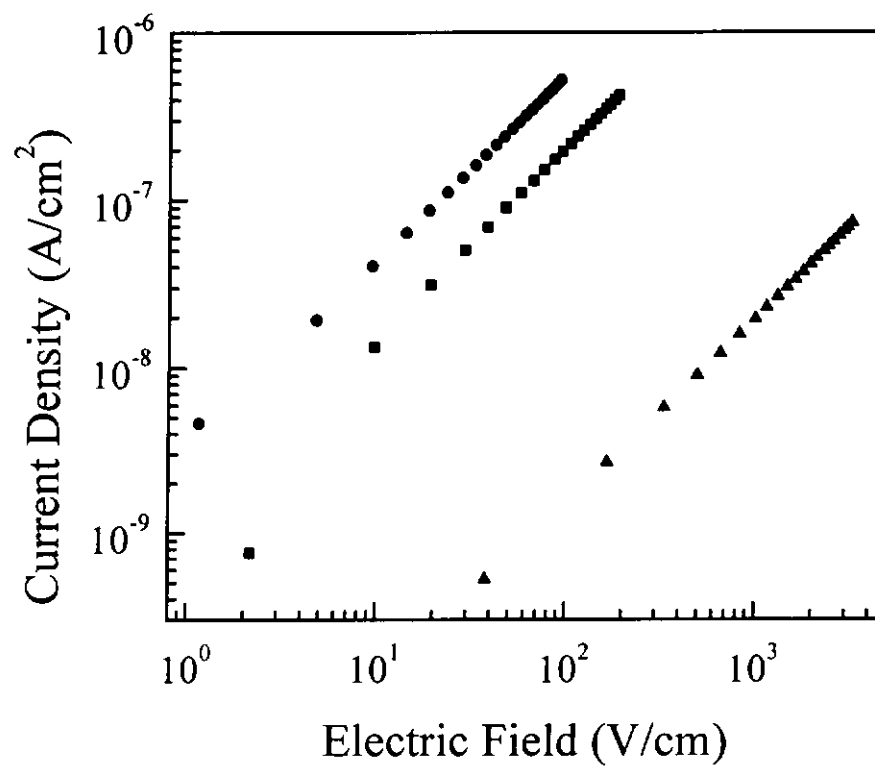
Figure 4.6b   *J-E* characteristic of 2 % CB/LCP composites in the
flow (■), transverse (●) and thickness (▲) directions
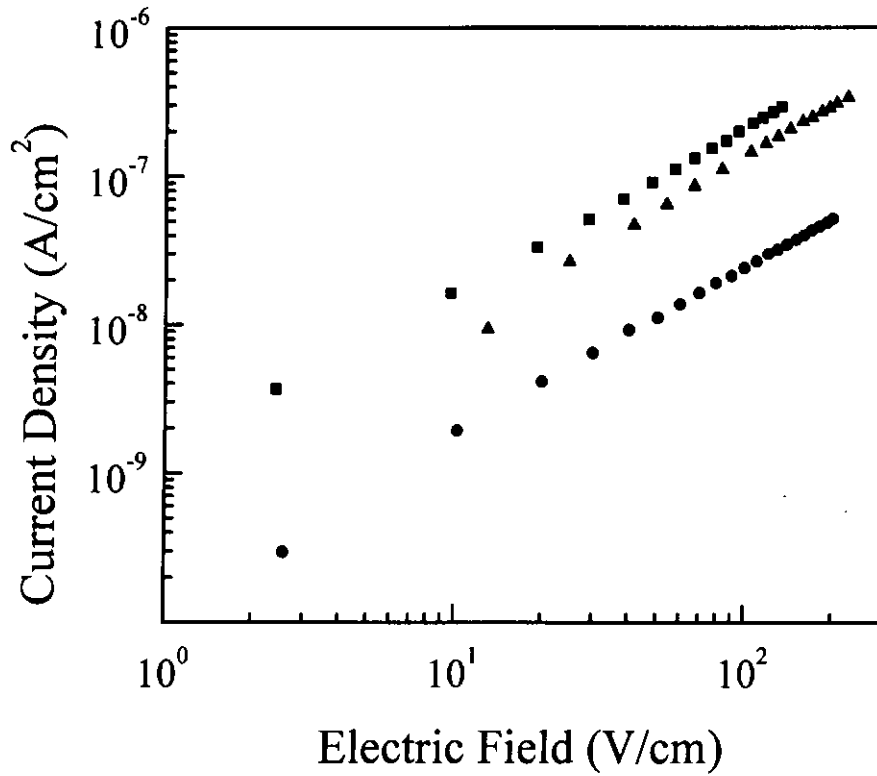
Figure 4.6c   *J-E* characteristic of 3 % CB/LCP composites in the
flow (■), transverse (●) and thickness (▲) directions
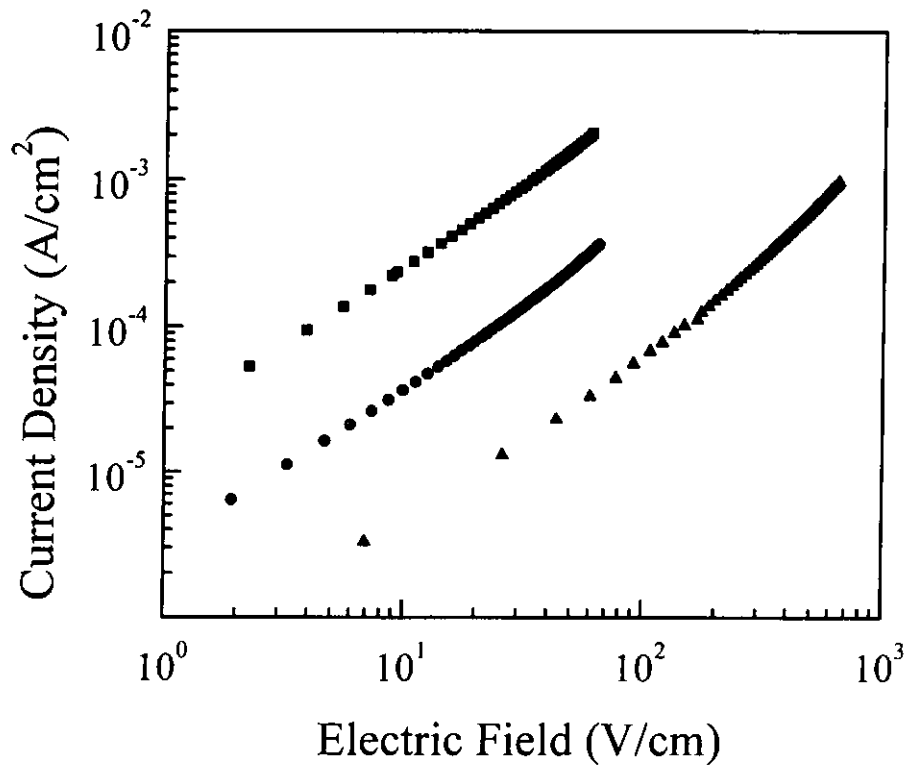
Figure 4.6d   *J-E* characteristic of 4 % CB/LCP composites in the
flow (■), transverse (●) and thickness (▲) directions
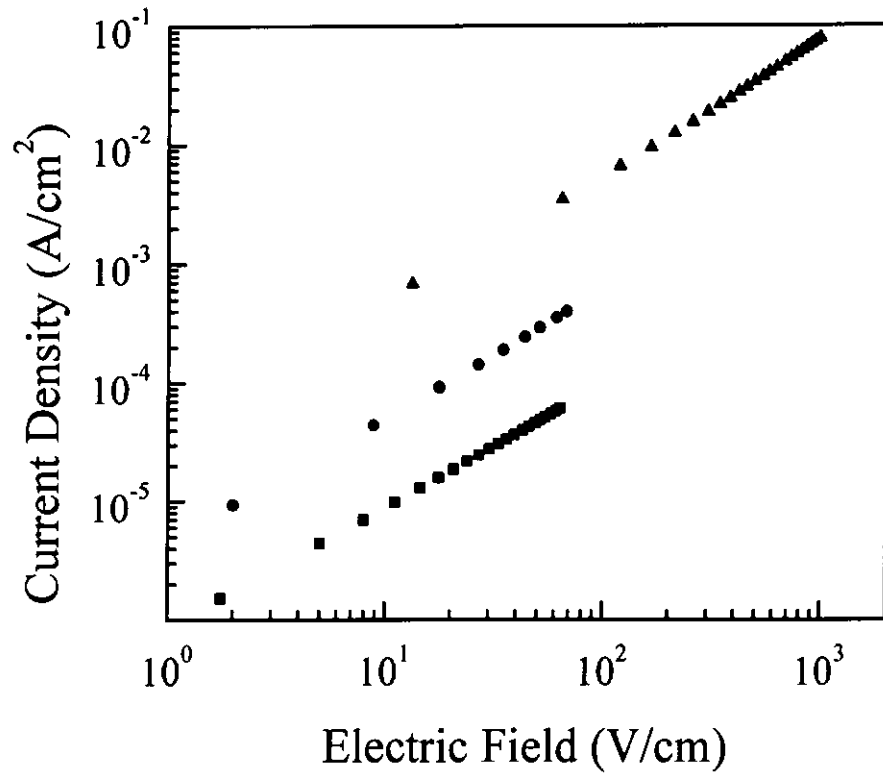
Figure 4.6e   *J-E* characteristic of 5 % CB/LCP composites in the
flow (■), transverse (●) and thickness (▲) directions
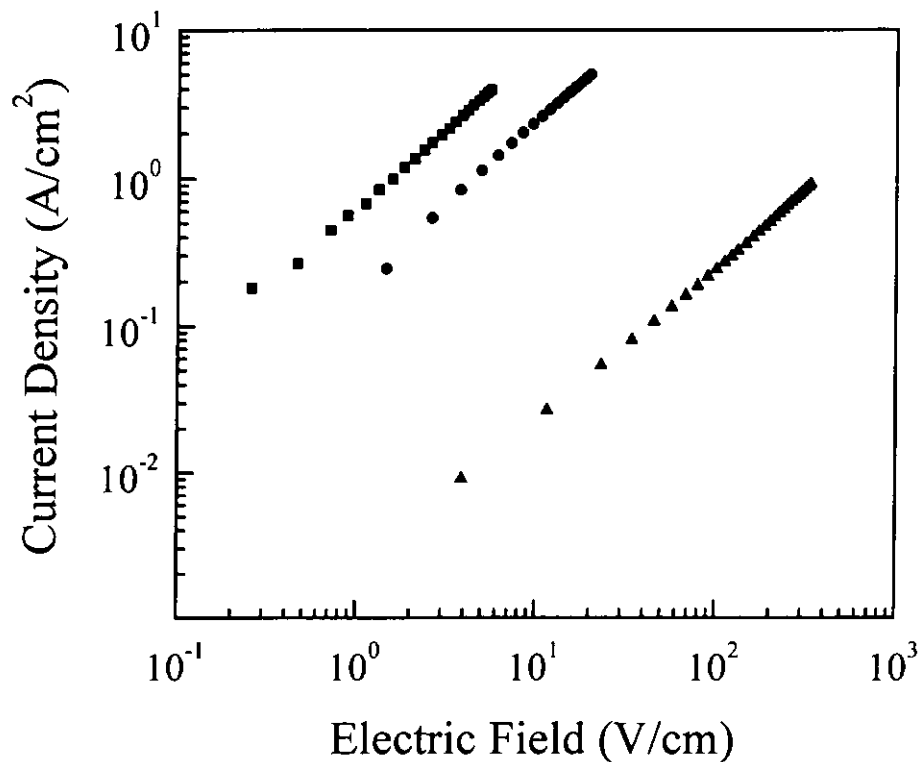
Figure 4.6f   *J-E* characteristic of 6 % CB/LCP composites in the
flow (■), transverse (●) and thickness (▲) directions
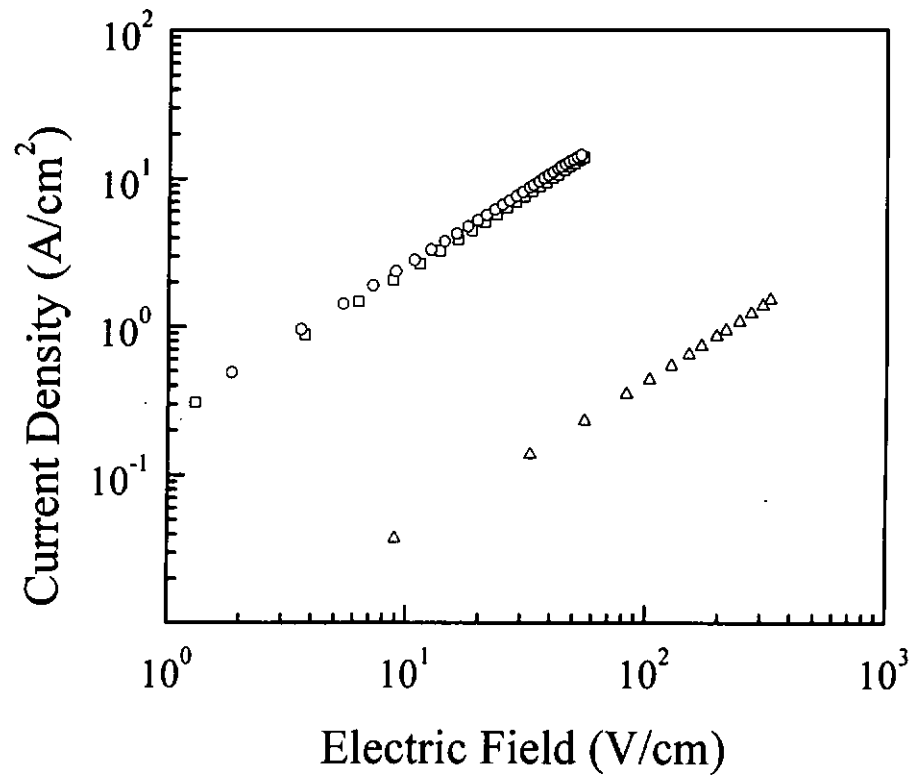
Figure 4.6g   *J-E* characteristic of 7 % CB/LCP composites in the flow (□), transverse (○) and thickness (△) directions
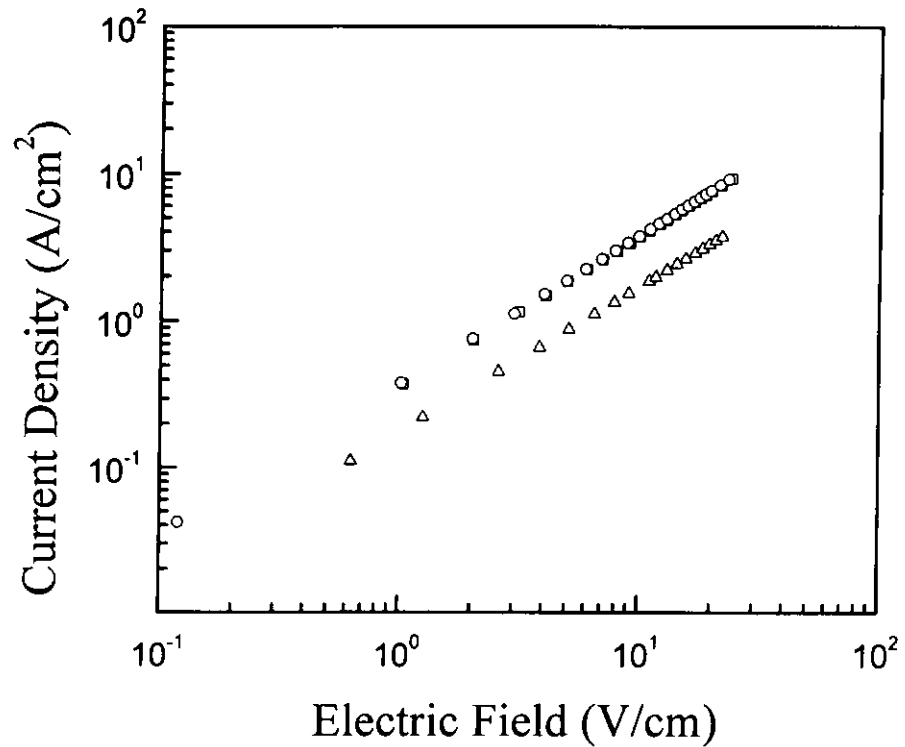
Figure 4.6h   *J-E* characteristic of 10 % CB/LCP composites in the flow (□), transverse (○) and thickness (△) directions

Volume Fraction Dependence of the Resistivity

The resistivities ρ of the CB/LCP composites in flow, transverse and thickness directions at room temperature depend critically on the volume fraction of carbon black as shown in Figure 4.7 (data were tabulated in Appendix E). For CB volume fraction below 3 %, the magnitudes of resistivity remain at the order of 10^9 Ω-cm, but there is a sudden drop in resistivity by almost eight orders of magnitude above 3 % up to 10 % CB. This 3 % critical volume fraction is known as the percolation threshold for this series of composites. It may be attributed to the percolation behavior of the conducting phase in the composites. It corresponds to the first continuous conducting path formed by the CB particles inside the LCP matrix. According to the percolation concept [Zallen, 1983], the conduction in these composites depends mainly upon the formation of CB clusters inside the LCP matrix. The formation of CB clusters require empty sites in which CB particles are able to form a long clusters and connect to become infinite conducting paths. Once the conducting network form and the resistivity decreased drastically.

It is seen that there are three volume fraction regions shown in Figure 4.7, each with a characteristic change in resistivity. As the CB volume fraction increase to the critical volume fraction, the resistivity almost independent on CB volume fraction. The CB particles distribute in the LCP matrix where adjacent particles are far apart so that the high resistivity region is defined as the insulative region. When the CB volume fraction increase further, the growing of CB clusters make themselves contacting with each other. The formation of conducting network inside the LCP matrix results a transition in

resistivity drops from 10^9 to 10^2 Ω-cm, as the CB volume fraction increase from 3 % to

6 % and this rapidly change in resistivity is defined as the percolation region. The well-

known percolation threshold occurs at about 3 %. An additional increase in the CB

volume fraction, the resistivity has a slight reduction because the infinite contiguous

particle chain has been formed already. This low resistivity range is defined as the

conductive region. Percolation region is the transition between insulative region and the

conductive region.

Figure 4.7   CB volume fraction dependence of resistivity of CB/LCP composites
in the flow (□), transverse (○), and thickness (△) directions

In the studies of percolation threshold, CB as filler network structure is clearly shown in the pictures of the carbon black/polymer composites of Michels [Michels *et al.*, 1989], which have a percolation threshold below 2 wt. % of carbon black. Other CB/polymer systems have higher percolation threshold, such as 11 %, 16 % to 18 % and 21 % studied by Nakamura *et al.*, Medalia and Abo-Hashem *et al.* respectively [Nakamura *et al.*, 1995, Medalia, 1986 and Abo-Hashem *et al.*, 1994].

Analysis by Scaling Law

According to [Sherman *et al.*, 1983] the site percolation threshold of a binary system which depends on the random close packing factor and the coordination number of the conducting phase. Kirpatrick [Kirkpatrick, 1973], also showed that at around the percolation threshold ϕ_c, the behaviour of the composite should follow the equation 2.2 which was shown in section 2.2. Kirkpatrick showed that this power law is valid within the range $\phi_c \leq \phi \leq 0.4$. According to percolation theory, the exponent β has a physical meaning which represents the average number of contacts per particle increase in the volume fraction of carbon black [Yacubowicz *et al.*, 1986]. When this average number reaches 1.0, the probability of formation of infinite chains becomes non-zero [Aharoni, 1972], thus reducing the resistivity of the system and enhancing the conduction. Thus the nature of the scaling power is unique and defined by particle geometry. By plotting the logarithm of ρ against the logarithm excess CB volume fraction above percolation threshold, a composite system obeying the percolation model should give a straight line according to equation 2.2. The negative value of the straight line's slope represents the scaling power β.

In studying the applicability of the scaling law for our system, a plots of log ρ against log(ϕ - ϕ_c) in the flow, transverse and thickness directions are shown in Figure 4.8. It shows that when ϕ_c is equal to 3.94 %, a least-squares linear regression of the data give the slopes (β) 1.91, 2.18 and 2.47 for the flow, transverse and thickness directions respectively. It seems that these are reasonable results, although it deviates from the percolation threshold value 3 for which the conducting particles are assumed to be

spherical and randomly distributed in the matrix. In other words, form the above β

values obtained, it is expected that the CB particles in the LCP matrix are aggregated in

clusters and thus render in irregular geometry and would be far from a random

distribution.
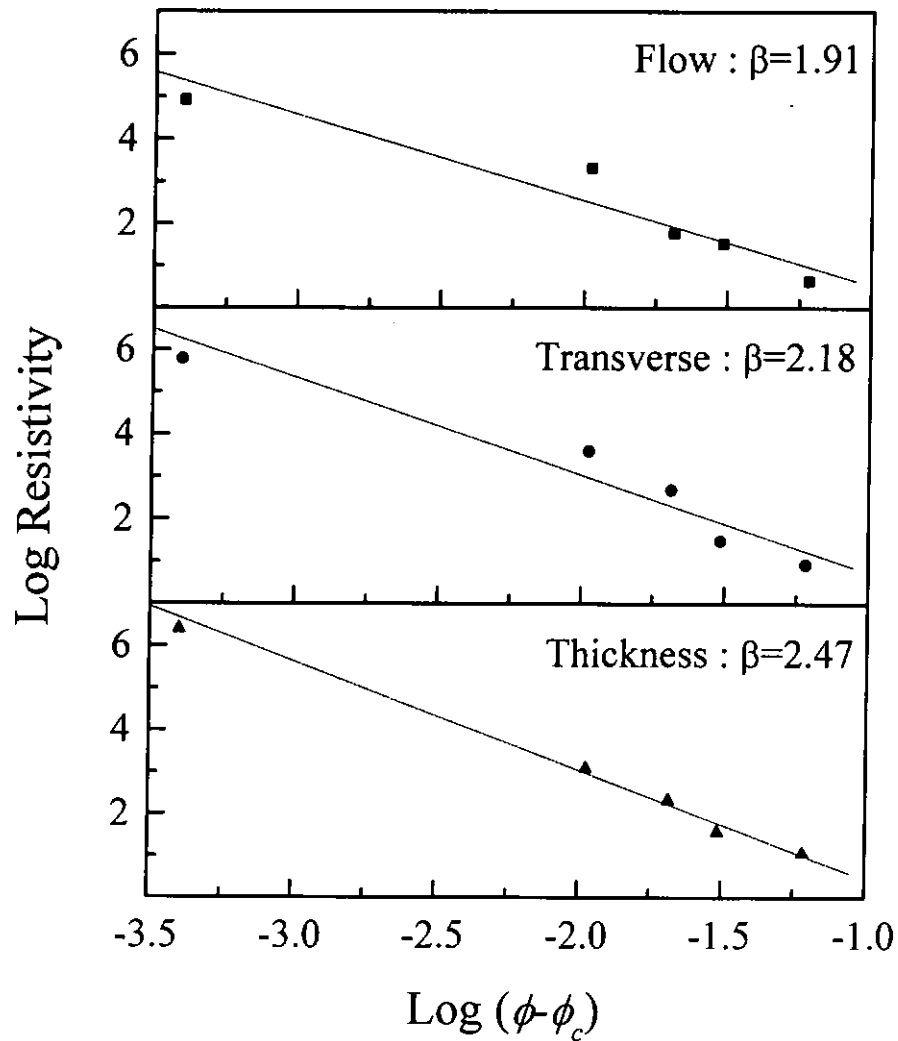
Figure 4.8   Linear regression fitting of the log-log plot of resistivity against excess volume fraction in the flow, transverse and thickness directions

Analysis by Effective Medium Theory

Base on the EMT equation 2.5 and 2.6, they have been used to fit the experimental data for the electrical resistivity. The result is shown in Figure 4.9, the dotted points are experimental data and the solid curve from 0 % to 4 % is obtained from equation 2.5 upon a conversion of conductivity to resistivity. Similar solid curve ranged from 4 % to 11 % is calculated from equation 2.6. The transition volume fraction is set at 3.94 % where α and x are taken to be 3.4 and 8×10^{-10} $(\Omega\text{-cm})^{-1}$ respectively. The value of α is the electrical conductivity of the carbon black powders provided by the manufacture. It seems that this effective medium model incorporated with the symmetrical Bruggeman equation even with one free parameter can give a good estimation of the resistivity of this aggregated CB/LCP composites in this volume fraction range.
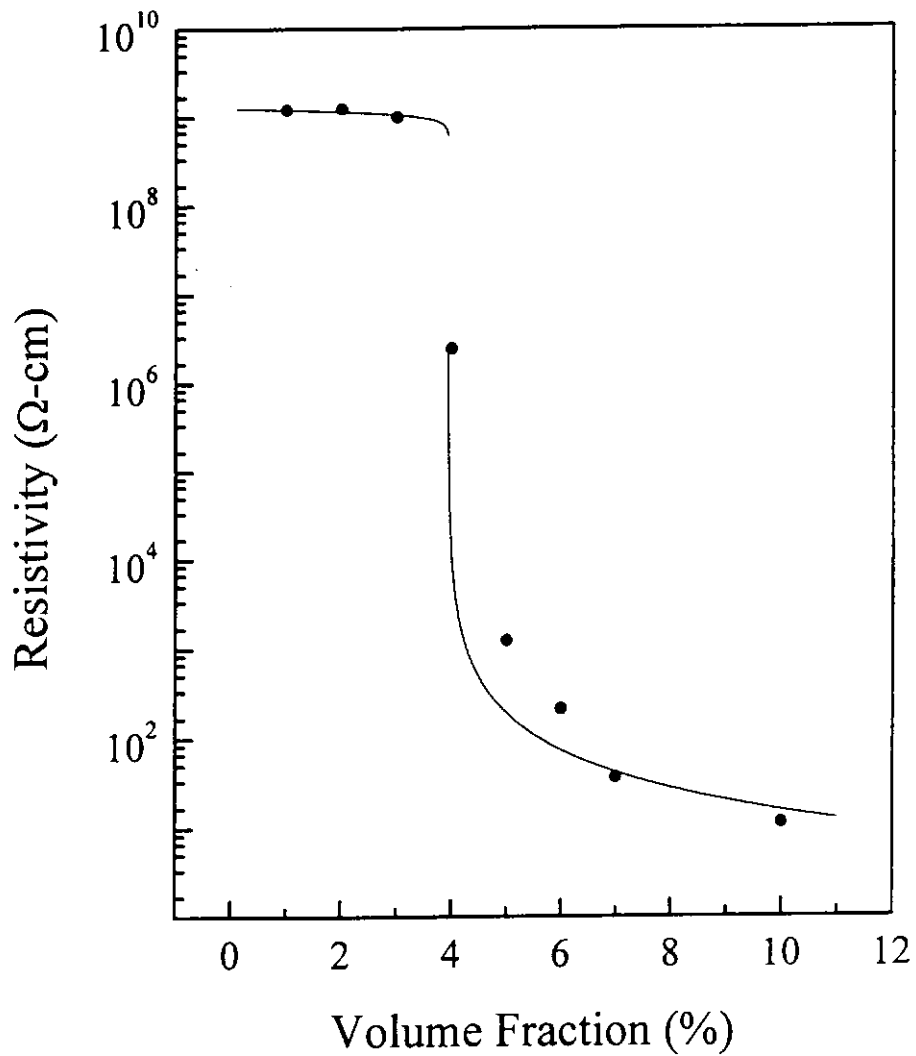
Figure 4.9   The resistivity versus volume fraction of CB for CB/LCP composite (●). The two solid curves (from 0 % to 4 % and 4 % to 11 %) through the data points were calculated using equation 2.5 and 2.6 respectively

Temperature Dependence of the Resistivity

The resistivities in the three directions as a function of temperature were measured in the range from room temperature to 200 °C. Figure 4.10a, 4.10b and 4.10c show the results for the flow, transverse and thickness direction measurements respectively (data were tabulated in Appendix F). Although there are not much differences in the temperature dependence for the three directions, the temperature dependence for below and above percolation threshold are completely different. For the composites of CB volume fraction below percolation threshold, they reveal a negative temperature coefficient (NTC) at the whole measurement range. The resistivities decrease from 10^9 Ω-cm at room temperature to 10^6 Ω-cm at 200 °C. They all gradually decrease at low temperature and there is an obvious drop in resistivity at around 55 °C and then follow a rapid decrease of almost three orders of magnitude so forth to 200 °C. It is interested to compare with the result as presented in Figure 4.7. A three orders of magnitude decrease in resistivity is equivalent to an increase in volume fraction to about 4 %. This thermally invoked percolative-like behaviour of the composites is still a question that cannot be easily understood neither by thermal expansion of the two phases nor by the glass transition of the LCP matrix. A further study of carbon black and LCP interface may help to explain this NTC effect.
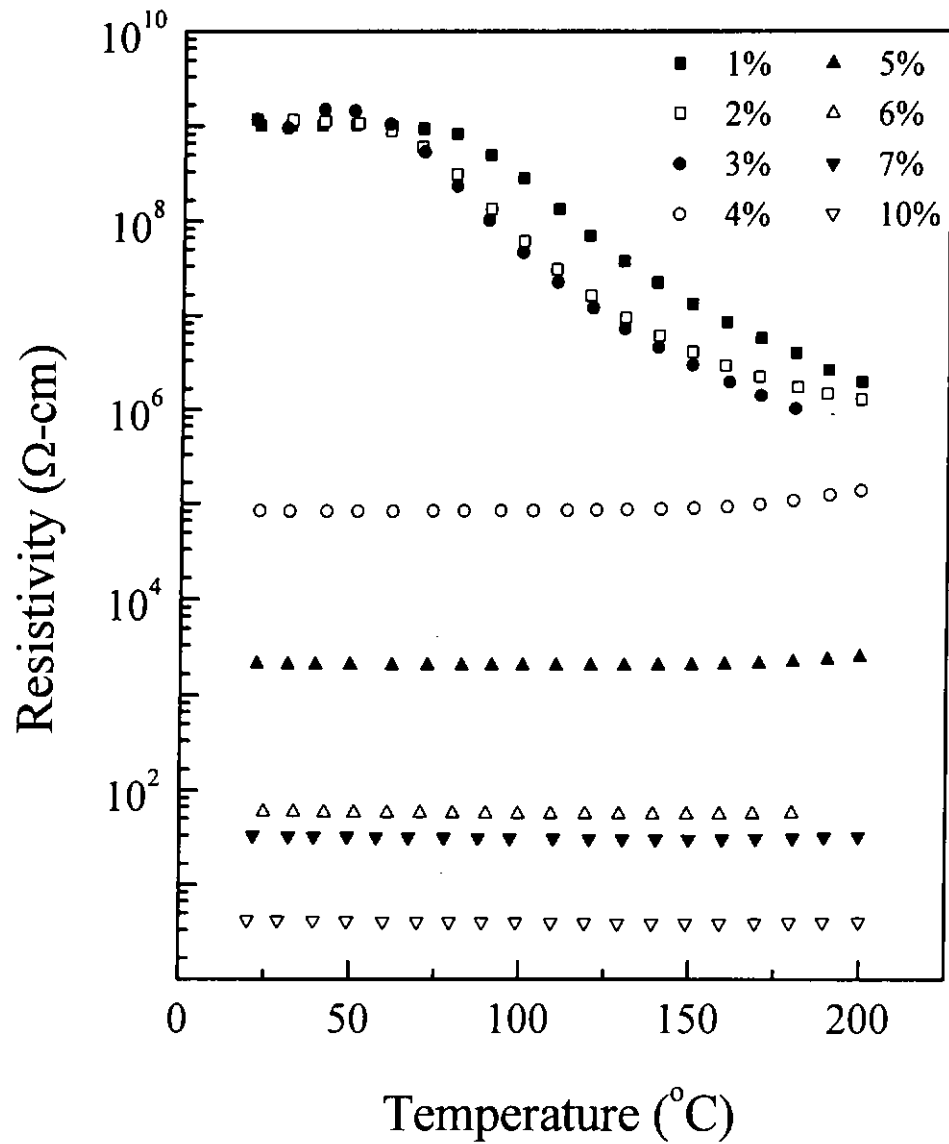
Figure 4.10a   Temperature dependence of resistivity of 1 % to
                10 % CB/LCP composites in the flow direction
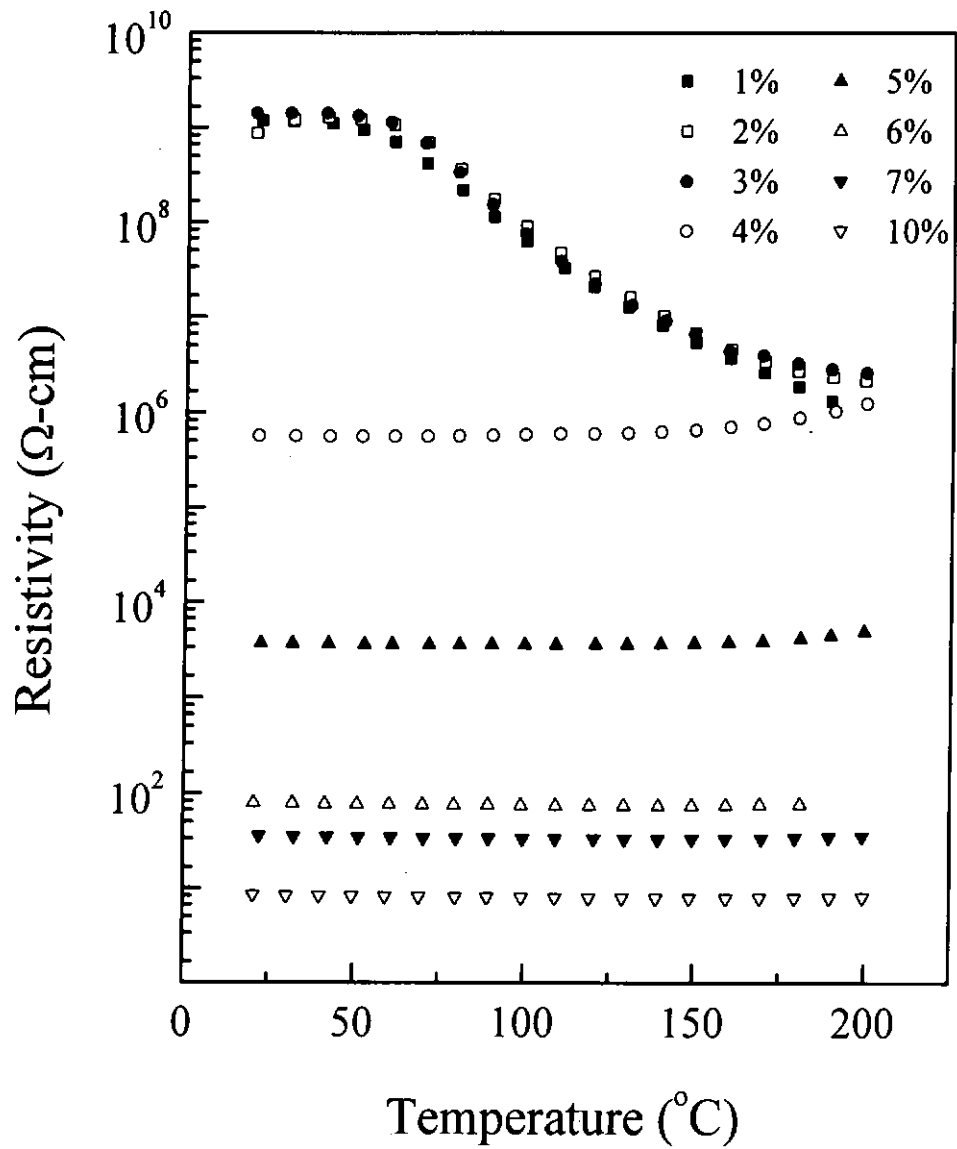
Figure 4.10b   Temperature dependence of resistivity of 1 % to 10 % CB/LCP composites in the transverse direction
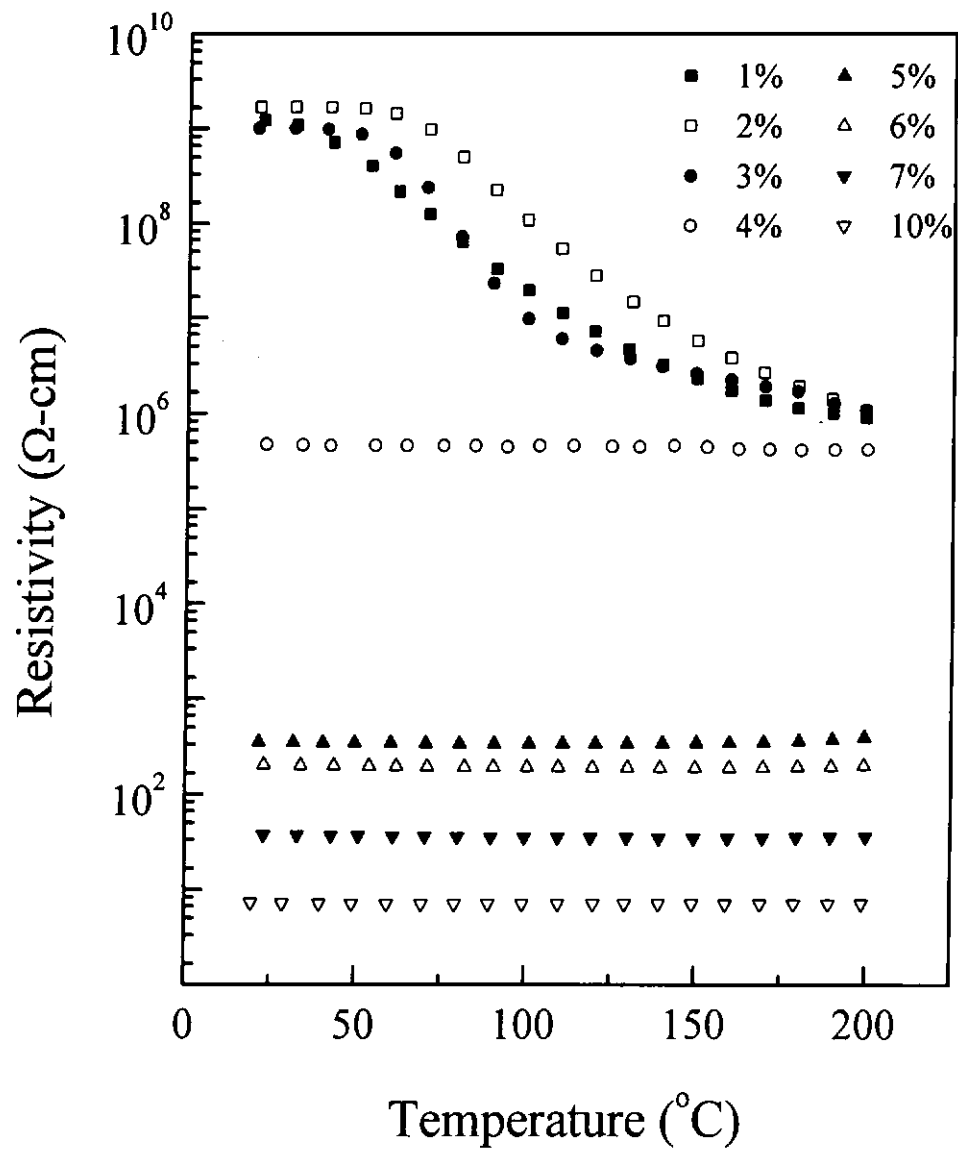
Figure 4.10c   Temperature dependence of resistivity of 1 % to 10 %
CB/LCP composites in the thickness direction

For those samples of CB volume fraction above percolation threshold, their temperature dependence are different compared with the low CB samples. Figure 4.11a and Figure 4.11b reveal the temperature behaviour of the group of composites at the percolation range. There is almost no change in the resistivity at low temperature but it increases at above 150 °C. For the high CB volume fraction composites, they are at the conductive range as shown in Figure 4.11c to Figure 4.11e. As the temperature increase, a transition point from negative slope to positive slope of resistivity occurs at about 150 °C, which is the same transition temperature as the percolative group of samples.

Another feature which is common to all measured samples, although they exhibit similar temperature dependence, the resistivities measured for the three directions are different. This may be a result of the slightly anisotropy of the LCP matrix, especially for those samples of low CB volume fraction and the conduction is mainly passing through the matrix. For those high CB volume fraction samples, the variation in resistivities in the three directions may be a result of different number of connecting paths in different direction. This is particularly true for highly aggregated CB composites. Furthermore, there is no consistence in the magnitude of resistivity in the three directions for different CB volume fraction sample, e.g. the 4 % sample exhibit the highest resistivity in the thickness direction as shown in Figure 4.11a, but the 5 % sample has the highest resistivity in the transverse direction as shown in Figure 4.11b. It is therefore no specific electrical anisotropic characteristic can be concluded in these CB/LCP composites. In other word, even though there is a slightly anisotropy found in the LCP matrix, it seems that it does not affect the charge transportation in the composites.
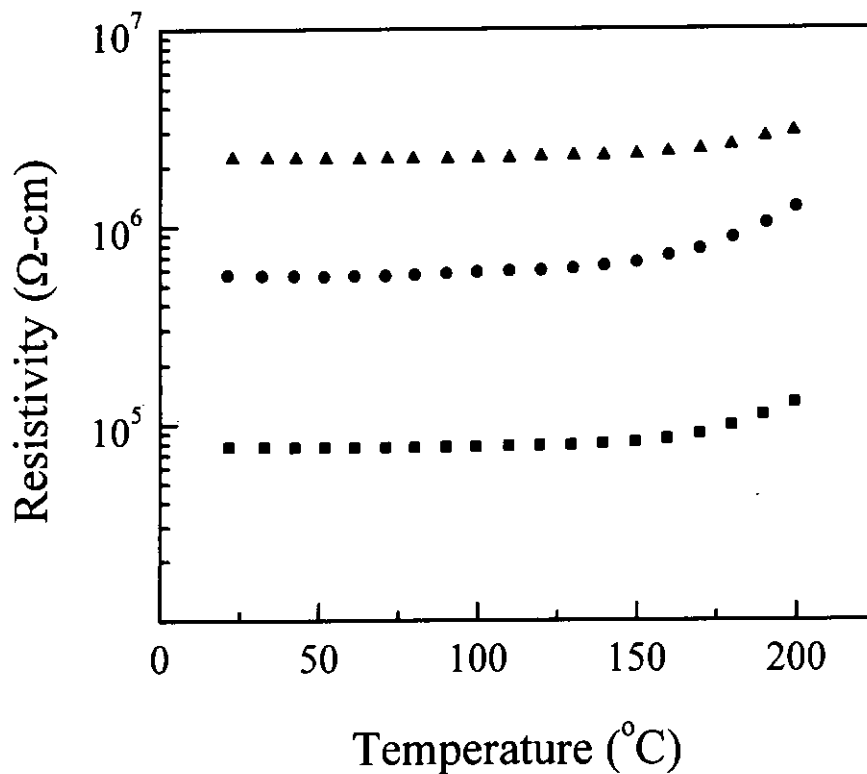
Figure 4.11a   Temperature dependence of resistivity of 4 % CB/LCP composites
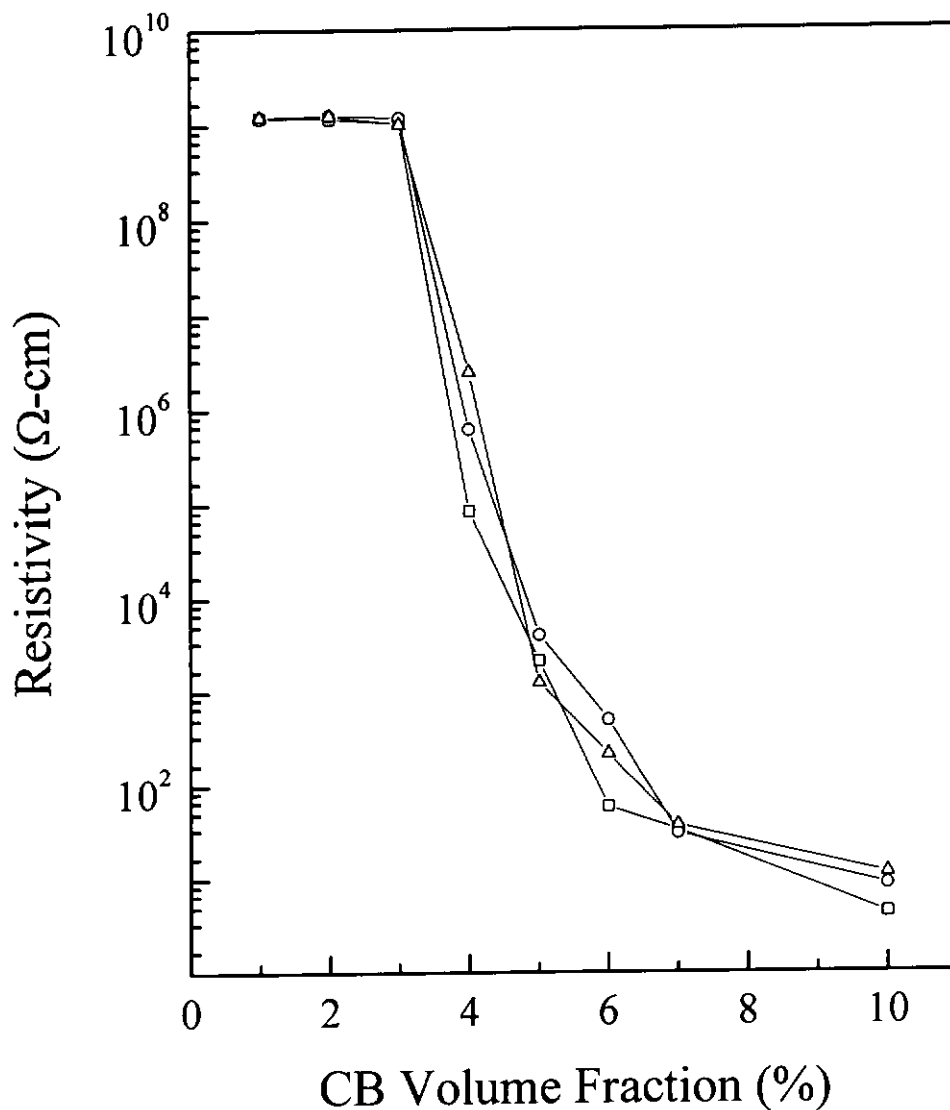   in the flow (■), transverse (●) and thickness (▲) directions
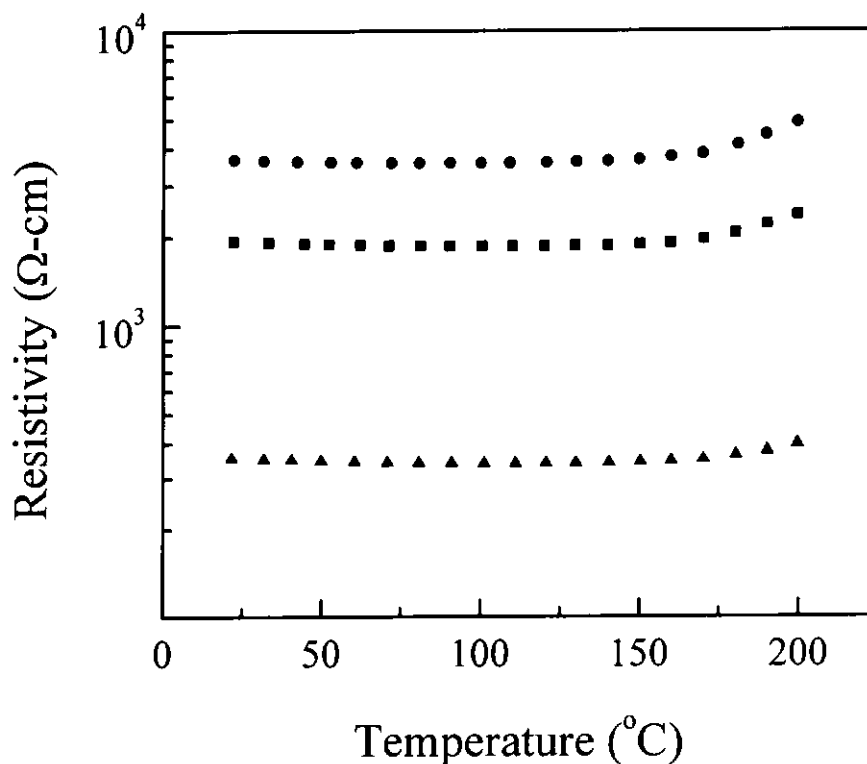
Figure 4.11b   Temperature dependence of resistivity of 5 % CB/LCP composites
                in the flow (■), transverse (●) and thickness (▲) directions
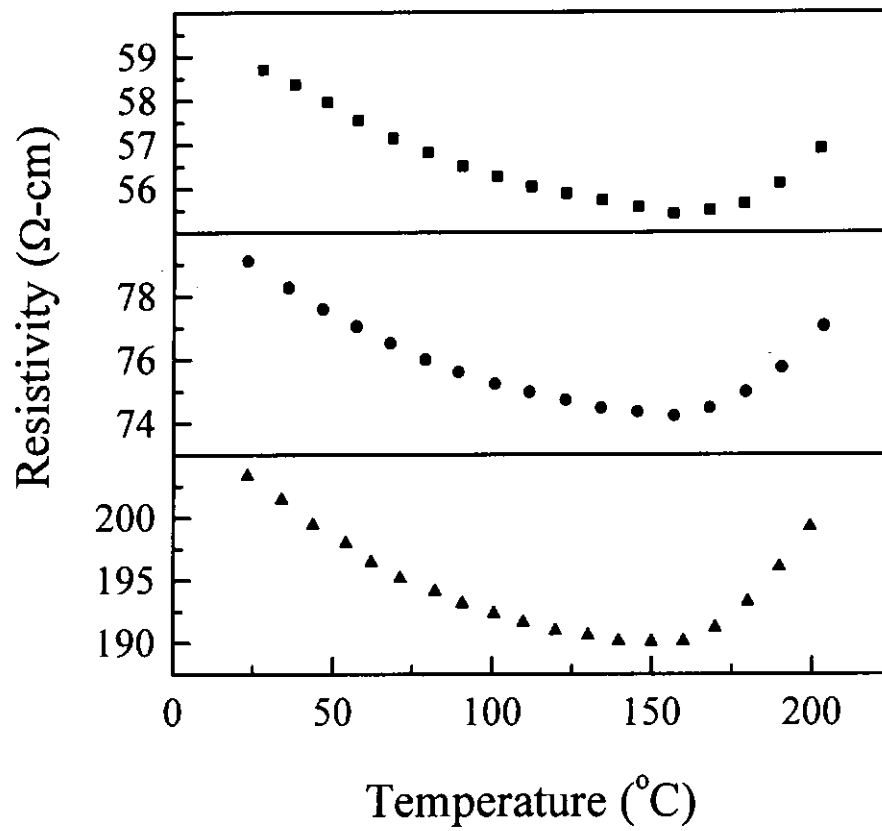
Figure 4.11c   Temperature dependence of resistivity of 6 % CB/LCP composites in the flow (■), transverse (●) and thickness (▲) directions
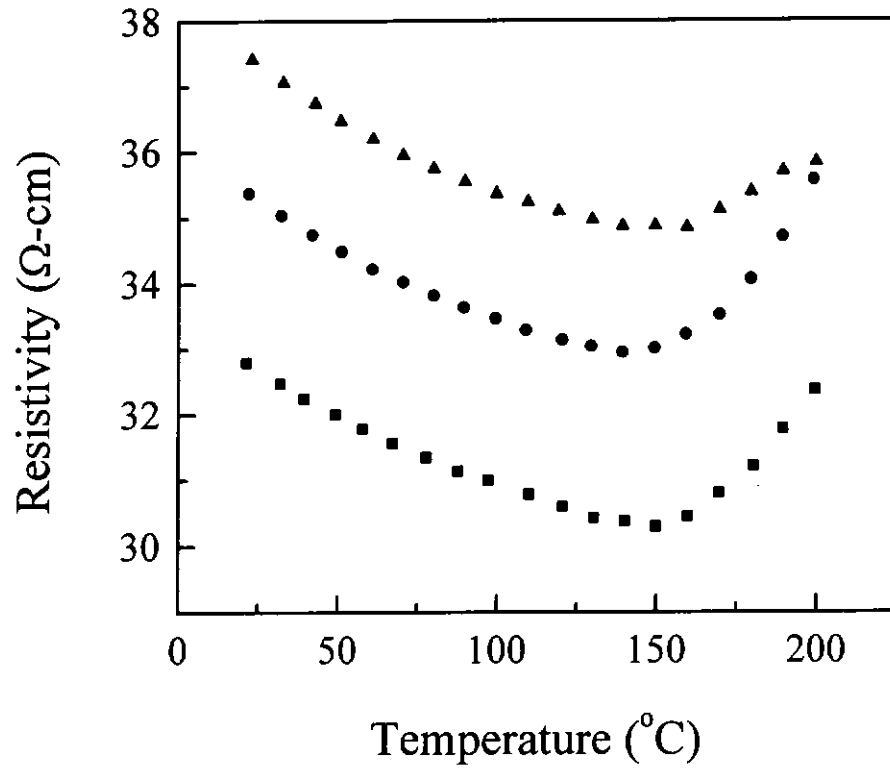
Figure 4.11d   Temperature dependence of resistivity of 7 % CB/LCP composites
in the flow (■), transverse (●) and thickness (▲) directions
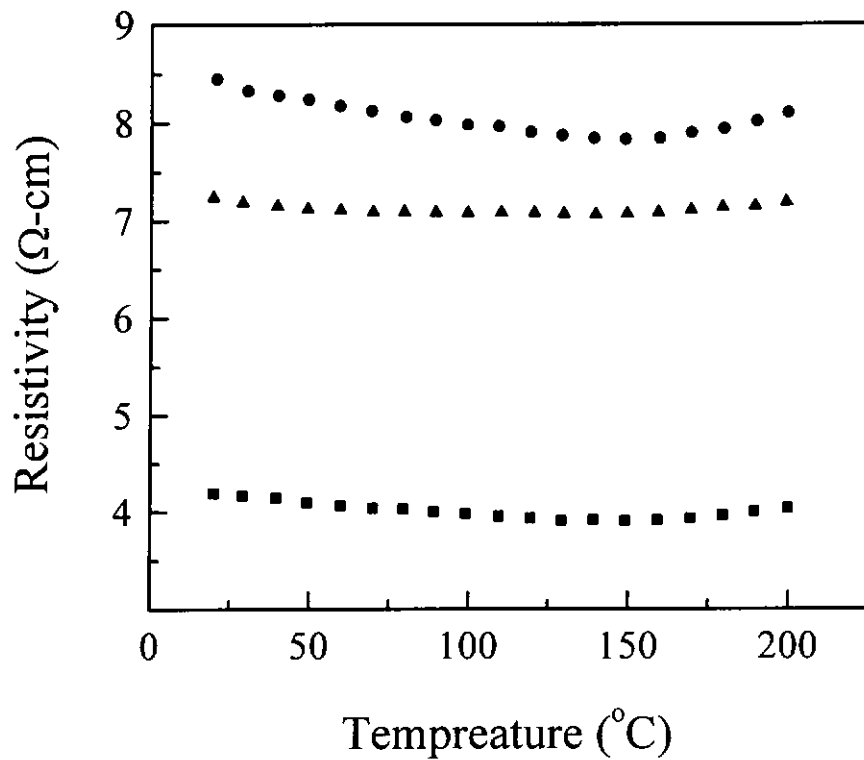
Figure 4.11e   Temperature dependence of resistivity of 10 % CB/LCP composites
in the flow (■), transverse (●) and thickness (▲) directions

5   Thermal Conductivity

To determine the thermal conductivity K of the samples, we have adopted the well-developed laser flash radiometry method [Choy *et al.*, 1987]. In fact, it is the thermal diffusivity D of the samples being determined by this method. K can then be obtained from the relation:

$$K = dC_pD \qquad\qquad (5.1)$$

where d and C_p are the density and specific heat of the samples respectively.

5.1   Laser Flash Radiometry Method for Thermal Diffusivity

The laser flash radiometry is a transient technique for measuring the thermal diffusivity of solid materials. A thin film sample is irradiated at the front surface with a pulse of energy from a high-power laser source. An infrared detector is used to measure the transient temperature change of the sample surface as a function of time. In practice, it is preferable to monitor the temperature change of the rear surface because of much less interference from the scattered laser.

Since the flash method has been introduced by Parker *et al.* in 1961 [Parker *et al.*, 1961], it has been studied extensively. The advent of pulse laser and infrared detector further enhanced its application on small and thin film samples.

The theory of laser flash radiometry method has been analyzed in detail by Leung and

Tam in 1984 [Leung *et al.*, 1984]. Its application on polymer films has been further

developed by Choy *et al.* [Choy *et al.* 1987]. According to their conclusion, a polymer

sample of lateral dimension ten times larger than its thickness could be treated by a one-

dimensional heat flow model. The heat loss mainly due to thermal radiation may be

neglected provided the polymer sample thickness is less than half of a millimeter.
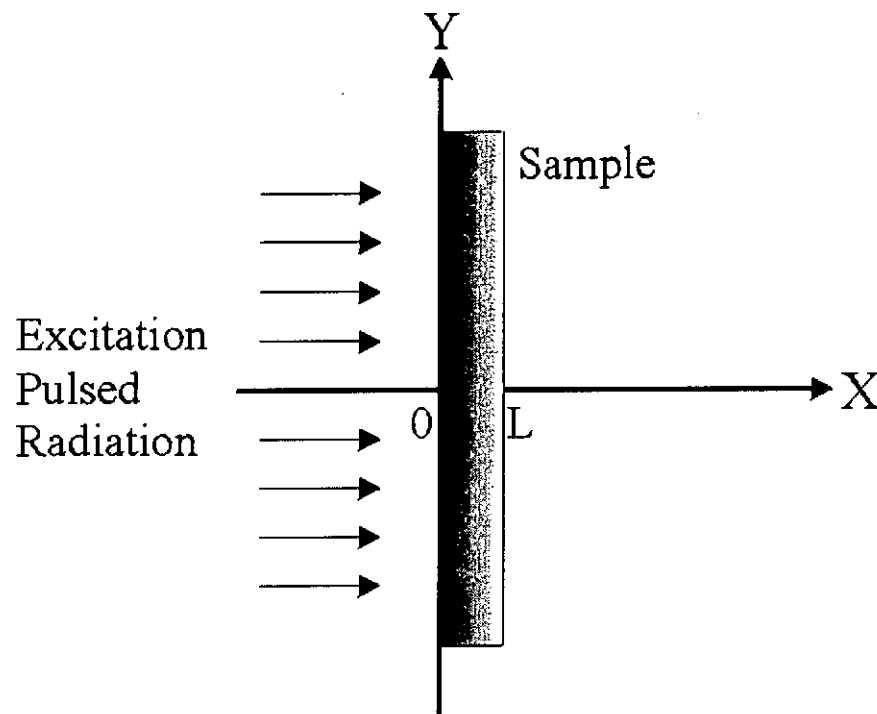
Figure 5.1   The laser flash on a thin solid sample
                in one-dimensional treatment

Consider a short laser pulse impinging onto the front surface of a thin film sample of thickness L as shown in Figure 5.1. Let $T(x, t)$ be the temperature rise above room temperature at position x in the sample at time t. The diffusion of the absorbed heat energy through the sample is governed by the one-dimensional heat diffusion equation [Leung *et al.*, 1984]:

$$\frac{\partial T(x,t)}{\partial t} = D\frac{\partial^2 T(x,t)}{\partial x^2}$$ (5.2)

where D is the thermal diffusivity.

Since a theoretical radiometric signal is developed by fitting the captured signal from the infrared detector to evaluate the thermal diffusion time constant τ, the thermal diffusivity D can then be calculated. The thermal conductivity K is related to the diffusivity through the equation 5.1.

5.1.1 Laser Flash Transmission Radiometry Measurement

A block diagram of the laser flash transmission radiometry measurement is shown in Figure 5.2. The Quanta-Ray GCR-16S Nd$^+$-YAG pulse laser serves as the pulsed radiation source of fundamental wavelength 1064 nm. Higher harmonics can be generated by inserting the KD*P nonlinear optical crystals into the laser beam path. Thus the laser system provides 1064, 532, 355 and 266 nm laser pulse wavelengths respectively. The second harmonic, a green radiation of wavelength 532 nm with pulse width about 10 ns was used as the excitation source in our experiment.

The vacuum chamber (Figure 5.3) is equipped with two windows, a fused-silica glass plate is used as the laser entrance window. A meniscus germanium *Ge* lens of focal length 4 cm attached at the opposite surface of the vacuum chamber serves to focus the emitted thermal radiation onto the liquid nitrogen cooled HgCdTe infrared detector (Infrared Associated, Inc). The sample was placed at a distance of 8 cm before the *Ge* lens, thus a one-to-one image of the rear surface of the sample was formed at 8 cm behind the *Ge* lens on the infrared detector. The active area of the detector was 0.25 mm ×0.25 mm and special range of 8 to 12 μm infrared radiation. The rise time of this photoconductive type detector is 0.3 μs.
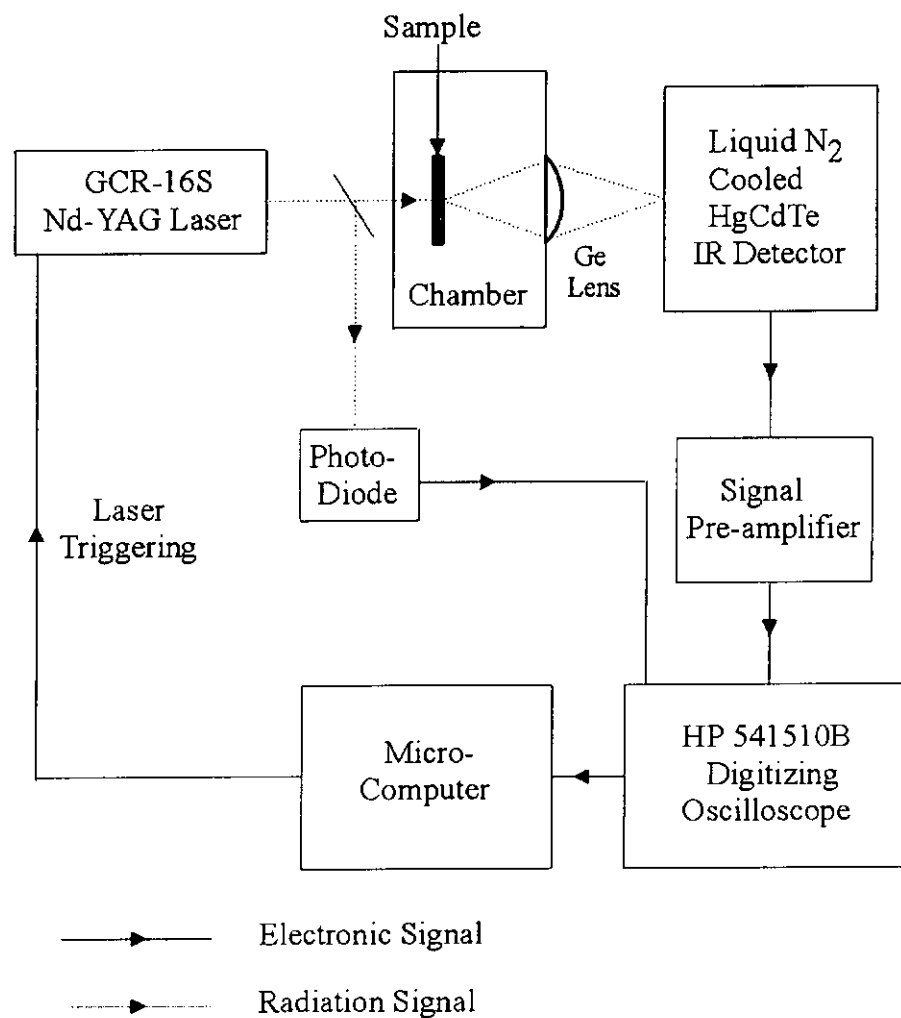
Figure 5.2   Block diagram for laser flash radiometry
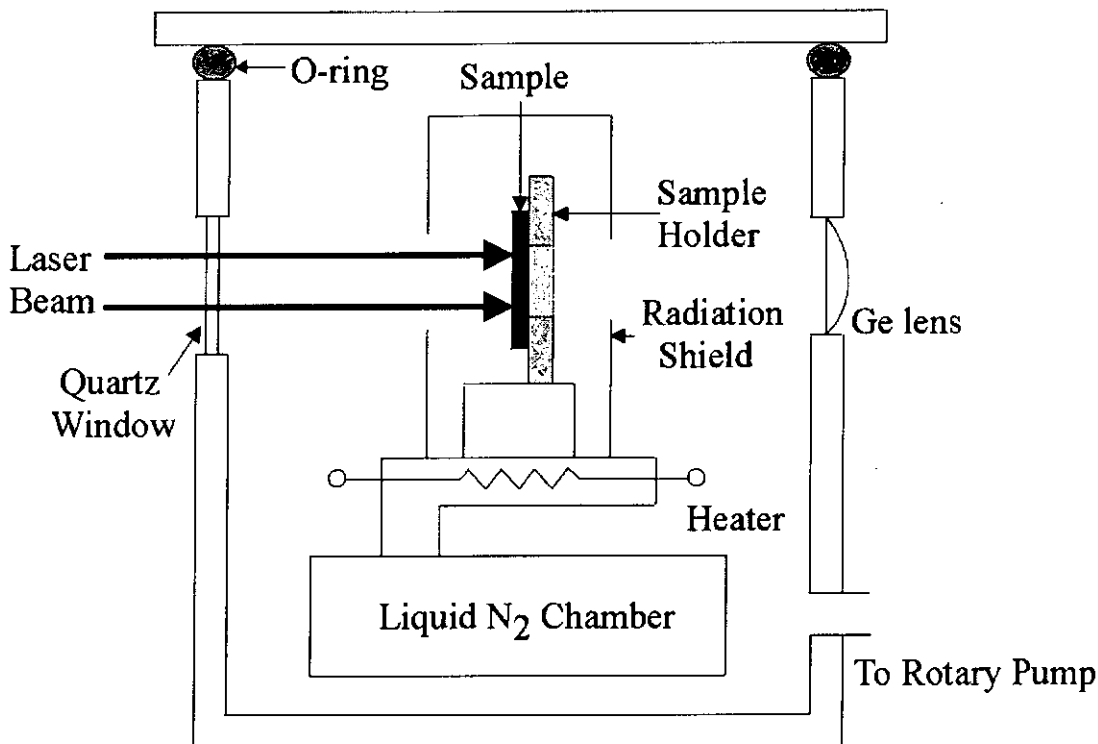
Figure 5.3   Vacuum chamber

The laser beam was slightly focused to have a spot size of approximately 10 mm diameter on the sample's front surface. The sample was clamped on its edge to the copper sample holder. Apertures of the same size as the sample to ensure that only the sample was irradiated by the laser beam and only the thermal radiation emitted by the sample was detected. Signal from the infrared detector was boosted by a pre-amplifier connected to a HP54510B digitizing storage oscilloscope (DSO). The bandwidth of the DSO was 350 MHz and the fastest digitizing rate was 1 giga-sample per second. Depending on the signal magnitude and the signal to noise ratio, the experiment is performed by averaging from 20 to 50 laser shots. The pulse period was about 10 to 20 s to allow the sample temperature decaying to ambient before firing the next pulse. The averaged signal was then transferred to a microcomputer and stored for analysis. The

thermal diffusivity was deduced from a recursive-fitting program which the captured data were fed [Leung *et al.*, 1984].

In this experiment, the front surface was entirely covered by an excitation light beam. This was done to ensure that heat flowed only along the thickness direction but not in the radial direction. It is not necessary to insulate the sample since radial conduction is negligible as long as the laser beam radius r is much larger than the sample thickness L. Donaldson had showed the effect of radial conduction becomes unimportant at $r/L > 10$ [Donaldson, 1972].

5.1.2 Laser Flash Transverse Radiometry Measurement

In the previous section, we have presented the method for the measurement of thermal diffusivity that is perpendicular to film surface. In the following discussion, we shall introduce the method for the determination of thermal diffusivity in the direction parallel to the film surface. The theory of this method has been analyzed by Choy *et al.* in 1997 [Choy *et al.*, 1997]. It is a modification of the transmission radiometry method discussed in the previous section. The pulsed laser was focused by a cylindrical lens given out a line-shaped beam which impinges on the surface of the sample. A slit of 0.2 mm width is placed at a distance of few millimeter away from the laser line at the opposite side of the sample surface as shown in Figure 5.4.
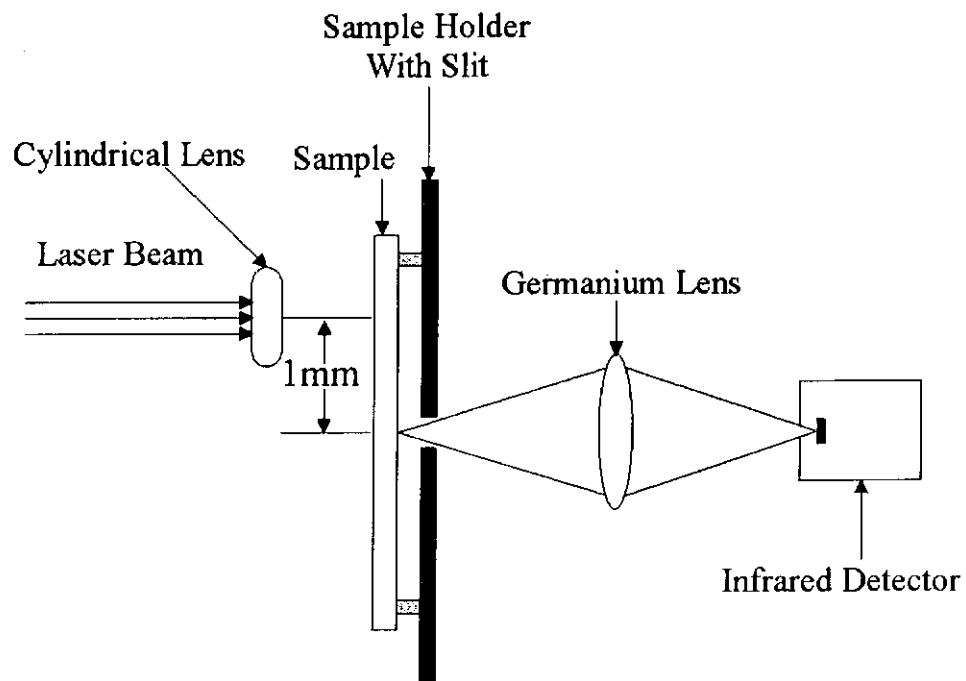
Figure 5.4   Experimental setup for thermal diffusivity
               measurement in the transverse direction

As if the sample length is 5 times longer than the excitation line-detection slit distance

x, the effect of the sample ends is negligible, then the temperature rise $T(x,t)$ can be

expressed as:

$$T(x,t) = \frac{Q}{2lWdC(\pi Dt)^{\frac{1}{2}}} \exp\left(-vt - \frac{x^2}{4Dt}\right) \qquad (5.3)$$

where D, d, and C_P are the thermal diffusivity, density and specific heat of the sample,

v is the dissipation constant, Q is the injected heat pulse energy, W and l are the width

and thickness of film sample.

The radiometry signal at the detector is proportioned to $T(x,t)$. Therefore, the thermal

diffusivity along the film surface direction can be obtained by fitting the observed signal

to equation 5.3.

In the present study, we have used the second harmonic of the YAG laser as the

excitation source. The pulse energy was adjusted to give a temperature rise of about 2 K

at x=1 mm. It has been found that a layer of air at the sample surface would effectively

enhance the diffusion process thus resulting in a higher value of D of the sample.

Therefore, the experiment should be performed in vacuum.

Depending on the signal to noise ratio, the experiment was performed by averaging the

captured signals for 20 to 100 laser shots. Then the digitized data were collected by a

microcomputer. There are two opposing conditions in the choice of the detection

distance. Since the temperature rise decreases inversely with increasing x, on the other

hand, the uncertainty of measuring x is about 0.04 mm, hence the accuracy increases as

x increases. Balancing between these two conditions, the value of x for our experiments is chosen to be 1mm. Taking with that distance, the accuracy in D is about 8 %. For each sample, several measurements were made to average the final value of D. By taking an average of these D values, it is estimated that an accuracy of 6 % has been achieved.

As long as the thermal diffusivity is determined, the thermal conductivity of the samples can be evaluated by the equation 5.1, provided the specific heat and density of the samples are known.

5.2 Pulsed Laser Induced Ultrasonic Wave Method for Sheet Modulus

Knowledge of the elastic modulus of composites is important since it represents the mechanical properties of the materials. It may also reveals the microscopic structure as well as the anisotropic characteristics after processing. Numerous methods have been developed for the measurement of elastic modulus. One of the commonly used techniques for polymeric materials is to measure the acoustic wave velocity as it is directly related to the elastic modulus.

In an infinite solid, two elastic wave modes can be generated: the longitudinal (also known as compression, particle motion is parallel to the direction of propagation) wave and transverse (shear, the particle motion is perpendicular to the direction of propagation) wave. If the medium occupies a half-space and has one free surface, then the surface stresses are zero. Wave of this type is referred to as Rayleigh waves. They propagate along the free surface and decay exponentially in the direction normal to the surface. The wave velocity in an infinite isotropic solid are related to the Young's modulus and Poisson's ratio v by [Scruby, 1990]:

$$V_L = \left(\frac{E(1-v)}{d(1+v)(1-2v)} \right)^{\frac{1}{2}} \tag{5.4}$$

and

$$V_S = \left(\frac{E}{2d(1+v)} \right)^{\frac{1}{2}} \tag{5.5}$$

where V_L is the velocity of the longitudinal wave, V_S is the velocity of the transverse wave and d is the density of the solid. Therefore, E and v of the material can be determined by measuring the wave velocities.

More elastic wave modes can be generated in the sample with finite dimensions due to the existence of free boundaries (the surfaces). Such vibration modes are more complicated than the longitudinal and shear waves.

For a film sample, if the two surfaces are sufficiently close together, the elastic wave motions on each surface will interact to produce a Lamb wave, whose propagation characteristics are partly a function of the separation between the two boundaries. The Lamb waves have two modes, the symmetric and antisymmetric modes. The symmetric modes are also termed extensional modes, while the antisymmetric modes are usually called flexural or torsional modes. Because of proximity of the two boundaries, the Lamb wave velocities are related to the thickness, and the waves are dispersive. However, if the wavelengths are large compared to the film thickness, the extensional mode tends to propagate at a single velocity, the sheet velocity V_{sh}, while the flexural mode becomes highly dispersed and propagates relatively slowly. An elastic modulus called the sheet modulus E_{sh} can be defined as [Greenough, 1987]

$$E_{sh} = dV_{sh}^{2} \qquad (5.6)$$

where d is the density. Its relationship with the Young's modulus is given by

$$E_{sh} = \frac{E}{1 - v^2} \qquad (5.7)$$

For solid materials, the Poisson's ratio is less than 0.5, e.g. ν of the Vectra pure LCP is about 0.45, so that the sheet modulus will be typically 25 % larger than the Young's modulus.

The most convenient way to produce an acoustic wave on polymeric film is to introduce a thermoelastic stress by a localized heat source. A pulsed laser will serve this purpose provided it could be absorbed by the sample material. As shown in Figure 5.5, the incident laser beam is radiated on the sample surface. The optical energy absorbed is converted to thermal energy and diffused into the sample. This sudden heating will produce a thermal elastic stress in the material. It will then transform into an ultrasonic wave and propagate away from the source.

Thermal Wave Field

Incident Laser Beam

Absorption of Electro-
Magnetic Radiation
Heat Surface Region

Ultrasonic Wave Field Generated
by Thermoelastic Stress
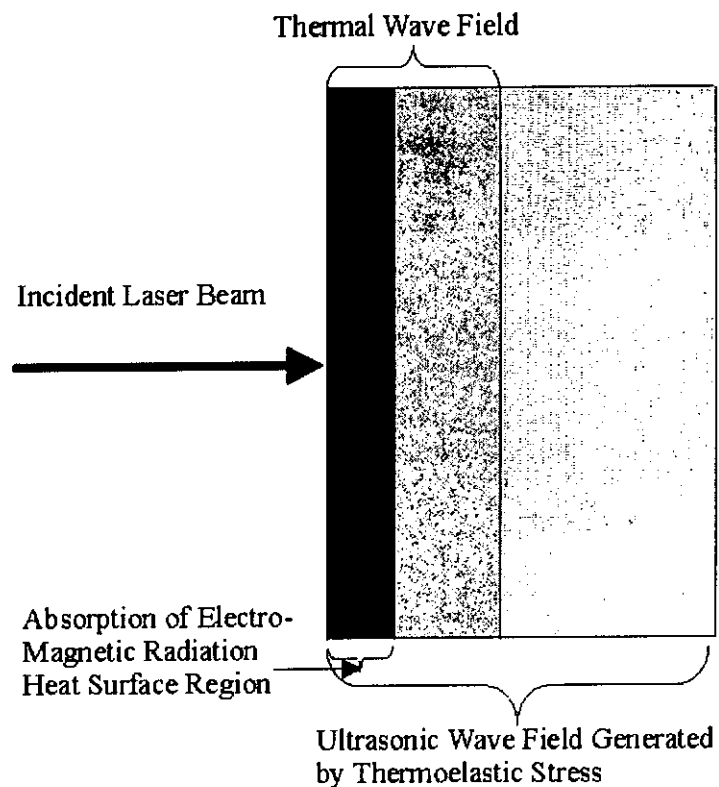
Figure 5.5   Electromagnetic radiation from the laser is absorbed
in the surface region of a sample, causing heating

Pulsed lasers have been used to generate ultrasonic wave for many years in various materials such as metals and composites [Piche, *et al.*, 1987, Scala *et al.*, 1989, Hutchins *et al.*, 1989 and Nakano *et al.*, 1991]. It has been widely used because it is nondestructive. Based on the measurement of the sheet velocity of the ultrasonic waves generated by a laser pulse, the elastic modulus can be deduced. Therefore, the elastic moduli in the two directions (flow and transverse) of the CB/LCP composites can be determined.

The schematic diagram of the setup for elastic modulus measurements is shown in Figure 5.6. A circular beam from the pulsed Nd/YAG laser (Quanta Ray GCR – 16S) was focused into a line shape of width 0.2 mm and flashed onto the surface of the CB/LCP samples. The line was oriented perpendicular to the length of the sample. The duration of the laser pulse was 10 ns. The wavelength used was the second harmonic 532 nm. Upon the absorption of the laser pulse, the irradiated region was heated and expanded. It leads to the generation of an ultrasonic wave which then propagated along the length of the sample.

The wave was detected by a piezoelectric PZT ceramic bar of length 15 mm, width 1.0 mm. The ceramic bar was adhered to a copper substrate which was used as one of the electrode. The other surface of the bar was coated with a thin layer of silver paint of thickness about 30 μm, which served as the other electrode. The transducer was mounted on an insulation support. The sample was lightly pressed onto the silver painted surface of the detector by a spring-loaded head as shown in Figure 5.6. The piezoelectric signal detected was fed to a pre-amplifier of bandwidth 100 MHz. A

digital storage oscilloscope (Hewlett Packard 54510B) with a maximum sampling rate 1

giga-sample per second was used to capture the amplified signal. The data were finally

transferred to a microcomputer and stored for further analysis.
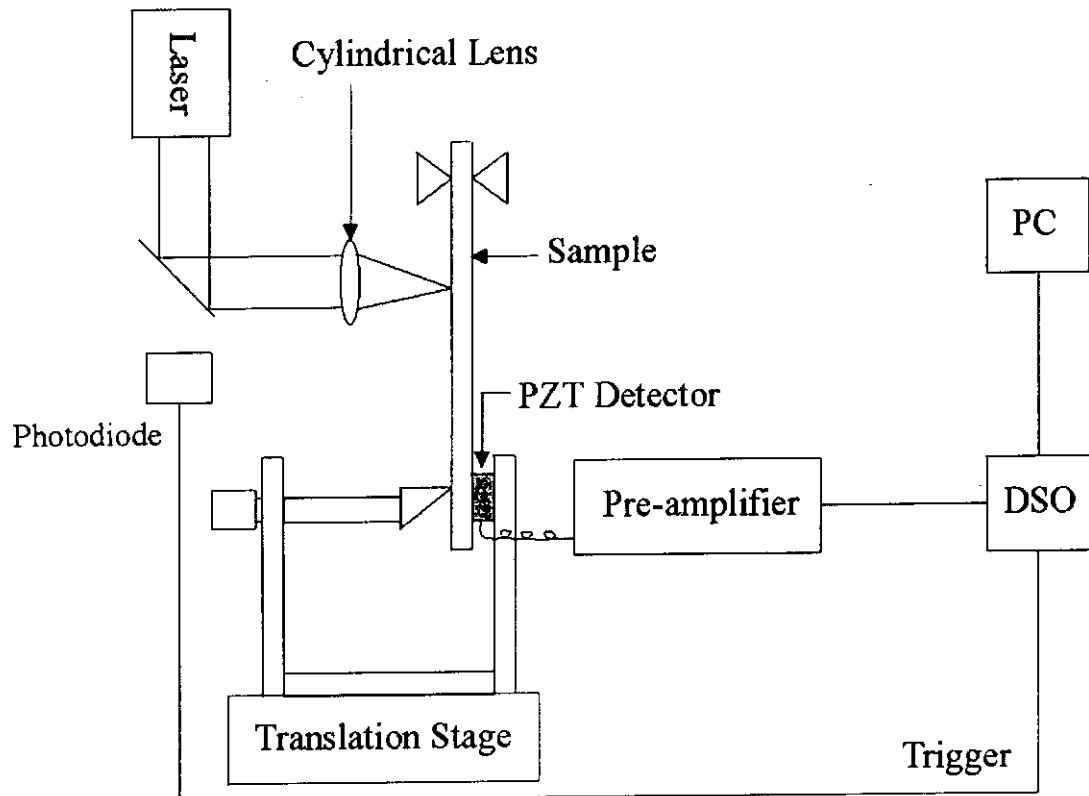
Figure 5.6   Experimental setup for laser induced ultrasonic wave measurement

The sample was placed on a translation stage which could be displaced along the length

direction of the sample so that the ultrasonic wave can be generated at various distance

from the detector. The displacement of the stage has a precision of 0.01 mm.

5.3   Results and Discussion

Thermal Conductivity

The volume fraction dependence of thermal diffusivity D and thermal conductivity K for the CB/LCP composites in the flow, transverse and thickness directions at room temperature are shown in Figure 5.7 and Figure 5.8 respectively (data were tabulated in Appendix G). Since the thermal conductivity is calculated from the equation 5.1, the specific heat and density do not show drastic CB volume fraction dependence (see Appendix B), therefore, both D and K exhibit similar dependence on CB volume fraction. From Figure 5.8, it can be seen that K in the flow direction decrease at low CB volume fraction and become constant at the high CB volume fraction. On the other hand, the K in the thickness direction increase at the low CB volume fraction and approach to the same value as K in flow direction at high CB volume fraction. The result of K in transverse direction almost constant at all volume fractions.

Due to the CB/LCP composites are injected from a mould tool. There is a certain amount of anisotropic in the samples. Pure LCP injected into the mould gap obtains high degree of molecular alignment in the flow direction. It is verified from the results of orientation function determination. The molecular alignment of the composites is the main factor which affects the thermal diffusion [Choy et al., 1995]. It can be realized that the covalent bonds along the chains are much stronger than the interchain van der Waals forces, therefore, we would expect a high thermal conductivity of a LCP sample in the flow direction.
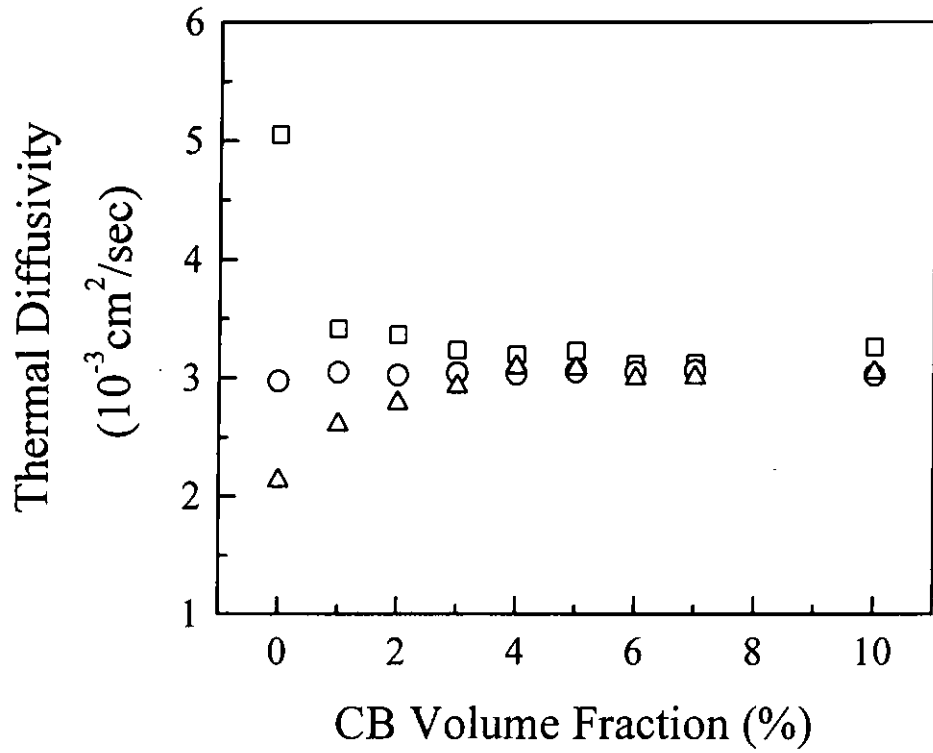
Figure 5.7   Thermal diffusivity of CB/LCP composites in the
                flow (□), transverse (○), and thickness (△) directions
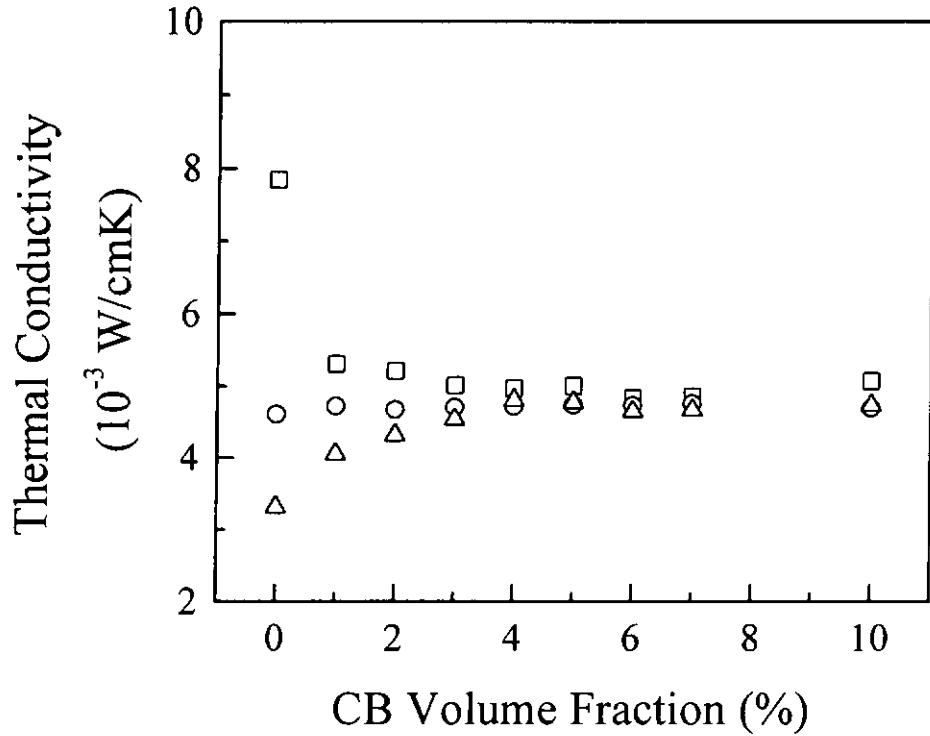
Figure 5.8   Thermal conductivity of CB/LCP composites in the
                flow (□), transverse (○), and thickness (△) directions

The cross-sectional schematic diagrams (Figure 5.9a and Figure 5.9b) depict the alignment of the rigid-rod LCP molecules for the three directions. For low CB volume fraction samples, there are more preferred molecules along the flow direction, which results in higher thermal conductivity in this direction. The thermal conduction in the transverse direction will face more interchain interactions, which means a lower conductivity. Moreover, the molecules were forced to flow through a small gap in the mould, the LCP molecules will tend to align in parallel with the mould wall, therefore, the thermal conductivity is the lowest.
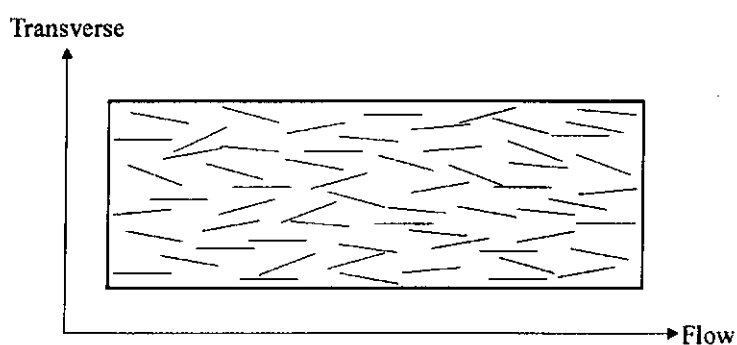
Figure 5.9a   Schematic diagram show the alignment of LCP
               molecules in the Transverse-Flow cross-section
               of the low CB volume fraction samples
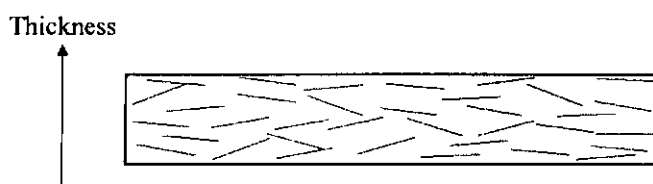
Figure 5.9b   Schematic diagram show the alignment of LCP
               molecules in the Thickness cross-section of the
               low CB volume fraction samples

As the CB volume fraction is increased, more CB particles in the composite hinder the LCP form fibrils, therefore reducing the orientation of molecular chains. It is evident that the more randomly oriented molecular, the more isotropic in thermal conduction of the composites (Figure 5.10a and Figure 5.10b), so the thermal conductivity measured for the three directions approach each other at a value just above 4.5 mW/cmK.
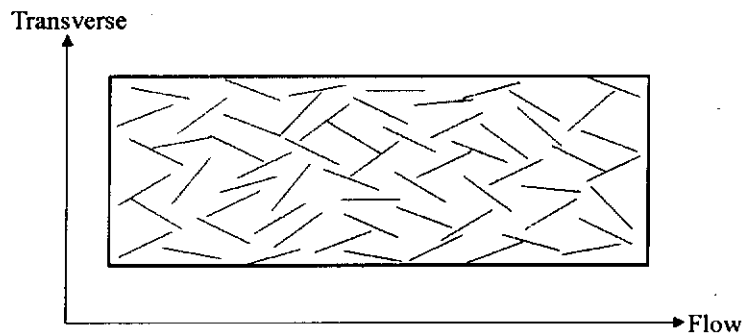
Transverse

Flow

Figure 5.10a   Similar diagram of Transverse-Flow cross-section with more random line distribution
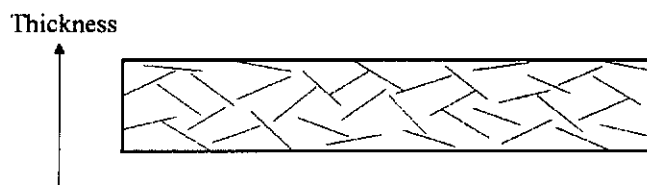
Thickness

Figure 5.10b   Similar diagram of Thickness cross-section with more random line distribution

According to William's study in the physical properties of CB [William, 1993], the thermal conductivity of CB is in the range of 1.55 to 3.75 mW/cmK. It's upper limit is about 3.75 mW/cmK. It seems that the thermal conduction of CB does not make too much contribution to the thermal conduction of the composites up to the 10 % volume fraction. We may conclude that up to this volume fraction, the dominant factor is the molecular alignment of the polymer matrix.

Sheet Modulus

We have also performed experiments on measuring the ultrasonic velocity of the composites. The experiment method has been described in detail in section 5.2. The sheet modulus which reflects the elastic property of the composite films can be directly deduced from the results of ultrasonic velocity measurements.

The sheet modulus against the CB volume fraction of the film samples in the flow and transverse directions are shown in the Figure 5.11. In the flow direction, pure LCP has relative high sheet modulus (12 GPa), data were tabulated in Appendix H. It gradually decreases as CB volume fraction increase and seems to be leveled off at high CB volume fraction. In the transverse direction, due to the short sample length, the experimental error is greater, the results have a large scattering. It ranges at 5.5 to 6.5 GPa for all CB volume fractions. The sheet modulus in high CB volume fraction in flow direction is close to that of transverse direction values.

Comparing the results of the sheet moduli and the thermal conductivity in the flow and transverse directions, the feature of the curves seems to be consistent. The amount CB loading inside the LCP matrix governed the orientation of the CB/LCP composites. Low CB loading may have higher degree of orientation. Since high molecular alignment in the flow direction results in a high modulus and thus more efficient for elastic wave propagation. Moreover, the inter-chain interaction is weaker in the transverse direction, the samples have lower modulus in this dirction.
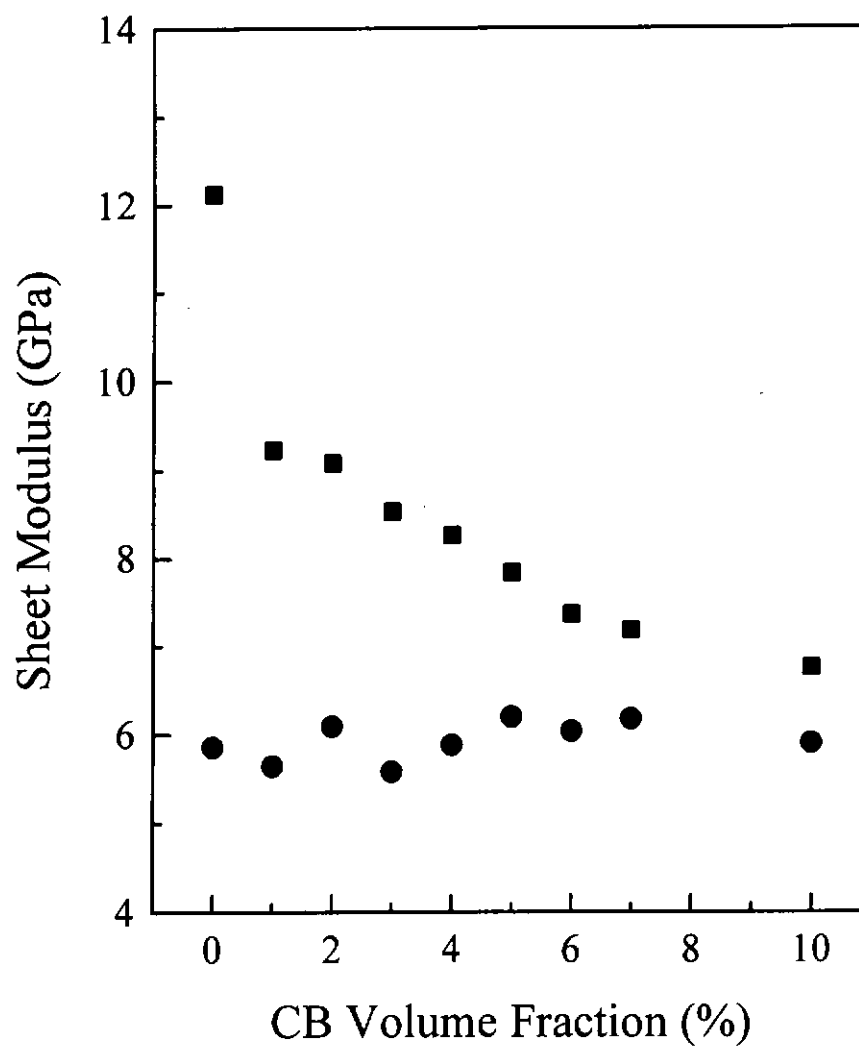
Figure 5.11   Sheet moduli of CB/LCP composites in the flow (■) and
transverse (●) directions as a function of CB volume fraction

6 Conclusions

A series of extrinsic conducting polymer has been prepared by mixing a highly conductive carbon black in various concentrations with a liquid crystalline polymer Vectra A950. The carbon black/liquid crystalline polymer composites have been investigated in various properties. From the experimental results obtained, it has been found that the electrical property is dominated by the CB particles distribution while the thermal and mechanical properties are sensitive to the molecular orientation of the LCP matrix.

From the morphology studies, both of the polarized optical and SEM micrographs reveal the aggregation of CB in the LCP matrix. As expected, when the CB volume fraction increases, the CB aggregates incorporated in form of clusters and grew in size. Obvious changes were observed between 3 % to 4 % of CB that large number of aggregates joined together forming a large scale clusters and made contact. Thus, resulted in a continuous CB network which changed the composite from insulator to conductor.

From the studies of orientation function in various CB volume fractions, lower CB volume fraction of samples exhibit larger orientation function values which means a comparatively higher degree of orientation. On the other hand, higher CB volume fraction composites have lower orientation function values which means almost no molecular orientation. In other words, the samples exhibit random molecular alignment.

The results of orientation function revealed that the CB clusters were hindrance to the LCP molecular alignment and weakened the anisotropy of the CB/LCP samples.

For the electrical study, the resistivities of the samples were measured in the flow, transverse and thickness directions. From the results of resistivity dependence on CB volume fraction, the sudden drop in resistivities in the three directions were observed at above 3 %. Furthermore, the volume fraction dependence of resistivity satisfies the scaling law and the least-squares fit of data to the scaling equation gives the slope of fitting line which is close to the percolation theoretical value.

The temperature dependence of the resistivity of the low CB volume fraction (below percolation threshold) samples reveal a negative temperature coefficient in the range from room temperature to 200 °C and the drop in resistivity is about three orders of magnitude at above 55 °C. For composites above the percolation threshold, they exhibit negative slope in low temperature range and change to positive slope in the high temperature range. The transition point occurs at about 150 °C.

On the other hand, the results of volume fraction dependence and temperature dependence of resistivities in the three directions of the samples do not show any trend between samples of different volume fraction. At above percolation threshold, although the resistivities in the three directions at one specific volume fraction exhibit almost one order of magnitude change, there is not any correlation between different volume fraction samples. Thus no conclusive anisotropy can be observed from these results.

The laser flash radiometry method was employed to obtain the thermal diffusivity of samples. It was then used to calculate the thermal conductivity. The pure LCP in the flow direction has a relative higher thermal conductivity, but it decreases rapidly for low CB volume fraction samples and becomes constant at high CB volume fraction. An opposite trend was found for thermal conductivity in the thickness direction. It increases at low CB volume fraction and approaches to similar value as those obtained in the flow direction at high CB volume fraction. The thermal conductivity in the transverse direction for all CB volume fractions was found almost constant, and was nearly the same as other two directions at high CB volume fraction. The results of thermal conductivity reveal that the volume fraction dependence of the thermal conductivity is highly dependent on the molecular chain orientation of the LCP matrix.

Similar results were found in the sheet modulus measurement. The sheet modulus in flow direction gradually decreases as the CB volume fraction increases and seems to be leveled off at high CB volume fraction. There is no obvious change found in the transverse direction. The results can be explained by the orientation of the LCP molecules and they are consistent with the results of thermal conductivity.

References

Abo-Hashem, A. "DC-conduction in butyl rubber (IIR) loaded with carbon black". *Journal of Polymer Science*, Vol. 45 pp.1733-1741 (1992)

Abo-Hashem, A., Saad, H.M. and Ashor, A.H. "Percolation concept and the electrical conductivity of carbon black-polymer composites: Butyl rubber mixed with SRF carbon black". *Plastic, Rubber and Composites Processing and Applications*, Vol. 21 pp.125-130 (1994)

Aharoni, S.M. "Electrical resistivity of a composite of conducting particles in an insulating matrix". *Journal of Applied Physics*, Vol. 43, pp.2463-2465 (1972)

Akhtar, S and Isayev, A.I. "Self-reinforced composites of two thermotropic liquid crystalline polymers". *Polymer Engineering and Science*, Vol. 33, pp.32-42 (1993)

Al-Allak, H.M., Brinkman, A.W. and Woods, J. "*I-V* characteristics of carbon black-loaded crystalline polyethylene". *Journal of Materials Science*, Vol. 28, pp.117-120 (1993)

Ali, M.H. and Abo-Hashem A., "Percolation concept and the electrical conductivity of carbon black-polymer composites 3-crystalline chloroprene rubber mixed with FEF carbon black". *Plastic, Rubber and Composites Processing and Application*, Vol. 24 pp.47-51 (1995)

Aminabhavi, T.M., Cassidy, P.E. and Thompson, C.M. "Electrical resistivity of carbon black-loaded rubbers". *Rubber Chemistry and Technology*, Vol. 63, pp.451-471 (1990)

Blaszkiewicz, M., McLachlan, D.S. and Newnham, R.E. "The volume fraction and temperature dependence of the resistivity in carbon black and graphite polymer composites: An effective media percolation approach". *Polymer Engineering and Science*, Vol. 32, pp.421-425 (1992)

Blizard, K.G. and Baird, D.G. "The morphology and rheology of polymer blends containing a liquid crystalline copolyester". *Polymer Engineering and Science*, Vol. 27, pp.653-662 (1987)

Blythe, A.R. "Conduction in polymers". Cahn, R.W. Thompson, M.W. and Ward, I.M. eds., *Electrical Properties of Polymers*, Press Syndicate of the University Cambridge, New York, pp.91-139 (1979)

Chen, X.B., Devaux, J., Issi, J-P. and Billaud, D. "The conducting behaviour and stability of conducting polymer composites". *Polymer Engineering and Science*, Vol. 35, pp.637-641 (1995)

Choy, C.L., Leung, W.P. and Ng, Y.K. "Thermal diffusivity of polymer films by the flash radiometry method". *Journal of Polymer Science: Part B: Polymer Physics*, Vol. 25, pp.1779-1799 (1987)

Choy, C.L., Leung, W.P. and Kwok, K.W. "Thermal diffusivity of an injection-moulded liquid crystalline polymer by flash radiometry". *Polymer Communications*, Vol. 32, pp.285-288 (1991)

Choy, C.L., Wong, Y.W., Lau, K.W.E., Yang, G.W. and Yee, A.F. "Thermal conductivity and thermal expansivity of thermotropic liquid crystalline polymers". *Journal of Polymer Science: Part B: Polymer Physics*, Vol. 33, pp.2055-2064 (1995)

Choy, C.L., Lau, K.W.E. and Wong, Y.W. "Elastic Moduli of a liquid crystalline polymer and its *in-situ* composites". *Polymer Engineering and Science*, Vol. 36, pp.1256-1265 (1996)

Choy, C.L. Yang, G.W. and Wong, Y.W. "Thermal diffusivity of polymer films by pulsed photothermal radiometry". *Journal of Polymer Science: Part B: Polymer Physics*, Vol. 35, pp.1621-1631 (1997)

Choy, C.L. "Elastic moduli of polymer liquid crystals". Witold, B. *Mechanical and Thermophysical Properties of Polymer Liquid Crystals*, Champman & Hall, New York, London, pp.495-510 (1998)

Coppard, R.W., Bowman, J., Dissado, L.A., Rowland, S.M. and Rakowski, R.T. "The effect of aluminium inclusions on the dielectric breakdown of polyethylene". *Journal of Physics D: Applied Physics*, Vol. 23, pp.1554-1561 (1990)

Deprez, N. and McLachlan, D.S. "The analysis of the electrical conductivity of graphite powers during compaction". *Journal of Physics D: Applied Physics*, Vol. 21, pp.101-107 (1988)

Ding, R. and Isayev, A.I. "Self-reinforced prepregs, laminates and injection mouldings of LCP/LCP blends". *Journal of Thermoplastic Composite Materials*, Vol. 8, pp.208-224 (1995)

Donaldson, A.B. "Radial conduction effects in the pulse method of measuring thermal diffusivity". *Journal of Applied Physics*, Vol. 43, pp.4226-4228 (1972)

Frisch, H.L. and Hammersley, J.M. "Percolation processes and related topics". *Journal of Society Industrial and Applied Mathematics*, Vol. 11, pp.894-918 (1963)

Ghofraniha, M. and Salovey, R. "Electrical conductivity of polymers containing carbon black". *Polymer Engineering and Science*, Vol. 28, pp.58-63 (1988)

Greenough, R.D., Dewhurst, R.J., and Edwards, C. "Magnetomechanical sensing of laser-generated ultrasound to assess structural change in metallic amorphous ribbons". *Journal of Applied Physics*, Vol. 62, pp.4728-4731 (1987)

Hammersley, J.M. "Percolation processes II. the connective constant". *Camb. Philos. Society*, Vol. 53, pp.642-645 (1957)

Hutchins, D.A. and Lundgren, K. "A laser study of transient Lamb waves in thin materials". *Journal of the Acoustical Society of American*, Vol. 85 pp.1441-1448 (1989)

Isayev, A.I. and Modic, M. "Self-rinforced melt processible polymer composites: extrusion, compression, and injection moulding." *Polymer composites*, Vol. 8, pp.158-175 (1987)

Isayev, A.I. "Self-reinforced composites of thermotropic liquid crystalline polymers". *SPE ANTEC*, Vol. 36, pp.908-912, (1991)

Isayev, A.I. "Self-Reinforced composites involving liquid-crystalline polymers" Isayev, A.I. Kyu, T and Cheng, Z.D., eds., *Liquid-Crystalline Polymer Systems Technological Advanced*, American Chemical Society, Anaheim, California pp.1-20 (1996)

Jackson, C.L. and Shaw, M.T. "Polymer liquid crystalline materials". *International Materials Review*, Vol. 36, pp.165-185 (1991)

Jackson, W.J. and Kuhfuss, H.F. "Liquid crystal polymers. I. Preparation and properties of p-hydroxybenzoic acid copolyesters". *Journal of Polymer Science: Polymer Chemistry*, Vol. 14, pp.2043-2058 (1976)

Jansson, J.F. "Application of LCP materials". Collyer, A.A. eds., *Liquid Crystal Polymers: From Structures to Applications*, Elsevier Applied Science, London and New York, pp.447-463 (1992)

Janzen, J. "On the critical conductive filler loading in antistatic composites". *Journal of Applied Physics*, Vol. 46, pp.966-969 (1975)

Jia, W. and Chen, X. "PTC effect of polymer blends filled with carbon black". *Journal of Applied Polymer Science*, Vol. 54, pp.1219-1221 (1994)

Karasek, L., Meissner, B., Asai, S. and Sumita, M. " Percolation concept: Polymer-filler gel formation, electrical conductivity and dynamic electrical properties of carbon-black-filled rubbers". *Polymer Journal*, Vol. 28, pp.121-126 (1996)

Kenig, S., DeMeuse, M.T. and Jaffe, M. "Properties of blends containing two liquid crystalline polymers". *Polymers for Advanced Technologies*, Vol. 2, pp.25-30 (1991)

Kirkpatrick, S. "Percolation and conduction". *Review of Modern Physics*, Vol. 45, pp.574-588 (1973)

Kiss, G. " In situ composites: blends of isotropic polymers and thermotropic liquid crystalline polymers". *Polymer Engineering and Science*, Vol. 27, pp.410-423 (1987)

Kozlowski, M. "Electrical conductive structured polymer blends". *Polymer Networks Blends*, Vol. 5, pp.163-172 (1995)

Kwan, S.H., Shin, F.G. and Tsui, W.L. "Direct current electrical conductivity of silver-thermosetting polyester composites". *Journal of Materials Science*, Vol. 15, pp.2978-2984 (1980)

Lee, B.L. "Electrically conductive polymer composites". *Polymer Engineering and Science*, Vol. 32, pp.36-42 (1992)

Lee, W.C., Dibenedetto, A.T. and Gromek, J.M. "Processing of thermotropic liquid crystalline polymers and their blends—analysis of melt-spinning TLCP fibers". *Polymer Engineering and Science*, Vol. 33, pp.156-165 (1993)

Leung, W.P. and Tam, A.C. "Techniques of flash radiometry". *Journal of Applied Physics*, Vol. 56, pp.153-161 (1984)

Li, J.X., Silverstein, M.S., Hiltner, A. and Baer, E. "Morphology and mechanical properties of fibers from blends of a liquid crystalline polymer and poly(ethylene terephthalate)". *Journal of Applied Polymer Science*, Vol. 44, pp.1531-1542 (1992)

Lu, G., Li, X., Jiang, H. and Mao, X. "Electrical conductivity of carbon fibers/ABS resin composites mixed with carbon blacks". *Journal of Applied Polymer Science*, Vol. 62, pp.2193-2199 (1996)

Lundberg, B. and Sundqvist, B. "Resistivity of a composite conducting polymer as a function of temperature, pressure, and environment: Applications as a pressure and gas concentration transducer". *Journal of Applied Physics*, Vol. 60, pp.1074-1079 (1986)

Lux, F. "Review models proposed to explain the electrical conductivity of mixtures made of conductive and insulating materials". *Journal of Materials Science*, Vol. 28, pp.285-301 (1993)

Magagnini, P.L., Paci, M., La Mantia, F.P. and Valenza, A. "A study of polycarbonate-liquid crystal polymer blends". *Polymer International*, Vol. 28, pp.271-275 (1992)

Malliaris, A and Turner, D.T. "Influence of particle size on the electrical resistivity of compacted mixtures of polymeric and metallic powders". *Journal of Applied Physics*, Vol. 42, pp.614-618 (1971)

McLachlan, D.S., Blaszkiewicz, M. and Newnham, R.E. " Electrical resistivity of composites". *Journal of the American Ceramic Society*, Vol. 73, pp.2187-2203 (1990)

Medalia A.I. "Electrical conduction in carbon black composites". *Rubber Chemistry and Technology*, Vol. 59, pp.432-454 (1986)

Michels, M.A.J., Brokken-Zijp, J.C.M., Groenewoud, W.M. and Knoester, A. " Systematic study of percolative network formation and effective electric response in low-concentration-carbon-black/polymer composites". *Physica A*, Vol. 157, pp.529-534 (1989)

Modine, F.A., Duggal, A.R., Robinson, D.N. Churnetski, E.L., Bartkowiak, M., Mahan, G.D., and Levinson, L.M. "Electrical properties of polyethylene highly filled with carbon". *Journal of Materials Research*, Vol. 11 pp.2889-2894 (1996)

Mucha, M. "Thermo-optical analysis as a complementary method in the study of phase transitions of thermotropic liquid crystalline polymer and its blends with polycarbonate". *Colloid and Polymer Science*, Vol. 267, pp.876-880 (1989)

Nakamura, S., Inoue, K., Saito, K., Ohkawa, T. and Sawa, G. "Resistivity and dielectric properties of carbon black (MA600)-polyethylene composites". *Proceeding of the Symposium on Electrical Insulating Materials 1995*, Institute of Elastical Engineers of Japan, Tokyo, Japan, pp.125-128 (1995)

Nakamura, S., Saito, K. Sawa, G. and Kitagawa, K. " Percolation threshold of carbon black-polyethylene composites". *Journal of Applied Physics*, Vol. 36, pp.5163-5168 (1997)

Nakano, H. and Nagai, S. "Laser generation of antisymmetric Lamb waves in thin plates". *Ultrasonics*, Vol. 29, pp.230-234 (1991)

Ober, C.K. and Weiss, R.A. "Current topics in liquid-crystalline polymers". Weiss, R.A. and Ober, C.K., eds., *Liquid Crystalline Polymers*, American Chemical Society, Washington, pp.1-13 (1990)

Ouyang, M. and Chan, C.M. "Electrical and mechanical properties of pre-localized polyprrole/poly(vinyl chloride) conductive composites". *Polymer Engineering and Science*, Vol. 36, pp.2676-2682 (1996)

Parker, W.J., Jenkins, R.J., Butler, C.P. and Abbott, G.L. "Flash method of determining thermal diffusivity, heat capacity and thermal conductivity". *Journal of Applied Physics*, Vol. 32, pp.1679-1684 (1961)

Piche, L., Champagne, B. and Monchalin, J.P. "Laser Ultrasonics measurement of elastic constants of composites". *Materials Evaluation*, Vol. 45, pp.74-79 (1987)

Probst, N. "Conducting carbon black". Donnet, J.B. Bansal R.C. and Wang, M.J. eds., *Carbon Black*, Marcel Dekker, Inc., New York, pp.271-288 (1993)

Roviello, A. and Sirigu, A. "Mesophasic structures in polymers. A preliminary account on the mesophases of some poly-alkanoates of p, p'-di-hydroxy-α, α'-di-methyl benzalazine". *Journal of Polymer Science: Polymer Letter*, Vol. 13, pp.445 (1975)

Scala, C.M. and Doyle, P.A. "Time-and frequency-domain characteristics of laser-generated ultrasonic surface waves". *Journal of the Acoustical Society of American*, Vol. 85, pp.1569-1576 (1989)

Scruby, C.B and Drain, L.E. "Ultrasonic generation by laser". De Barr, A.E. eds., *Laser Ultrasonics Techniques and Applications*, Adam Higher, New York, pp.223-324 (1990)

Shante, V.K.S. and Kirkpatrick, S. "An introduction to percolation theory". *Advanced Physics*, Vol. 20, pp.325-357 (1971)

Sheng, P., Sichel, E.K. and Gittleman, J.I. "Fluctuation-induced tunneling conduction in carbon-polyvinylchloride composites". *Physical Review Letters*, Vol. 40, pp.1197-1200 (1978)

Sherman, R.D., Middleman, L.M. and Jacobs, S.M. "Electron transport processes in conductor-filled polymers". *Polymer Engineering and Science*, Vol. 23, pp.36-46 (1983)

Shin, F.G., Yeung, Y.Y and Tsui, W.I. "On symmetrical dielectric binary mixture formulas". Journal of Material Science Letters, Vol. 9, pp.948-950 (1990)

Sichel, E.K., Gittleman, J.I. and Sheng P. "Transport properties of the composite material carbon-poly(vinyl chloride)". *Physical Review B*, Vol. 18, pp.5712-5716 (1978)

Stauffe, D. "Cluster number". *Introduction to Percolation Theory*, Taylor & Francis, Philadelphia, pp.15-58 (1985)

Tang, H., Chen, X. Tang, A. and Luo, Y. "Studies on the electrical conductivity of carbon black filled polymers". *Journal of Applied Polymer Science*, Vol. 59 pp.383-387 (1996)

Viswanathan, R. and Isayev, A.I. "Blends of a PPO-PS alloy with a liquid crystalline polymer". *Journal of Applied Polymer Science*, Vol. 55, pp.1117-1129 (1995)

Voet, A. "Temperature effect of electrical resistivity of carbon black filled polymers". *Rubber Chemistry and Technology*, Vol. 54, pp.42-50 (1981)

Weiss, R.A., Huh, W. and Nicolais, L. "Novel reinforced polymers based on blends of polystyrene and a thermotropic liquid crystalline polymer". *Polymer Engineering and Science*", Vol. 27, pp.684-691 (1987)

William, M.H. "Microstructure, morphology and general physical properties". Donnet, J.B. Bansal R.C. and Wang, M.J. eds., *Carbon Black*, Marcel Dekker, Inc., New York, pp.271-288 (1993)

Xu, Q., Leng, Y. and Mai, Y.W. "Injection moulding of PC/PBT/LCP ternary *in situ* composite". *Polymer Engineering and Science*, Vol. 36, pp.769-777 (1996)

Yacubowicz, J. and Narkis, M. "Dielectric behavior of carbon black filled polymer composites". *Polymer Engineering and Science*, Vol. 26, pp.1568-1573 (1986)

Yacubowicz, J. and Narkis, M. "Electrical and dielectric properties of segregated carbon black-polyethylene systems". *Polymer Engineering and Science*, Vol. 30, pp.459-468 (1990)

Zallen, R. "The percolation model". *The Physics of Amorphous Solids*, Wiley Interscience, New York (1983)

Appendix

Appendix A Conversion of Weight Fraction to Volume Fraction

Weight % of CB in CB/LCP composites (W_f)	Volume % of CB in CB/LCP composites (ϕ)
1.60	1
3.18	2
4.74	3
6.28	4
7.80	5
9.30	6
10.79	7
15.01	10

Appendix **B**   Data-table of Density and Specific Heat of CB/LCP Composites

CB/LCP Composites (CB %)	Density (g/cm^3)	Specific Heat (J/gK)
0	1.4018	1.1080
1	1.4030	1.1082
2	1.4078	1.1007
3	1.4116	1.0985
4	1.4226	1.0953
5	1.4216	1.0906
6	1.4316	1.0854
7	1.4358	1.0845
10	1.4386	1.0820

Appendix **C1** Operation Information of DSC

Parameters   Conditions

Final Temp:	40 °C		End Condition:	Load
Start Temp:	-10 °C		Load Temp:	-10 °C
Scanning Rate:	10 °C /min.		Go to Temp Rates:	10 °C /min.
Time at T Start:	2 min.		Event 1 Time:	0 min.
Time at T Final:	2 min.		Event 2 Time:	0 min.
Y Range:	50 mW		Y Initial Value:	20 mW
Sample Weight:	*		Y Cal. Factor:	1

*   Sample weight of CB/LCP composites were measure by a electronic
       Balance (Mettler AT201) with precision of 0.01 mg

Appendix **C2** Operation Information of TMA

Parameters   Conditions

Temp Final:	200 °C		End Condition:	Load
Temp Start:	30 °C		Load Temp:	30 °C
Scanning Rate:	10 °C		Go to Temp Rate:	10 °C
Y Range:	1 mm		/min.Event 1 Time:	0.0 min.
Applied Force:	100 mN		Event 2 Time:	0.0 min.
Sample Height:	Read by the		Sample Probe Type:	Expansion
	Quartz Probe		Delay Time:	0
			Y Initial Value:	0.5 mm

Appendix **D** Data-Table of Orientation Function of CB/LCP Composites

Volume Fraction of CB (%)	Orientation Function
0	0.35
1	0.23
2	0.20
3	0.15
4	0.13
5	0.12
6	0.11
7	0.08
10	0.06

Appendix E   Data-Table of CB Volume Fraction
Dependence of Resistivity

CB/LCP composites

Volume Fraction (CB %)	Resistivity (Ω-cm)		
	Flow	Transverse	Thickness
1	1.21×10^9	1.19×10^9	1.22×10^9
2	1.16×10^9	1.26×10^9	1.25×10^9
3	1.04×10^9	1.19×10^9	1.01×10^9
4	8.40×10^4	6.13×10^5	2.49×10^6
5	2.11×10^3	4.10×10^3	1.23×10^3
6	59.00	497.00	216.00
7	33.00	30.60	37.00
10	4.30	8.63	11.47

Appendix F   Data-Table of Temperature Dependence of Resistivity

1 % CB/LCP composites

Flow direction		Transverse direction		Thickness direction	
Temperature (°C)	Resistivity (10^6 Ω-cm)	Temperature (°C)	Resistivity (10^6 Ω-cm)	Temperature (°C)	Resistivity (10^6 Ω-cm)
21.2	1207	21.5	1189	21.8	1218
32.1	1188	30.6	1152	31.5	1084
40.8	1121	42.0	1101	42.2	714
50.6	1145	51.0	938	53.4	405
60.5	1059	60.5	701	61.6	217
70.5	851	70.0	420	70.5	125
81.8	532	80.5	216	80.0	63
92.0	287	89.8	113	90.3	33
102.8	141	99.4	61	99.8	19
113.0	71	110.4	32	109.7	11
121.2	43	119.2	21	119.3	7.12
131.5	26	129.4	13	129.5	4.64
140.7	168	139.4	8.26	139.6	3.21
150.5	1.09	149.4	5.45	149.7	2.31
160.5	7.04	159.6	3.72	159.6	1.73
170.0	5.04	169.6	2.64	169.6	1.37
180.2	3.69	179.7	1.87	179.3	1.13
190.5	3.02	189.0	1.32	189.5	0.99
199.3	2.44			199.3	0.90

2 % CB/LCP composites

Flow direction		Transverse direction		Thickness direction	
Temperature (°C)	Resistivity (10^6 Ω-cm)	Temperature (°C)	Resistivity (10^6 Ω-cm)	Temperature (°C)	Resistivity (10^6 Ω-cm)
21.0	1163	20.0	1465	20.6	1691
31.5	1157	30.6	1667	31.0	1691
41.0	1125	40.4	1704	41.4	1678
51.0	1068	50.2	1643	51.3	1629
60.4	888	60.1	1544	60.4	1440
69.7	604	70.5	1134	70.5	976
79.9	311	79.7	615	80.3	500
90.0	134	89.4	251	90.1	226
99.8	611	99.5	103	99.5	108
109.5	308	109.4	49	109.4	53
119.6	16	119.4	26	119.5	28
129.9	9.49	129.6	14	130.4	15
139.7	6.16	139.8	8.65	139.5	9.26
149.6	4.15	149.4	5.65	149.7	5.73
159.3	2.97	159.3	3.92	159.5	3.82
169.3	2.26	169.2	2.95	169.3	2.66
180.5	1.74	179.6	2.38	179.4	1.92
189.2	1.49	189.4	2.06	189.2	1.41
199.2	1.29	199.3	1.96	199.2	1.06

3 % CB/LCP composites

Flow direction		Transverse direction		Thickness direction	
Temperature (°C)	Resistivity (10^6 Ω-cm)	Temperature (°C)	Resistivity (10^6 Ω-cm)	Temperature (°C)	Resistivity (Ω-cm)
21.2	1039	20.3	1159	20.2	1012
30.9	925	30.5	1210	30.9	1003
40.5	1099	39.8	1210	40.5	990
50.8	768	50.5	1166	50.3	875
61.3	387	59.5	977	60.4	556
70.8	153	69.5	629	69.9	240
80.4	55	80.8	284	80.0	72
90.0	20	89.5	147	89.5	23
99.8	7.38	99.5	71	99.8	9.83
109.8	3.67	109.6	38	109.7	6.03
119.5	2.62	119.4	22	119.9	4.56
129.5	2.01	129.7	13	129.8	3.75
139.6	1.62	139.6	9.09	139.4	3.12
149.2	1.34	149.7	6.39	149.5	2.62
159.7	1.22	160.5	4.64	159.7	2.26
169.6	1.24	170.2	3.77	169.6	1.92
179.6	1.00	179.5	3.27	179.2	1.70
		189.7	2.92	189.8	1.28
		199.5	2.66	199.3	1.09

4 % CB/LCP composites

Flow direction		Transverse direction		Thickness direction	
Temperature (°C)	Resistivity (10^3 Ω-cm)	Temperature (°C)	Resistivity (10^3 Ω-cm)	Temperature (°C)	Resistivity (10^3 Ω-cm)
21.7	77.00	21.2	568.63	22.7	2215
32.8	76.66	32.0	564.23	33.7	2209
42.4	76.26	42.0	562.92	42.7	2203
51.9	76.21	51.6	559.80	52.1	2194
61.2	76.14	61.2	562.39	62.6	2183
71.0	76.36	70.9	563.12	71.4	2193
80.1	7640	80.1	569.98	79.5	2192
90.1	76.68	90.1	578.47	90.4	2188
99.3	77.01	99.7	589.12	99.9	2199
109.7	7756	109.8	597.98	109.7	2208
119.4	78.22	119.8	600.94	119.7	2243
129.3	78.85	129.8	612.97	130.0	2263
139.2	79.94	139.6	631.91	139.4	2266
149.4	81.29	149.8	657.29	149.8	2289
159.4	84.18	159.9	711.96	159.7	2360
169.6	89.75	169.6	767.45	169.7	2437
179.5	98.21	180.0	879.63	179.4	2557
189.4	111.65	190.5	1035	190.1	2810
199.2	127.91	199.7	1246	199.0	3003

5 % CB/LCP composites

Flow direction		Transverse direction		Thickness direction	
Temperature (°C)	Resistivity (Ω-cm)	Temperature (°C)	Resistivity (Ω-cm)	Temperature (°C)	Resistivity (Ω-cm)
22.1	1936	22.3	3675	21.6	353
33.1	1916	31.6	3645	31.7	350
44.4	1900	42.1	3617	40.4	348
52.3	1890	52.7	3598	49.8	345
62.0	1879	60.9	3587	60.4	343
71.1	1870	71.8	3574	70.7	341
81.0	1865	80.7	3570	80.6	339
90.2	1861	90.2	3571	90.8	339
100.2	1861	99.9	3568	101.1	338
109.8	1861	109.0	3577	110.9	338
119.9	1864	120.6	3590	120.6	339
129.6	1867	130.0	3600	130.0	340
139.9	1873	139.9	3620	140.4	341
150.0	1891	149.8	3676	150.3	343
159.7	1911	159.8	3760	160.0	346
170.1	1973	169.7	3839	170.0	350
180.0	2064	180.8	4115	180.3	362
190.0	2219	189.6	4438	190.1	347
199.4	2382	199.4	4889	199.5	395

6 % CB/LCP composites

direction		Transverse direction		Thickness direction	
Temperature (°C)	Resistivity (Ω-cm)	Temperature (°C)	Resistivity (Ω-cm)	Temperature (°C)	Resistivity (Ω-cm)
24.7	58.71	20.6	79.11	23.2	203.33
33.5	58.37	32.0	78.27	33.9	201.43
42.5	57.95	41.5	77.59	43.7	199.41
51.2	57.54	50.9	77.06	54.1	197.95
61.0	57.14	60.4	76.53	62.1	196.41
70.7	56.82	70.2	76.01	71.2	195.13
80.3	56.50	79.4	75.62	82.1	194.09
90.0	56.27	89.5	75.24	90.7	193.12
99.5	56.03	99.1	74.99	100.6	192.33
109.2	55.88	109.2	74.73	109.7	191.61
119.3	55.73	119.2	74.49	119.8	190.94
129.3	55.57	129.3	74.36	130.1	190.55
139.2	55.42	139.5	74.24	139.7	190.10
149.2	55.50	149.4	74.49	150.0	190.06
158.8	55.65	159.4	74.99	160.0	190.09
168.5	56.11	169.3	75.75	169.9	191.17
180.0	56.90	181.0	77.06	180.0	193.25
				189.8	196.01
				199.4	199.22

7 % CB/LCP composites

Flow direction		Transverse direction		Thickness direction	
Temperature (°C)	Resistivity (Ω-cm)	Temperature (°C)	Resistivity (Ω-cm)	Temperature (°C)	Resistivity (Ω-cm)
21.5	32.79	22.2	35.38	23.2	37.41
32.0	32.47	32.4	35.04	33.0	37.06
39.5	32.24	42.1	34.75	43.0	36.74
49.3	32.00	51.3	34.49	51.0	36.47
57.8	31.78	60.9	34.22	61.1	36.19
67.3	31.56	70.5	34.03	70.6	35.95
77.8	31.34	80.1	33.82	80.2	35.74
87.8	31.13	89.6	33.64	90.0	35.54
97.2	30.99	99.6	33.47	99.9	35.36
110.0	30.79	109.1	33.29	109.7	35.23
120.3	30.60	120.5	33.13	119.4	35.09
130.4	30.43	129.6	33.04	130.0	34.96
140.2	30.38	139.4	32.94	139.5	34.86
149.8	30.30	149.5	33.01	149.7	34.87
159.7	30.45	159.2	33.22	159.7	34.84
169.5	30.81	169.8	33.52	169.8	35.11
180.3	31.21	179.6	34.07	179.7	35.39
189.5	31.78	189.5	34.71	189.7	35.70
199.5	32.36	199.3	35.57	200.0	35.83

10 % CB/LCP composites

Flow direction		Transverse direction		Thickness direction	
Temperature (°C)	Resistivity (Ω-cm)	Temperature (°C)	Resistivity (Ω-cm)	Temperature (°C)	Resistivity (Ω-cm)
20.0	4.20	20.6	8.45	19.6	7.24
29.0	4.17	30.4	8.33	28.8	7.19
39.5	4.15	40.0	8.28	39.6	7.15
49.3	4.10	49.5	8.24	49.2	7.12
59.9	4.06	59.3	8.18	59.5	7.11
70.0	4.04	69.3	8.12	69.7	7.09
79.5	4.03	80.0	8.06	79.4	7.09
89.1	4.00	89.3	8.03	89.3	7.08
99.1	3.98	99.4	7.98	99.4	7.08
109.4	3.95	109.2	7.96	109.9	7.08
119.3	3.93	119.2	7.90	120.2	7.08
129.1	3.91	129.1	7.87	129.5	7.07
139.1	3.91	139.0	7.84	139.5	7.06
149.1	3.91	148.9	7.83	149.3	7.07
159.1	3.91	159.5	7.84	159.1	7.08
169.4	3.93	169.4	7.90	169.3	7.11
179.5	3.96	179.6	7.94	179.1	7.13
189.3	4.00	189.8	8.01	189.2	7.15
199.8	4.04	199.6	8.11	199.0	7.19

Appendix **G1** Data-Table of Thermal Diffusivity

CB/LCP composites

Volume Fraction (CB %)	Thermal Diffusivity (10^{-3} cm/s)		
	Flow	Transverse	Thickness
0	5.05	2.97	2.13
1	3.41	3.04	2.60
2	3.36	3.02	2.79
3	3.23	3.04	2.93
4	3.19	3.03	3.09
5	3.22	3.05	3.08
6	3.11	3.05	2.99
7	3.12	3.06	3.00
10	3.23	3.02	3.04

Appendix **G2** Data-Table of Thermal Conductivity

CB/LCP composites

Volume Fraction (CB %)	Thermal Conductivity (mW/cmK)		
	Flow	Transverse	Thickness
0	7.84	4.61	3.31
1	5.30	4.73	4.05
2	5.21	4.68	4.32
3	5.01	4.71	4.54
4	4.97	4.72	4.81
5	5.00	4.74	4.78
6	4.83	4.74	4.65
7	4.86	4.76	4.67
10	5.07	4.70	4.74

Appendix **H**   Data-table of Sheet Modulus

CB/LCP composites

Volume Fraction (CB %)	Sheet Modulus (GPa) Flow	Transverse
0	12.12	5.86
1	9.23	5.65
2	9.08	6.09
3	8.53	5.58
4	8.26	5.88
5	7.83	6.19
6	7.36	6.04
7	7.18	6.17
10	6.75	5.90